On the Time-Resolved Atomic Force Microscopy

by

Mohammad SAFIKHANI-MAHMOUDI

THESIS PRESENTED TO ÉCOLE DE TECHNOLOGIE SUPÉRIEURE
IN PARTIAL FULFILLMENT FOR THE DEGREE OF
DOCTOR OF PHILOSOPHY
Ph.D.

MONTREAL, JUNE 16, 2026

ÉCOLE DE TECHNOLOGIE SUPÉRIEURE
UNIVERSITÉ DU QUÉBEC

BOARD OF EXAMINERS

THIS THESIS HAS BEEN EVALUATED

BY THE FOLLOWING BOARD OF EXAMINERS

Dr. Omur E. Dagdeviren, Thesis supervisor
Department of Mechanical Engineering at École de technologie supérieure

Dr. Ricardo Izquierdo, Chair, Board of Examiners
Department of Electrical Engineering at École de technologie supérieure

Dr. Nicole R. Demarquette, Member of the Jury
Department of Mechanical Engineering at École de technologie supérieure

Dr. Mohammad Jahazi, Member of the Jury
Department of Mechanical Engineering at École de technologie supérieure

Dr. Elmira Moosavi, Member of the Jury
Department of Mechanical Engineering at École de technologie supérieure

Dr. Yoichi Miyahara, External Independent Examiner
Department of Physics at Texas State University

THIS THESIS WAS PRESENTED AND DEFENDED

IN THE PRESENCE OF A BOARD OF EXAMINERS AND THE PUBLIC

ON "APRIL 20, 2026"

AT ÉCOLE DE TECHNOLOGIE SUPÉRIEURE

ACKNOWLEDGEMENTS

I would like to express my sincere gratitude to my supervisor, Dr. Omur E. Dagdeviren, for his guidance, encouragement, and mentorship throughout the course of this research. His scientific insight, thoughtful feedback, and continuous support were essential to the successful completion of this work and to my development as an independent researcher.

I am deeply grateful to my master's supervisor, Dr. Arash Bahrami, whose early guidance and mentorship played an important role in shaping my research foundations and academic path.

I am grateful to my colleagues Bugrahan Guner and Nuray Basaran for their collaboration, technical discussions, and support during various stages of this research. I also thank Simon Laflamme from the university staff for his assistance with administrative and technical matters, which greatly facilitated the progress of this work.

I would like to thank my friends Ali Bahri, Sina Ghofrani, Mehrdad Noori, Moslem Yazdanpanah, Reza Tangestani, Arash Ebrahimian, and my cousin Reza Farzadnia for their friendship, encouragement, and moral support throughout my graduate studies. Their presence and understanding made this journey both manageable and meaningful.

Finally, I would like to express my deepest gratitude to my parents, Farkhondeh and Abdollah, for their unconditional love, patience, and unwavering support. Their sacrifices, belief in me, and constant encouragement have been the foundation of all my achievements, and this work would not have been possible without them.

This work was supported by the Fonds de recherche du Québec – Nature et technologies (FRQNT), the Natural Sciences and Engineering Research Council of Canada (NSERC), Canada Economic Development for Quebec Regions (CED), and the Fonds de recherche en coopération intersectorielle (FRECC).

Sur la microscopie à force atomique résolue en temps

Mohammad SAFIKHANI-MAHMOUDI

RÉSUMÉ

La compréhension de la dynamique des porteurs de charge et des processus médiés par les défauts à l'échelle nanométrique est essentielle pour améliorer les performances et la fiabilité des matériaux fonctionnels à base d'oxydes métalliques. Dans des systèmes tels que le dioxyde de titane (TiO_2), le comportement électronique est régi par une interaction complexe entre le transport de charge, les défauts de lacunes d'oxygène, l'énergétique de surface et les stimuli externes, notamment l'illumination, la température et l'excitation électrique. Beaucoup de ces processus sont spatialement hétérogènes et fortement dépendants du temps, pourtant les techniques de caractérisation conventionnelles ne fournissent souvent que des informations moyennées spatialement ou temporellement, limitant la compréhension des mécanismes qui contrôlent le comportement macroscopique des matériaux.

Cette thèse utilise des techniques avancées basées sur la microscopie à force atomique (AFM) pour sonder directement la dynamique des porteurs de charge et les phénomènes électrostatiques à l'échelle nanométrique sur plusieurs échelles de temps. En combinant la microscopie à force électrostatique, la microscopie à force à sonde Kelvin (KPFM) et les approches AFM résolues en temps, ce travail étudie comment les paysages de défauts locaux et les conditions d'excitation régissent le comportement électronique du TiO_2 dans des conditions de non-équilibre. Des mesures d'AFM résolues en temps sont utilisées pour quantifier la dynamique de relaxation des porteurs de charge sur des échelles de temps allant de la milliseconde à la seconde, révélant une cinétique spatialement hétérogène associée au transport médié par les défauts et au mouvement de charge coopératif. Les mesures dépendantes de la température permettent l'extraction de barrières de migration effectives, fournissant un aperçu du rôle des lacunes d'oxygène dans la régulation de la dynamique de transport.

Pour accéder à des processus électroniques plus rapides, l'AFM résolue en temps à l'échelle de la sous-microseconde est mise en œuvre par l'analyse du signal du levier en temps réel, permettant l'étude de la dynamique de redistribution rapide des charges qui complète les processus plus lents pilotés par les défauts. En parallèle, la KPFM est employée pour sonder le potentiel de surface local et l'évolution énergétique sous une illumination ultraviolette contrôlée. En faisant varier l'énergie des photons, la géométrie d'irradiation et les conditions interfaciales, la thèse élucide comment les lacunes d'oxygène de surface photo-induites et les interfaces métal-oxyde modulent les décalages du niveau de Fermi et la cinétique des porteurs de charge.

Collectivement, les résultats démontrent que la dynamique des porteurs de charge à l'échelle nanométrique dans le TiO_2 est très sensible à la distribution des défauts, à l'historique d'excitation et à l'échelle de temps de mesure. En intégrant les techniques d'AFM électrostatique et résolues en temps, cette thèse fournit un cadre unifié pour corréler l'énergétique locale avec le comportement de transport dynamique, faisant progresser la compréhension des processus pilotés par les

défauts dans les oxydes métalliques et établissant l'AFM résolue en temps comme un outil puissant pour la caractérisation nanométrique des matériaux fonctionnels.

Mots-clés: Microscopie à sonde locale, Microscopie à force atomique résolue en temps, Microscopie à force à sonde Kelvin, Différence de potentiel de contact, Dynamique des porteurs de charge, Lacunes d'oxygène de surface photo-induites, Mobilité des porteurs de charge, Barrières de migration

On the Time-Resolved Atomic Force Microscopy

Mohammad SAFIKHANI-MAHMOUDI

ABSTRACT

Understanding charge carrier dynamics and defect-mediated processes at the nanoscale is essential for advancing the performance and reliability of functional metal oxide materials. In systems such as titanium dioxide (TiO_2), electronic behavior is governed by a complex interplay between charge transport, oxygen vacancy defects, surface energetics, and external stimuli including illumination, temperature, and electrical excitation. Many of these processes are spatially heterogeneous and strongly time dependent, yet conventional characterization techniques often provide only spatially or temporally averaged information, limiting insight into the mechanisms that control macroscopic material behavior.

This thesis employs advanced atomic force microscopy (AFM)–based techniques to directly probe nanoscale charge carrier dynamics and electrostatic phenomena across multiple timescales. By combining electrostatic force microscopy, Kelvin probe force microscopy (KPFM), and time-resolved AFM approaches, this work investigates how local defect landscapes and excitation conditions govern electronic behavior in TiO_2 under nonequilibrium conditions. Time-resolved AFM measurements are used to quantify charge carrier relaxation dynamics over millisecond-to-second timescales, revealing spatially heterogeneous kinetics associated with defect-mediated transport and cooperative charge motion. Temperature-dependent measurements enable extraction of effective migration barriers, providing insight into the role of oxygen vacancies in governing transport dynamics.

To access faster electronic processes, sub-microsecond time-resolved AFM is implemented through real-time cantilever signal analysis, allowing investigation of rapid charge redistribution dynamics that complement slower defect-driven processes. In parallel, KPFM is employed to probe local surface potential and energetic evolution under controlled ultraviolet illumination. By varying photon energy, irradiation geometry, and interfacial conditions, the thesis elucidates how photoinduced surface oxygen vacancies and metal–oxide interfaces modulate Fermi-level shifts and charge carrier kinetics.

Collectively, the results demonstrate that nanoscale charge carrier dynamics in TiO_2 are highly sensitive to defect distribution, excitation history, and measurement timescale. By integrating electrostatic and time-resolved AFM techniques, this thesis provides a unified framework for correlating local energetics with dynamic transport behavior, advancing the understanding of defect-driven processes in metal oxides and establishing time-resolved AFM as a powerful tool for nanoscale characterization of functional materials.

Keywords: Scanning probe microscopy, Time-resolved atomic force microscopy, Kelvin probe force microscopy, Contact potential difference, Charge carrier dynamics, Photoinduced surface oxygen vacancies, charge carrier mobility, migration barriers

TABLE OF CONTENTS

Page

INTRODUCTION 1
0.1 Metal Oxides and TiO_2 as a Model System for Nanoscale Charge Dynamics 3
0.2 Fundamentals of Atomic Force Microscopy 6
0.3 Electrostatic and Time-Resolved Atomic Force Microscopy Techniques 9
0.3.1 Electrostatic Interactions in AFM 10
0.3.2 Kelvin Probe Force Microscopy and Local Energetics 10
0.3.3 Time-Resolved AFM for Slow Charge Carrier Dynamics 11
0.3.4 Sub-Microsecond Time-Resolved AFM for Fast Dynamics 12
0.3.5 Advantages of Combining Electrostatic and Time-Resolved AFM 13
0.4 Research Objectives, Key Questions, and Thesis Contributions 14

CHAPTER 1 ULTRAVIOLET IRRADIATION PENETRATION DEPTH ON TiO_2 ... 17
1.1 Abstract 17
1.2 Introduction 17
1.3 Results and Discussion 19
1.4 Conclusions 26
1.5 Experimental Methods and Sample Preparation 26
1.5.1 Preparation of polycrystalline TiO_2 films 26
1.5.2 Preparation of TiO_2 (100) single crystal 27
1.5.3 Back illumination of samples with ultraviolet illumination 28
1.5.4 Time-Resolved Atomic Force Microscopy Measurements 29

CHAPTER 2 TIME-RESOLVED MAPPING OF CHARGE CARRIER DYNAMICS AND DEFECT-MEDIATED MIGRATION BARRIERS IN TiO_2 33
2.1 Abstract 33
2.2 Introduction 33
2.3 Methods 35
2.3.1 Preparation of the TiO_2 Single Crystal 37
2.3.2 Experimental Setup 37
2.3.3 Conventional Time-Resolved Atomic Force Microscopy Measurements .. 37
2.3.4 Submicrosecond Time-Resolved Atomic Force Microscopy Measurements 38
2.3.5 Surface Irradiation 39
2.4 Results and Discussion 40
2.5 Conclusions 47

CHAPTER 3 DEFECT- AND GEOMETRY-CONTROLLED FERMI-LEVEL DYNAMICS IN TiO_2 49
3.1 Abstract 49
3.2 Introduction 50

3.3 Summary of Methods 51
3.4 Results and Discussion 53
3.5 Conclusions 59

CONCLUSION AND RECOMMENDATIONS 61

APPENDIX I SUPPLEMENTAL INFORMATION OF THE ARTICLE ”ULTRAVIOLET IRRADIATION PENETRATION DEPTH ON TIO_2” . 75

APPENDIX II SUPPLEMENTAL INFORMATION OF THE ARTICLE ”TIME-RESOLVED MAPPING OF CHARGE CARRIER DYNAMICS AND DEFECT-MEDIATED MIGRATION BARRIERS IN TIO_2” 77

APPENDIX III SUPPLEMENTAL INFORMATION OF THE ARTICLE ”DEFECT- AND GEOMETRY-CONTROLLED FERMI-LEVEL DYNAMICS IN TIO_2” 83

APPENDIX IV SUPPLEMENTAL INFORMATION: DETAILED MEASUREMENT PARAMETERS FOR KPFM METHOD 87

BIBLIOGRAPHY 93

LIST OF TABLES

Page

Table 1.1 Time-resolved atomic force microscopy measurements on a 500 μm-thick, undoped TiO_2 (100) single crystal at different ultraviolet (UVC) back illumination levels 24

LIST OF FIGURES

Page

Figure 1.1 High-energy UVC irradiation transmission measurements on TiO_2 samples 20

Figure 1.2 Measurement of charge carrier dynamics on a 500 μm-thick TiO_2 single crystal 22

Figure 1.3 Measurement of charge carrier dynamics on a 46nm-thick polycrystalline TiO_2 film 25

Figure 1.4 Schematic explanation of UVC transmission measurements 28

Figure 1.5 Schematic explanation of the time-resolved AFM setup and charge carrier dynamics 30

Figure 2.1 Schematic representation of conventional and submicrosecond TR-AFM measurements 36

Figure 2.2 TR-AFM measurements of the characteristic time constant τ^* on TiO_2 .. 41

Figure 2.3 Effective activation barrier for electron–hole pair migration in TiO_2 43

Figure 2.4 Evolution of charge migration dynamics under repeated electrical pulses 45

Figure 2.5 Spatial extent of history-dependent charge carrier migration on TiO_2 46

Figure 3.1 Schematic of simultaneous topography and KPFM measurements under UV irradiation 52

Figure 3.2 Time-dependent CPD response of TiO_2 under front- and back-side UVC irradiation 54

Figure 3.3 Time-dependent CPD response under varying UVC illumination geometries 56

Figure 3.4 Effect of back-side UVC irradiation density on the CPD of TiO_2 57

Figure 3.5 Effect of gold nanoparticle decoration on the CPD dynamics of TiO_2 ... 59

LIST OF SYMBOLS AND UNITS OF MEASUREMENTS

AFM	Atomic Force Microscopy
AM-AFM	Amplitude Modulation Atomic Force Microscopy
CB	Conduction Band
CPD	Contact Potential Difference
FFT	Fast Fourier Transform
FM-AFM	Frequency Modulation Atomic Force Microscopy
FWHM	Full Width at Half Maximum
GXSM	Gnome-X Scanning Microscopy
KPFM	Kelvin Probe Force Microscopy
MO / MOS	Metal Oxide / Metal Oxide Semiconductor
NP	Nanoparticle
PCE	Photoelectrochemical
PI-SOV	Photoinduced Surface Oxygen Vacancy
PID	Proportional–Integral–Derivative
PL	Photoluminescence
PLL	Phase-Locked Loop
SPM	Scanning Probe Microscopy
STM	Scanning Tunneling Microscopy
TR-AFM	Time-Resolved Atomic Force Microscopy

UV	Ultraviolet
UVA / UVC	Ultraviolet-A / Ultraviolet-C
VB	Valence Band
XPS	X-ray Photoelectron Spectroscopy
XRD	X-ray Diffraction
C	Tip–sample capacitance
E_{bg}	Bandgap energy
F_{el}	Electrostatic force between tip and sample
f_0	Natural resonance frequency of the cantilever
Δf	Resonance frequency shift
k	Cantilever spring constant
k_{ts}	Tip–sample force gradient
t	Time
V	Potential difference between tip and sample
z	Tip–sample separation distance
β	Stretching exponent (collective motion parameter)
λ	Wavelength of incident light
τ	Characteristic time constant
τ^*	Effective time constant of charge carrier relaxation

V_o	Oxygen vacancy
V_o^0	Neutral oxygen vacancy
V_o^+	Singly charged oxygen vacancy
V_o^{2+}	Doubly charged oxygen vacancy

INTRODUCTION

Human progress has long been driven by the pursuit of improved quality of life through the development of new technologies. Central to this progress is the understanding and manipulation of materials, which has enabled the creation of increasingly sophisticated tools and devices. Historically, major technological eras—from the Bronze Age and Iron Age to the modern Silicon Age—have been defined by advances in material knowledge and the ability to control material properties with increasing precision.[1] As scientific understanding expanded, materials were no longer viewed merely as passive structural components, but as active functional elements whose electronic, mechanical, and chemical properties could be tailored for specific applications.[2]

For much of human history, direct observation using the naked eye and tactile interaction were the primary means of gathering information about materials. While these approaches were sufficient for macroscopic systems, they imposed severe limitations on the ability to probe phenomena occurring at smaller length scales. The development of optical microscopy marked a significant milestone by extending observational capabilities beyond natural human perception. Nevertheless, optical techniques are fundamentally constrained by diffraction limits, restricting access to processes that occur at nanometer and sub-nanometer scales.[3] As modern technologies increasingly rely on nanoscale functionality, these limitations have become more pronounced.

In contemporary scientific and engineering fields—including nanoelectronics, renewable energy, photocatalysis, and sensing—the performance of materials is often governed by processes occurring at surfaces, interfaces, and defects.[4] At these scales, properties such as charge carrier transport, defect formation, and local energetic variations play a dominant role in determining device efficiency, stability, and lifetime. Importantly, many of these processes are not only spatially heterogeneous but also time dependent, evolving over a wide range of timescales from microseconds to seconds. As a result, characterization techniques that provide spatially averaged

or time-averaged information are often insufficient to capture the mechanisms that ultimately control macroscopic behavior.[5]

Scanning probe microscopy (SPM) techniques have emerged as powerful tools for addressing these challenges by enabling direct, local probing of material properties at the nanometer scale.[6;7] Among these techniques, atomic force microscopy (AFM) is particularly versatile due to its ability to operate on a wide range of materials, including insulating and semiconducting systems, and under diverse environmental conditions.[8;9] Unlike electron-based microscopies,[10] AFM relies on mechanical interactions between a sharp probe and the sample surface, allowing access to topographical, mechanical, and functional properties with high spatial resolution.[11;12]

Beyond conventional imaging, AFM has evolved into a multifunctional platform capable of probing local electrical, electrostatic, and dynamic processes.[7;13] Electrostatic AFM modalities, such as Kelvin probe force microscopy (KPFM), provide access to local surface potential and work function variations, offering insight into electronic structure and energetic landscapes at the nanoscale.[14;15] These capabilities are particularly valuable for studying semiconductors and metal oxides, where local changes in defect density, charge trapping, or surface chemistry can induce measurable shifts in electronic energetics.[16;17]

Despite these advances, significant challenges remain in understanding how nanoscale electronic and defect-related processes evolve in time and space. Many AFM-based measurements focus on steady-state behavior, while dynamic processes—such as charge carrier migration, defect formation and recovery, and history-dependent electrostatic effects—remain less explored.[18;19] Moreover, external stimuli such as illumination, temperature, and electrical excitation can strongly influence these dynamics, often in ways that depend on both spatial location and prior excitation history.[20] Capturing such coupled spatiotemporal behavior requires measurement approaches that combine nanometer-scale spatial resolution with high temporal sensitivity.[21;22]

Time-resolved atomic force microscopy has emerged as a promising strategy to bridge this gap.[23] By monitoring the time-dependent response of the cantilever following controlled electrical or optical excitation, time-resolved AFM enables direct access to charge carrier dynamics over timescales ranging from microseconds to seconds.[24;25] When combined with electrostatic detection schemes, this approach provides a powerful framework for investigating how local electronic processes evolve under operando-like conditions.[26] Importantly, time-resolved AFM allows simultaneous interrogation of fast electronic responses and slower, defect-mediated processes, offering a more complete picture of nanoscale material behavior.[27;28]

This thesis focuses on the development and application of time-resolved AFM and electrostatic AFM techniques to investigate charge carrier dynamics and defect-mediated processes in metal oxide systems, with a particular emphasis on titanium dioxide (TiO_2).[29;30] By leveraging controlled illumination, temperature variation, and electrical excitation, this work aims to elucidate how local defect landscapes and excitation history govern nanoscale electronic behavior.[20;31] Through these investigations, the thesis seeks to advance the understanding of dynamic processes that underpin the functionality of oxide-based materials and devices, and to demonstrate the unique capabilities of time-resolved AFM as a tool for nanoscale characterization.[32;33]

0.1 Metal Oxides and TiO_2 as a Model System for Nanoscale Charge Dynamics

Metal oxides constitute a broad and technologically important class of materials whose functional properties arise from the interplay between electronic structure, ionic defects, and surface chemistry.[17;34] Owing to their chemical stability, tunable band structure, and compatibility with diverse operating environments, metal oxides are widely employed in applications ranging from photocatalysis and photoelectrochemical energy conversion to sensing, memristive electronics, and protective coatings.[35;36] In many of these systems, device performance is governed not by

the bulk crystal alone, but by processes occurring at surfaces, interfaces, and near-surface defect states.[16;37]

A defining characteristic of metal oxides is their sensitivity to point defects, particularly oxygen vacancies.[38;39] Oxygen vacancies act as intrinsic donors in many oxide semiconductors and can strongly modify electronic properties by introducing localized states within the bandgap, altering band bending, and influencing charge carrier trapping and recombination.[40;41] Even small variations in vacancy concentration can produce substantial changes in conductivity, surface reactivity, and charge transport pathways.[42] As a result, oxygen vacancies play a dual role: they can enhance functionality by promoting charge separation or catalytic activity, while simultaneously acting as recombination centers that degrade performance if uncontrolled.[43;44]

Titanium dioxide (TiO_2) has emerged as a canonical model system for studying defect-mediated phenomena in metal oxides.[16;29] As a wide-bandgap semiconductor, TiO_2 is transparent to visible light while strongly absorbing ultraviolet radiation, making it a cornerstone material in photocatalysis, photovoltaics, and optoelectronic devices.[30;45] Beyond its technological relevance, TiO_2 offers well-defined crystal structures, relatively simple chemistry, and reproducible surface terminations, which together enable systematic investigation of defect formation and charge transport mechanisms.[46;47]

The electronic behavior of TiO_2 is highly sensitive to oxygen stoichiometry.[48] Oxygen vacancies can donate electrons to the conduction band or form localized trap states that influence carrier lifetime and mobility.[49;50] These defects affect not only steady-state electronic properties, such as conductivity and work function, but also the dynamic response of the material under external stimuli.[51] In photoactive environments, ultraviolet illumination can induce the formation of photoinduced surface oxygen vacancies, which persist beyond the illumination period and modify surface energetics over extended timescales.[31;52] Such photoinduced defects can lower migration

barriers for charge carriers, reshape local band alignment, and introduce history-dependent behavior that is invisible to equilibrium measurements.[20;26]

Importantly, the influence of oxygen vacancies in TiO_2 is not spatially uniform.[27] Even in single-crystal samples, local variations in defect density, coordination environment, and surface chemistry can lead to pronounced heterogeneity in charge carrier dynamics.[25;28] These variations are further amplified under external perturbations such as illumination, temperature changes, and applied electric fields.[19;20] Consequently, macroscopic measurements that average over large areas or long timescales often fail to capture the localized processes that ultimately govern material performance.[21;23]

In addition to defect concentration, the energetic landscape of TiO_2 is strongly affected by the Fermi level and its evolution under nonequilibrium conditions.[53;54] The Fermi level determines charge distribution, band bending, and interfacial energetics, thereby controlling charge transfer across interfaces and the driving force for redox reactions.[55;56] Under illumination or electrical excitation, the Fermi level can shift dynamically due to changes in carrier population and defect states.[57;58] These shifts are particularly relevant at surfaces and interfaces, where even millivolt-scale variations can significantly alter reaction kinetics and transport behavior.[54;59] Understanding how the Fermi level evolves locally and in time is therefore essential for rational design of oxide-based devices.[60]

Despite extensive study, many fundamental questions regarding charge carrier dynamics and defect-mediated processes in TiO_2 remain unresolved.[29;30] Conventional spectroscopic and electrical techniques typically provide spatially averaged information or probe bulk properties, limiting their ability to resolve local variations in dynamics.[21;25] Time-resolved optical methods offer high temporal resolution but often lack the spatial specificity required to distinguish nanoscale heterogeneity.[61;62] Conversely, scanning probe techniques provide exceptional spatial resolution but have historically focused on static or quasi-equilibrium measurements.[8;11]

These limitations motivate the use of advanced atomic force microscopy–based approaches to probe TiO_2 at the relevant spatial and temporal scales[23;63]. By combining nanoscale resolution with sensitivity to local electrostatic forces, AFM-based techniques enable direct interrogation of charge carrier behavior, defect dynamics, and energetic variations under controlled external stimuli.[64;65] When augmented with time-resolved measurement schemes, AFM becomes uniquely capable of capturing both fast electronic responses and slower, defect-mediated processes within the same experimental framework.[18;20]

In this thesis, TiO_2 serves as a model system through which the capabilities of time-resolved and electrostatic AFM techniques are explored and demonstrated.[26;28] By leveraging controlled ultraviolet illumination, temperature variation, and electrical excitation, this work aims to elucidate how oxygen vacancies and excitation history govern charge carrier migration, energetic relaxation, and electrostatic memory effects at the nanoscale.[20;31] Insights gained from this model system are broadly applicable to a wide range of oxide materials and devices, providing general principles for defect engineering and nanoscale characterization in functional metal oxides.[17;35]

0.2 Fundamentals of Atomic Force Microscopy

Atomic force microscopy (AFM) is a scanning probe technique that enables surface characterization with nanometer and sub-nanometer spatial resolution by exploiting the interaction forces between a sharp probe and a sample surface[6;7] Unlike electron-based microscopies[10], AFM does not rely on charged particle beams and therefore can operate on conductive, semiconductive, and insulating materials alike. This versatility, combined with its ability to function under ambient, vacuum, or controlled environmental conditions, has made AFM an indispensable tool for nanoscale science and engineering.[8;9]

At the core of AFM is a microfabricated cantilever equipped with a sharp tip, typically with a radius of curvature on the order of tens of nanometers or less.[8] As the cantilever approaches the sample surface, a variety of tip–sample interaction forces arise, including van der Waals forces, electrostatic forces, capillary forces, and short-range repulsive interactions.[11;12] These forces cause measurable deflections or changes in the oscillatory behavior of the cantilever, which are detected using an optical beam deflection system or, in some configurations, piezoresistive or interferometric detection schemes.[7]

AFM can be operated in several modes depending on how the cantilever interacts with the surface. In contact mode, the tip remains in continuous contact with the sample, and surface topography is obtained by monitoring the static deflection of the cantilever.[8] While this mode offers straightforward interpretation, it can induce significant lateral forces that may damage soft samples or alter surface chemistry.[7] To mitigate these effects, dynamic modes were developed in which the cantilever oscillates near its resonance frequency and interacts intermittently with the surface.[11]

In tapping mode and non-contact mode, the cantilever oscillates with a finite amplitude, and surface information is extracted from changes in oscillation amplitude, phase, or frequency.[66;67] These dynamic modes significantly reduce shear forces and allow sensitive detection of weak long-range interactions.[11] Among them, frequency modulation AFM (FM-AFM) is particularly well suited for high-resolution measurements, as it detects changes in the cantilever's resonance frequency arising from tip–sample force gradients rather than forces themselves.[68]

For a cantilever oscillating near its fundamental resonance frequency f_0, the interaction with the sample modifies the effective force gradient k_{ts}, leading to a resonance frequency shift Δf. In the small-amplitude limit, this shift can be approximated as:

$$\Delta f \approx \frac{f_0}{2k}\langle k_{ts}\rangle \tag{1}$$

where k is the cantilever spring constant and the brackets denote averaging over one oscillation cycle.[68;69] This relationship highlights the sensitivity of AFM to local force gradients, enabling detection of subtle variations in mechanical, chemical, and electrostatic properties at the nanoscale.

A key advantage of AFM lies in its ability to decouple topographical information from functional contrasts by selectively enhancing sensitivity to specific interaction forces.[70] By controlling the excitation frequency, oscillation amplitude, and applied bias voltage, AFM can be configured to probe mechanical stiffness, adhesion, magnetic interactions, or electrostatic forces.[71;72] This flexibility has led to the development of numerous AFM-based modalities tailored to specific physical phenomena.

Of particular relevance to this thesis are electrostatic interactions, which arise from capacitive coupling between the conductive AFM tip and the sample surface.[73] These forces are long-ranged and depend on local charge distribution, surface potential, and dielectric properties.[15;74] Electrostatic forces can be deliberately enhanced by applying a bias voltage between the tip and sample, enabling the detection of local electrical properties even in insulating or weakly conducting materials.[75] Because electrostatic forces act over tens to hundreds of nanometers, they are especially sensitive to subsurface charges and defect-mediated processes.[25;76]

Beyond static or quasi-static measurements, AFM is inherently suited to dynamic investigations.[23] By monitoring the cantilever response as a function of time following a controlled perturbation—such as an electrical bias pulse or optical excitation—it becomes possible to access time-dependent material behavior.[21;22] The temporal resolution of AFM-based measurements spans a wide range, from milliseconds to microseconds, depending on the detection scheme and signal

processing methods employed.[18;24] This capability distinguishes AFM from many other nanoscale characterization techniques, which often trade temporal resolution for spatial specificity or vice versa.[23]

Importantly, AFM measurements are inherently local.[7] Each data point reflects the response of a nanometer-scale interaction volume defined by the tip geometry, lift height, and force range.[8;74] This locality enables direct interrogation of spatial heterogeneity arising from defects, interfaces, or compositional variations, even in nominally uniform single-crystal materials.[19] As a result, AFM is uniquely positioned to reveal how nanoscale variations influence macroscopic behavior[11].

In the context of functional materials such as metal oxides, these attributes are particularly valuable[17]. Charge carrier migration, defect formation, and energetic relaxation often occur over length scales comparable to or smaller than the AFM probing volume, and over timescales accessible by dynamic AFM measurements[26;31]. Consequently, AFM provides a natural platform for studying coupled spatiotemporal phenomena that are difficult to resolve using conventional electrical or spectroscopic techniques.[21;25]

The following section builds upon these fundamentals by introducing electrostatic AFM modalities and time-resolved AFM approaches that extend conventional AFM into the temporal domain.[23;63] These methods form the experimental foundation of this thesis and enable direct investigation of charge carrier dynamics, defect-mediated processes, and history-dependent electrostatic effects in metal oxide systems.[20;28]

0.3 Electrostatic and Time-Resolved Atomic Force Microscopy Techniques

While conventional AFM provides high-resolution topographical information, many functional properties of materials—particularly in semiconductors and metal oxides—are governed by electrical and electrostatic phenomena that are not directly accessible through purely mechanical

interactions.[72] To address this limitation, a family of electrostatic AFM techniques has been developed to probe local charge distribution, surface potential, and electronic energetics[63] When combined with time-resolved measurement schemes, these approaches enable direct investigation of dynamic electronic processes at the nanoscale.[21;23]

0.3.1 Electrostatic Interactions in AFM

Electrostatic forces between an AFM tip and a sample arise from capacitive coupling and depend on the local electrostatic potential, charge distribution, and dielectric environment.[73;74] For a conductive tip positioned above a sample surface, the electrostatic force F_{el} can be expressed as:

$$F_{el} = \frac{1}{2}\frac{\partial C}{\partial z}V^2 \tag{2}$$

where C is the tip–sample capacitance, z is the tip–sample separation, and V is the potential difference between the tip and the sample.[69;73] This quadratic dependence allows electrostatic forces to be selectively enhanced or suppressed by applying controlled bias voltages.[15]

Electrostatic forces are inherently long-ranged compared to short-range mechanical interactions and therefore probe a larger interaction volume that can include subsurface regions.[74;76] As a result, electrostatic AFM techniques are particularly sensitive to buried charges, defect states, and near-surface carrier redistribution—features that are critical in oxide semiconductors and photoactive materials.[25;31]

0.3.2 Kelvin Probe Force Microscopy and Local Energetics

Kelvin probe force microscopy (KPFM) is a widely used electrostatic AFM modality that enables measurement of the local contact potential difference (CPD) between the AFM tip and the sample surface.[14] The CPD reflects the difference in work function between the tip and the

local sample region and is directly related to the local electrostatic potential and Fermi-level position.[54;77]

In KPFM, an alternating voltage is superimposed on a constant bias applied between the tip and the sample. This modulation generates an oscillating electrostatic force component that is detected by the cantilever. By adjusting the applied DC bias to nullify the oscillating force, the CPD can be extracted.[15] Depending on the implementation, KPFM can be operated in amplitude-modulated or frequency-modulated configurations, each offering distinct trade-offs between spatial resolution, sensitivity, and quantitative accuracy.[63;76]

For semiconductor and oxide materials, CPD variations can arise from changes in band bending, charge carrier density, defect states, or surface adsorbates.[16;65] Importantly, CPD is not a purely static quantity; it can evolve dynamically under external perturbations such as illumination, temperature variation, or electrical excitation.[64] Consequently, time-dependent KPFM measurements provide access to the evolution of local energetics and Fermi-level shifts under nonequilibrium conditions.[55] These capabilities make KPFM particularly well suited for investigating defect-mediated electronic processes in photoactive oxides.[20;28]

0.3.3 Time-Resolved AFM for Slow Charge Carrier Dynamics

Although KPFM provides valuable energetic information, it does not directly reveal the kinetics of charge carrier migration or relaxation. Time-resolved atomic force microscopy (TR-AFM) addresses this limitation by monitoring the cantilever response as a function of time following a controlled perturbation, such as an applied bias pulse.[23]

In conventional TR-AFM, the AFM tip is positioned at a fixed height above the sample surface, and a step-like bias voltage is applied between the tip and the sample. This bias induces redistribution of charge carriers within the material, which in turn modifies the electrostatic force acting on the cantilever.[25] The resulting change in the cantilever's resonance frequency,

Δf, is recorded as a function of time. The temporal evolution of Δf reflects the underlying charge carrier dynamics within the probed volume.[78]

The relaxation behavior observed in TR-AFM measurements is often well described by a stretched exponential function:

$$\Delta f(t) = \Delta f_0 \exp\left[-\left(\frac{t}{\tau}\right)^{\beta}\right] \tag{3}$$

where τ is a characteristic time constant and β is the stretching factor.[79;80] The parameter τ provides a measure of the timescale over which charge redistribution occurs, while β reflects the degree of collective or correlated motion among charge carriers.[81] Values of $\beta < 1$ are indicative of non-single-exponential behavior, often associated with cooperative processes or heterogeneous energy landscapes.[82]

By performing TR-AFM measurements at different temperatures, activation energies associated with charge carrier migration can be extracted through Arrhenius analysis.[83;84] This approach enables direct quantification of effective migration barriers for charge carriers and provides insight into the role of defects and thermal activation in governing transport dynamics.[19] Importantly, because TR-AFM measurements are inherently local, they can reveal spatial variations in dynamics that are obscured in macroscopic measurements.[20;28]

0.3.4 Sub-Microsecond Time-Resolved AFM for Fast Dynamics

While conventional TR-AFM is well suited for probing slow processes occurring over seconds, many electronic phenomena—such as electron redistribution and fast polarization responses—occur on much shorter timescales.[21;22] To access these fast dynamics, sub-microsecond time-resolved AFM techniques have been developed.[13;18]

In sub-microsecond TR-AFM, the real-time cantilever deflection signal is recorded with high temporal resolution following a rapid electrical excitation.[22] Rather than relying on phase-locked loop demodulation, the raw oscillation signal is numerically processed to extract the instantaneous phase of the cantilever motion.[21] The time derivative of this phase yields the instantaneous resonance frequency shift, $\Delta f(t)$, with microsecond resolution.[22]

A key metric in this approach is the time to the first peak in $\Delta f(t)$, which serves as a relative indicator of fast charge carrier dynamics.[21] Although the absolute value of this timescale can be influenced by experimental parameters such as cantilever properties and signal processing filters, relative changes under different conditions—such as temperature or illumination—provide meaningful insight into fast electronic processes[20]. This technique enables separation of fast electronic responses from slower, defect-mediated dynamics, offering a more complete picture of charge transport behavior.[26]

0.3.5 Advantages of Combining Electrostatic and Time-Resolved AFM

The combination of electrostatic AFM, KPFM, and time-resolved AFM provides a powerful and complementary toolkit for investigating functional materials.[23] KPFM offers access to local energetic landscapes and Fermi-level evolution,[55] while TR-AFM probes the kinetics of charge carrier redistribution across multiple timescales.[78] Together, these methods enable correlation between energetic shifts and transport dynamics at the nanoscale.[64]

Crucially, these techniques allow systematic investigation of how external stimuli—such as illumination wavelength, irradiation geometry, temperature, and excitation history—modulate both the energetics and dynamics of charge carriers.[20;28] This integrated approach is particularly valuable for studying metal oxides, where defect formation, charge trapping, and carrier migration are strongly coupled and evolve under nonequilibrium conditions.[17;31]

In this thesis, these advanced AFM-based techniques are employed to investigate charge carrier dynamics and defect-mediated processes in TiO_2.[26] By combining slow and fast time-resolved measurements with electrostatic probing, this work aims to uncover how local defect landscapes, illumination conditions, and prior excitation history shape nanoscale electronic behavior.[20;31] The following sections build upon this methodological foundation to present the specific research questions, experimental findings, and contributions of the thesis.

0.4 Research Objectives, Key Questions, and Thesis Contributions

Despite significant advances in atomic force microscopy and electrostatic scanning probe techniques, a comprehensive understanding of nanoscale charge carrier dynamics in metal oxides remains incomplete. In particular, existing approaches often emphasize either spatial resolution or temporal resolution, but rarely achieve both simultaneously across multiple timescales. Furthermore, many studies focus on steady-state or quasi-equilibrium behavior, while dynamic processes—such as defect-mediated charge migration, photoinduced energetic relaxation, and history-dependent electrostatic effects—are less well understood. These limitations are especially pronounced in photoactive oxides, where illumination, temperature, and prior excitation can strongly influence electronic behavior in ways that are both spatially heterogeneous and time dependent.

The overarching objective of this thesis is to develop and apply time-resolved and electrostatic AFM-based methodologies to directly probe charge carrier dynamics and defect-mediated processes in metal oxide materials at the nanoscale. By combining high spatial resolution with sensitivity to temporal evolution, this work seeks to bridge the gap between static nanoscale characterization and dynamic electronic behavior under nonequilibrium conditions. Titanium dioxide (TiO_2) is employed as a model system to systematically investigate how oxygen vacancies, illumination conditions, and excitation history govern charge carrier migration and local energetic landscapes.

More specifically, this thesis addresses the following key scientific questions:

1. **How do charge carrier dynamics vary spatially across nominally uniform oxide surfaces?**

   Even in well-prepared single-crystal materials, local variations in defect density and surface chemistry can lead to heterogeneous electronic behavior. This thesis seeks to quantify such spatial heterogeneity by mapping characteristic charge carrier timescales at the nanoscale using time-resolved AFM.

2. **What role do oxygen vacancies play in mediating charge carrier migration and relaxation dynamics?**

   Oxygen vacancies are known to modify electronic structure and transport properties, yet their influence on time-dependent charge dynamics remains difficult to quantify locally. This work investigates how intrinsic and photoinduced oxygen vacancies alter migration barriers, relaxation times, and cooperative transport behavior.

3. **How do external stimuli such as illumination wavelength, irradiation geometry, and temperature influence nanoscale dynamics?**

   Illumination can induce both transient charge carrier excitation and persistent defect formation, depending on photon energy and exposure conditions. By systematically varying illumination parameters and temperature, this thesis explores how these stimuli modulate both fast electronic responses and slower defect-mediated processes.

4. **To what extent does excitation history influence nanoscale electrostatic behavior?**

   Many functional materials exhibit memory effects, where prior electrical or optical excitation affects subsequent response. This thesis examines history-dependent charge dynamics and electrostatic relaxation, including the spatial extent over which such memory effects persist.

To address these questions, the thesis is structured around three interrelated studies, each contributing a distinct but complementary perspective on nanoscale charge dynamics:

Structure of the Thesis

This thesis follows a paper-based format and consists of research articles that have been published or are under review in peer-reviewed journals.

Chapter 2 is based on the article entitled *Ultraviolet Irradiation Penetration Depth on TiO_2*, published in *Communications Chemistry*, 8, 83 (2025).

Chapter 3 is based on the article entitled *Time-Resolved Mapping of Charge Carrier Dynamics and Defect-Mediated Migration Barriers in TiO_2*, published in *Journal of Physical Chemistry C*, 129, 16879–16886 (2025).

Chapter 4 is based on the manuscript entitled *Defect- and Geometry-Controlled Fermi-Level Dynamics in TiO_2*, currently under review in *Advanced Materials*.

Minor modifications have been made to formatting and figure numbering to ensure consistency within the thesis structure.

CHAPTER 1

ULTRAVIOLET IRRADIATION PENETRATION DEPTH ON TIO_2

Bugrahan Guner[1,4] , Mohammad Safikhani-Mahmoudi[1,4] , Fengmiao Li[2,3] , Ke Zou[2,3] , Omur E. Dagdeviren[1]

[1]Department of Mechanical Engineering, École de technologie supérieure,
1100 Notre-Dame Ouest, Montréal, Québec, Canada H3C 1K3
[2]Department of Physics and Astronomy, University of British Columbia,
6224 Agricultural Road, Vancouver, BC, Canada V6T 1Z1
[3]Quantum Matter Institute, University of British Columbia,
6224 Agricultural Road, Vancouver, BC, Canada V6T 1Z1
[4]These authors contributed equally.

Article published in *Communications Chemistry*, 8, 83 (2025).
DOI: https://doi.org/10.1038/s42004-025-01487-1

1.1 Abstract

High-energy ultraviolet (UVC) irradiation of metal oxides (MOs, e.g., TiO_2) results in photoinduced surface oxygen vacancies (PI-SOVs), which can change the charge carrier (e.g., electrons and holes) migration dynamics. Although PI-SOVs alter the electronic and chemical properties of MOs, there is no consensus on the penetration depth of the UVC irradiation, which induces PI-SOVs and is an important variable for the design and operation of MO-based systems. Here, we performed optical transmission and time-resolved atomic force microscopy (TR-AFM) measurements on back-illuminated TiO_2 samples. Our experiments show that the effect of UVC irradiation on MOs can be observed hundreds of micrometers across the bulk, i.e., orders of magnitude larger than previously postulated values. We believe that our findings would be important both for the fundamental understanding of UVC irradiation/penetration and for device design/fabrication processes.

1.2 Introduction

Metal oxides (MOs), e.g., TiO_2, are widely used for solar energy, battery, sensor, and biomedical applications.[16;85–90] The ability to tune their properties (e.g., electrical, chemical)

without altering desired characteristics and their relatively low cost are major reasons for their widespread.[35;52;91;92] To this end, it is known that the ultraviolet (UV) irradiation of MOs plays an important role in many applications.[34;38;93] More specifically, high-energy UV (a.k.a., UVC) irradiation can change surface stoichiometry and chemistry by introducing photoinduced surface oxygen vacancies (PI-SOVs) and through resulting chemical reactions (e.g., formaldehyde formation of methanol on Ti_{5c} sites).[28;31;52;94;95]

TiO_2, a wide bandgap semiconductor ($E_{bg} >\sim 3$ eV), absorbs light ($\lambda <\sim 400$ nm).[35;43;96] However, PI-SOVs are sensitive to irradiation wavelength and are induced only by UVC irradiation ($\lambda < 280$ nm).[31;52;94;97] Although the existence of PI-SOVs is well-supported, there is no agreement on the penetration depth of the UVC.[30;98–101] Being the nucleus of a decades-old interest, the claims of the penetration depth of UVC range between 10-30 nm up to the micrometer level.[30;98–104] The uncertainty of the UVC penetration depth not only hinders the complete understanding of UVC-sample interaction but also impedes the longevity of sample systems where TiO_2 is used as an electron transfer and/or UV protection layer. Formerly, Raman spectroscopy and time-resolved atomic force microscopy (TR-AFM) were utilized to explore the effect of PI-SOVs.[26;28;31;52;94] In our previous works, we performed TR-AFM measurements to understand the influence of UVC irradiation and/or photocatalytic reactions on the charge carrier dynamics of TiO_2 and similar sample systems.[26;28;31]

Here, we measured the transmission and the effect of back illumination of UVC ($\lambda = 255$ nm) irradiation on a polycrystalline TiO_2 film and a single-crystal TiO_2 sample. Our measurements show two major findings, which are important for the basic understanding of UVC-MO interaction and potentially, for MO-based device design. First, even though the majority of incident UVC is absorbed within the first few tens of nanometers, the UVC irradiation has a measurable transmission even through 500 μm-thick samples. Moreover, as expected, the measured transmission is inversely proportional to the TiO_2 thickness and the illumination density. Second, the effect of back illumination of UVC has a dominant influence on the charge carrier dynamics, which has been quantified via TR-AFM measurements as a function of UVC illumination density for the single crystal TiO_2 sample. We believe that the observed variation of charge carrier

dynamics and its dependence on back illumination power density originates from the PI-SOVs and their collective motion. Our results reveal that the effect of UVC irradiation on MOs can extend through hundreds of micrometers and alter carrier dynamics in TiO_2 across the bulk. We believe our results are important for a fundamental understanding of the interaction of UVC with MOs and for the design of sample systems utilizing MOs in which TiO_2 is employed either as an electron transfer or UV protection layer.

1.3 Results and Discussion

We performed measurements to reveal the penetration depth of UVC irradiation and its effect on charge carrier dynamics. First, we performed optical transmission measurements via back illumination (vide infra) on a fused silica glass substrate, polycrystalline TiO_2 film, and 500 μm-thick, undoped TiO_2 (100) single crystal. The optical transmission measurements of fused silica reveal ~90% of UVC transmission, as classified by the manufacturer.

Figure 1.1 summarizes that the optical transmission is inversely proportional to the luminance of the UVC source, i.e., with increasing illuminance, the UVC transmission of both polycrystalline TiO_2 film, and 500 μm-thick, undoped TiO_2 (100) single crystal decreases asymptotically. We believe that this inverse relation with illuminance is associated with the PI-SOV density. It is well-known that UVC irradiation results in oxygen vacancies on the surface (vide supra).[31;52;94;97] With increasing PI-SOV and electron/hole concentration, mid-gap states are introduced, and as our experiments show, the absorption of UVC irradiation increases.[105–107] Normally, defect engineering is performed in TiO_2 to enhance the optical absorption in the visible spectrum for enhanced photocatalytic performance.[51;108–111] However, our measurements demonstrate that the optical absorption of TiO_2 increases (i.e., optical transmission decreases) even for UVC irradiation. We also experimentally measured the relation between the film thickness and the optical transmission. Although the 46 nm-thick TiO_2 film absorbs almost 99% of UVC irradiation, the 500 μm-thick TiO_2 (100) single crystal has a measurable UVC transmission across the sample (0.6 – 1% depending on the illuminance). For this reason, our optical transmission measurements show that even though a major part of UVC irradiation (~ 99%) is

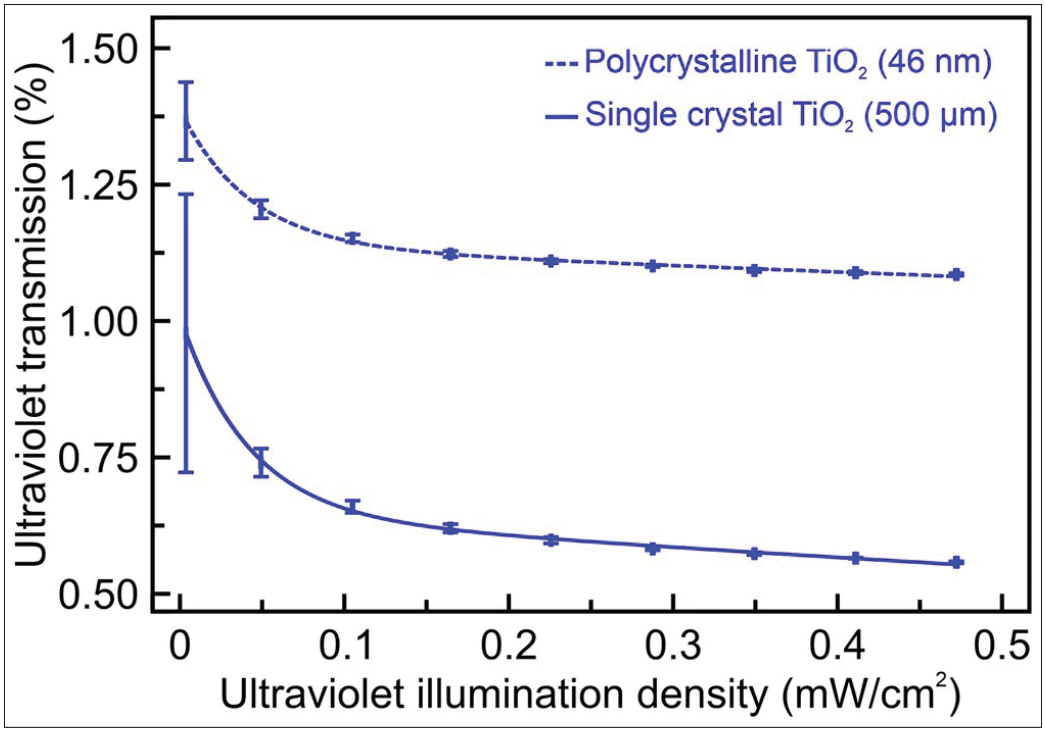

Figure 1.1 High-energy ultraviolet (a.k.a., UVC) irradiation (λ = 255 nm) transmission measurements on a 46 nm-thick polycrystalline TiO_2 film and a 500 μm-thick TiO_2 (100) single crystal as a function of UVC illumination density

Our measurements on 46 nm-thick TiO_2 polycrystalline film show that ~99% of UVC irradiation was absorbed within the first tens of nanometers. However, the optical transmission measurements of the 500 μm-thick TiO_2 (100) single crystal show that the rest of the UVC (~1%) can penetrate through the entire crystal for hundreds of micrometers. Our measurements for both 46nm-thick and 500 μm-thick samples display that with increasing UVC illumination power density, the optical transmission decreases, i.e., absorption increases. We believe that the enhanced absorption is associated with mid-gap states introduced by the photoinduced oxygen vacancies generated by UVC irradiation.

absorbed within the first tens of nanometers, the rest can penetrate through the entire crystal for hundreds of micrometers. Even though the optical transmission decreases with increasing illumination density monotonically, at very low illumination density levels, i.e., closer to zero, the error propagation is dominated by the operation principle of the UVC diode, as the power

consumption, so the illumination of the diode oscillates for voltages closer to the threshold voltage of the diode.

We also performed TR-AFM measurements on a TiO_2 single crystal and a 46 nm-thick polycrystalline film as a function of the back illumination density of UVC irradiation, as shown in Fig. 1.2. Surface oxygen vacancies in TiO_2 (V_o) can have multiple different charge states, where they can be neutral (i.e., V_o^0) or charged (e.g., V_o^+ and V_o^{2+}).[50;112] Former theoretical work showed that the V_o^+ state is the thermodynamically most favorable state and has the greatest influence on the TiO_2 sample conductivity.[31;50;112] Thus, we expect to mainly induce the V_o^+ vacancies and measure their effect on the charge carrier migration dynamics.[95]

Our TR-AFM measurements on TiO_2 single crystal show that the time constant associated with charge carrier migration, τ^*, decreases with the existence of UVC illumination. The charge transfer of MOs is mainly governed by holes, electrons, and ions.[16;95;113] For TiO_2 samples, in addition to a supplemental ion influence, mainly, electrons and holes govern the sample conductivity.[16;29;30;48;62;95] Based on the timescale of the measurement (from hundreds of milliseconds to a few seconds), it is expected that we are measuring the migration of slow charge carriers in the sample, i.e., holes as part of small polarons.[26;38;49;95;114] More specifically, for a single point measurement, τ^* values decrease from 3.31 ± 0.87 seconds to 2.05 ± 0.19 seconds even for the lowest illuminance density of 0.03 mW/cm^2. In addition, with increasing UVC illuminance, however, τ^* decreases almost an order of magnitude compared to UVC off case, i.e., decreases to 0.36 ± 0.08 seconds from 3.31 ± 0.87 seconds for UVC illumination density of 0.47 mW/cm^2. It is known that the mobility and velocity of charge carriers are linearly correlated to the measured time constant. For this reason, the decrease in the τ^* implies a decrease in the mobility of charge carriers. Moreover, we observed a prominent decrease in β values with increasing UVC illuminance, i.e., β decrease from 0.66 ± 0.05 (no UVC illumination) to 0.31 ± 0.06 (UVC illumination density of 0.47 mW/cm^2). The decrease in β values implies that the charge carriers move more collectively with increasing PI-SOV density. Hence, we believe that the enhanced collective motion can be explained by the increased density of charge traps formed by PI-SOVs.[115–118] Nevertheless, as Fig. 1.1 shows, ~99% of incident UVC were observed

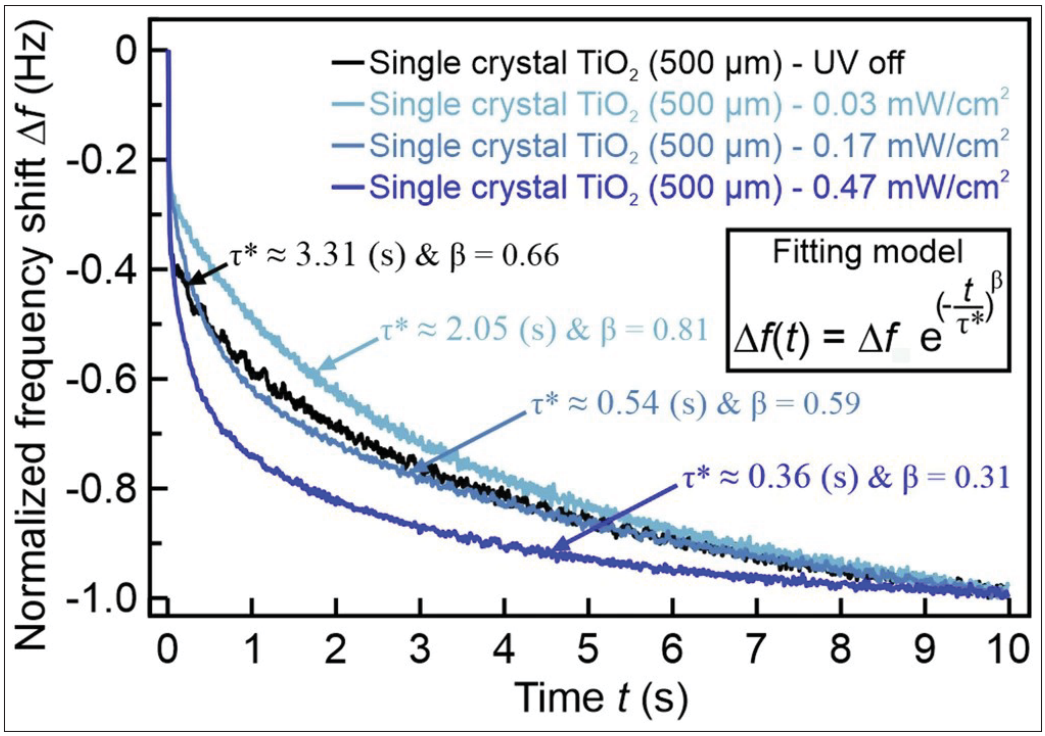

Figure 1.2 Measurement of charge carrier dynamics on a 500 μm-thick, undoped TiO_2 (100) single crystal, which was back illuminated using a high-energy ultraviolet (UVC, λ = 255 nm) source with different irradiation levels

Charge carrier dynamics were accessed by fitting a stretched exponential function to the resonance frequency shift, Δf, as a function of time, t: $\Delta f(t) = \Delta f_0 \exp[-(t/\tau^*)^\beta]$. The time constant, τ^*, is associated with the decay of the electrostatic interaction within the probing volume and is linked to the charge carrier migration. The stretching factor of the exponential fit, β, is related to the collective motion of charge carriers. We normalized the resonance frequency shifts to enable the comparison of decays for different back illumination levels. Data show that with increasing back illumination irradiation density, measured τ^* values decrease monotonically. The decrease of τ^* implies an attenuation of charge carrier migration velocity and mobility, which can be associated with enhanced vacancy concentration. The variation of β implies that charge carriers interact more collectively at high irradiation levels. Data presented in this figure were recorded on the same sample region, i.e., the only change between different data points is the UVC illumination densities.

within the first few tens of nanometers, i.e., only ~0.6% of the incident UVC reaches the front side of the 500 μm-thick sample. For this reason, it may be claimed that the transmitted UVC may be responsible for the observed variation of τ^* and β by introducing PI-SOVs on the front side. Even though the transmitted UVC, i.e., ~0.6% of the back illumination density (~2.4 μW/cm^2) may be capable of promoting PI-SOVs on the front side of the sample, the former study has shown that the variation of τ^* is linearly correlated with the illumination density and even for significantly higher front illumination densities, the variation of τ^* was significantly lower.[28] For this reason, in this study, the strong variation of τ^* (i.e., 10-fold variation) implies that the remaining UVC density is, potentially, not responsible for the observed change. Also, for the back-illuminated sample, the value of β, a parameter for collective motion, decreases by 50%. However, for front-illuminated samples, the variation of β is inert to UVC irradiation. Hence, driven by the concentration variations, we propose that PI-SOVs at the back side of the sample may migrate across the bulk. Nevertheless, back-surface-illuminated X-ray photoelectron spectroscopy measurements or atomic resolution scanning probe microscopy measurements under ambient conditions are required to directly quantify the diffusion of PI-SOVs. However, such measurements are beyond the scope of this work. To distinguish the contribution of PI-SOVs and holes as part of small polarons, we performed complementary back illumination measurements with a low-energy UV (UVA) irradiation (λ = 375 nm), which only introduces electrons and holes but not PI-SOVs.[31;52;94;97] Our optical transmission measurements for UVA show that, similar to the UVC case, UVA transmission decreases with increasing illumination density asymptotically. However, UVA measurements revealed that the τ^* decreases only 50% upon back illumination of the single crystal TiO_2 sample, and the corresponding β change is only 10%. To this end, the comparison of UVA and UVC measurements also implies that PI-SOVs dominate the dynamic properties of holes as part of small polarons.

We challenged the reproducibility of our TR-AFM results on a single-crystal TiO_2 sample by performing measurements over a span of two weeks under different UVC illumination levels, as Table 1 summarizes. To this end, we conducted successive measurements on ten different sample regions. We performed measurements at a minimum of 25 different points at each region

and repeated measurements 40 times at each point, i.e., a total of a thousand measurements for each region. Our repetitive experiments on different sample regions and/or under different illumination levels undoubtedly showed that the observed variation originates from high-energy UVC irradiation.

Table 1.1 Time-resolved atomic force microscopy measurements on a 500 μm-thick, undoped TiO_2 (100) single crystal at different ultraviolet (UVC) back illumination levels

High-energy Ultraviolet (UVC) Irradiation of Single Crystal TiO_2 (100) Sample	**Time Constant, τ^* (ms)**	**Stretching factor, β**
UVC OFF	3077.8 ± 751.4	0.68 ± 0.05
UVC ON - 0.03 mW/cm^2	2053.3 ± 193.7	0.81 ± 0.04
UVC ON - 0.17 mW/cm^2	626.6 ± 71.0	0.65 ± 0.06
UVC ON - 0.47 mW/cm^2	301.4 ± 81.9	0.35 ± 0.07

The data presented in above table were recorded at different regions across the sample in a mixed order on different days.[27] We performed 25 different point measurements with 40 repetitions for each experimental set.[27] Our measurements show that the effect of back illumination of UVC is reproducible across the sample.[27]

Our measurements on 46 nm-thick polycrystalline film show that the τ^* values are significantly smaller compared to the single crystal sample regardless of the UVC irradiation, as shown in Fig. 1.3. Former TR-AFM measurements on similar TiO_2 films also disclosed smaller time constants compared to single crystals.[31] We measured the average grain size of our polycrystalline film as 8.7 ± 4.0 nm. The significantly smaller time constants may be associated with the grain size, orientation, and the (degree of) polycrystallinity of the films.[42;47;119–123] The grain size and orientation may affect the formation of PI-SOVs and electron/hole pairs, altering the charge carrier migration dynamics.[47;121;122] However, the identification of the intrinsic contribution of such effects is beyond the scope of this work. Even though oxygen vacancy formation due to UVC irradiation is expected to be a surface phenomenon, as ~99% of incident UVC is absorbed within the first tens of nanometers, our TR-AFM measurements show that the effect of UVC irradiation can penetrate deep into the bulk and can alter electronic properties for hundreds of

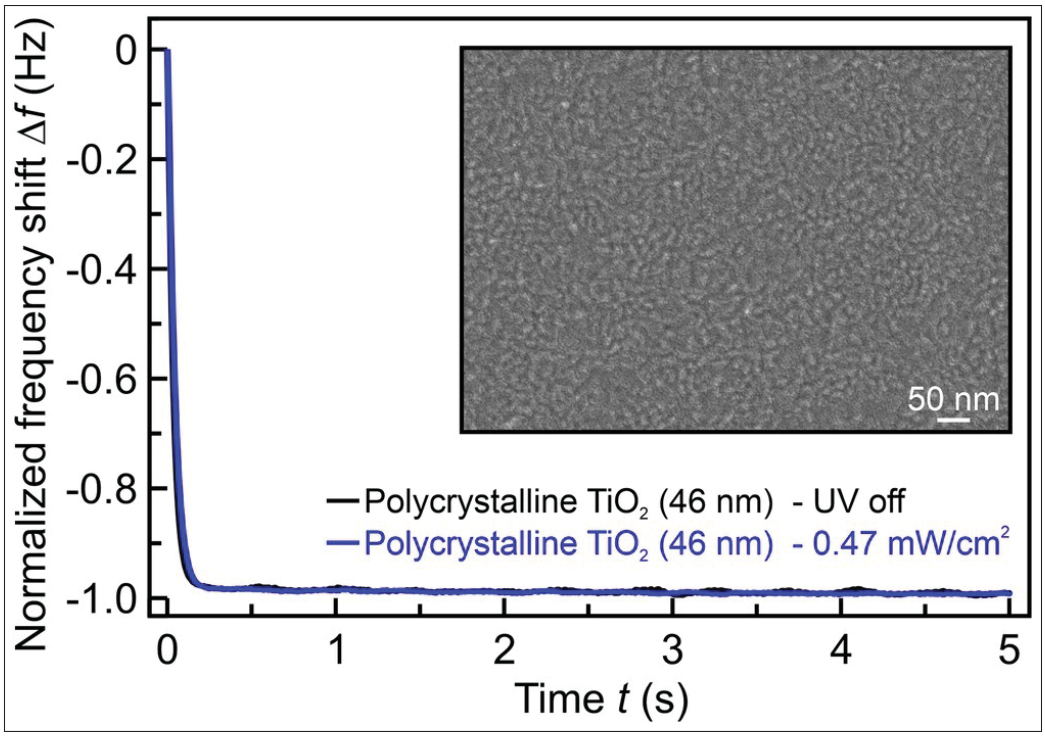

Figure 1.3 Measurement of charge carrier dynamics on a 46nm-thick polycrystalline TiO_2 film grown on a fused silica glass substrate, which was back illuminated with a high-energy ultraviolet (UVC, λ = 255 nm) source

Our measurements show that the time constant associated with the charge carrier migration is significantly smaller than the single crystal TiO_2, regardless of the existence of UVC irradiation. As the measured time constant is very close to the detection limit, we do not deliver a numerical value. As shown in the inset, we performed scanning electron microscopy measurements, which revealed that the average grain size has an equivalent circular diameter of 8.7 ± 4.0 nm. We believe that the smaller time constant is related to the grain size, orientation, and degree of polycrystallinity of the film (see main text for details).

micrometers across the sample. This result is important not only for the basic understanding of the variation of charge carrier dynamics due to PI-SOVs in MOs but also for sample systems that employ MOs as a charge transfer layer or protecting layer for underlying photocatalytic activities.

1.4 Conclusions

We performed optical transmission and TR-AFM measurements on back-illuminated (with high-energy ultraviolet (UVC) irradiation, λ = 255 nm) metal oxide (MO) samples, i.e., a 500 μm-thick, undoped TiO_2 (100) single crystal and a 46 nm-thick polycrystalline TiO_2 film grown on fused silica glass. Our optical transmission measurements show that even though ~99% of incident UVC was absorbed within the first tens of nanometers, the residual illuminance (i.e., ~1%) can penetrate through the bulk for hundreds of micrometers. Moreover, we revealed that the optical transmission is inversely correlated with the illumination density. We think that this inverse relation between the optical transmission and the illumination density arises from the enhanced concentration of mid-band gap states prompted by photoinduced surface oxygen vacancies. Our TR-AFM measurements show that the time constant associated with the charge carrier migration is strongly affected by the back illumination density and can decrease almost by an order of magnitude with increasing UVC irradiation density. Moreover, the collective nature of charge carrier migration is more pronounced with increasing irradiation density. Also, the charge carrier migration dynamics and its control are important for other oxides such as $SrTiO_3$ and $KTaO_3$.[124–126] It is important to note that atomic scale identification of oxide-based devices and correlating the measured dynamic characteristics at the interface of different material systems as a function of their intrinsic properties (e.g., bandgap, intrinsic and extrinsic doping, roughness), external stimulation (e.g., temperature variation, chemicals), and transient formation/recovery of PI-SOVs remain to be explored. For this reason, we believe our results will lay the foundation for a more fundamental understanding of UVC penetration and MO-based sample systems.

1.5 Experimental Methods and Sample Preparation

1.5.1 Preparation of polycrystalline TiO_2 films

46 nm-thick polycrystalline TiO_2 film was prepared on a fused silica glass substrate using molecular beam epitaxy (MBE).[127;128] The silica glass (by MTI Corporation, UV Grade Fused

Silica Glass) was cleaned at 500 °C in a 2.0×10^{-6} Torr O_2 atmosphere for 60 mins in the ultra-high vacuum chamber before the growth. The TiO_2 film was later prepared in the same MBE chamber. The substrate temperature was at 500 °C during the growth. The Ti flux of ~1.1 $\times 10^{13}$ atoms·cm^{-2}·s^{-1} (measured using quartz crystal microbalance) was employed. The O_2 partial pressure was 2.0×10^{-6} Torr during the growth. The film thickness was confirmed by fitting X-ray diffraction reflectivity measurements.

1.5.2 Preparation of TiO_2 (100) single crystal

We utilized a 500 μm-thick, undoped TiO_2 single crystal (by MSE Supplies LLC). We followed an established recipe, as detailed elsewhere.[19;26;28;31;129] Briefly, TiO_2 crystal was annealed at 1000 °C for 10 hours, in addition to heating and cooling periods (~3 hours each). This method creates rutile-terminated, atomically flat terraces that are free of carbon clusters (please see Section 1 of the Supplementary Information for further details).[31] Avoiding large clusters of contamination is important both for the stability of the TR-AFM measurements and to be able to extract intrinsic properties of MBE-grown thin films (vide supra) and single crystals.

We used a rutile-terminated surface, as the anatase termination is more susceptible to particles in the air under UVC irradiation and ambient conditions.[46;130–133] For this reason, adsorbed, undesired particles could impede the characterization of charge carrier dynamics and their variation with PI-SOVs.

Being a slightly more stable configuration compared to the (110) surface, in TiO_2 (110), Ti atoms can have either five or six coordination numbers, while the coordination number of the (100) surface is constant and five.[40;134;135] Our focus in this work is to understand the penetration depth of the UVC irradiation and its electronic effects across the sample, rather than revealing site-dependent variation of charge carrier dynamics. For these reasons, to eliminate any coordination number-dependent variation of time-resolved properties, we employed a TiO_2 (100) surface as our single crystal sample.

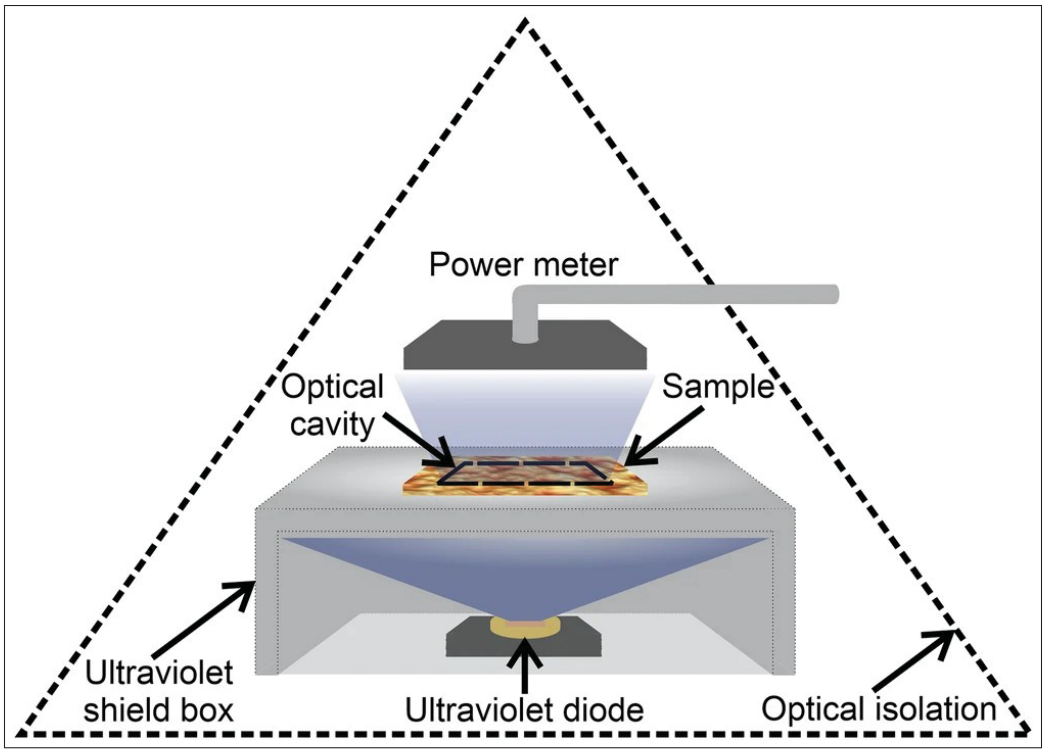

Figure 1.4 Schematic explanation of high-energy ultraviolet (UVC) transmission measurements

A UVC diode (λ = 255 nm) was employed to back illuminate samples as a function of metal oxide (MO) thickness and illumination density. The UVC transmission was measured with a power meter. The UVC diode was shielded within a metal box with an optical cavity under the sample, eliminating any UVC leak to the optical power meter. Additionally, the entire measurement setup was optically isolated to prevent any external influence on measurements.

1.5.3 Back illumination of samples with ultraviolet illumination

We used a constant wavelength (λ = 255 nm), UVC light-emitting diode (LED, OP255-10P-SM by Crystal IS). As Fig. 1.4 shows, the UVC source was shielded to ensure that the surface was only back illuminated via the cavity underneath the sample. The power density of the transmitted light was measured with a power meter (Slim Photodiode Power Sensor, S130VC by Thorlabs). The measurement setup was optically isolated to ensure no external light affected the measurement. We tuned the power of the UVC source to understand the effect of illumination

density. The distance between the power meter and the sample was kept constant for each measurement. The back illumination of the sample is uniform and covers the entire back side of the sample, as the illumination angle of the UVC diode is 120°, and the optical cavity is ~1 cm away and right above the UVC diode.

We positioned the UVC diode on a large stainless steel heatsink with an embedded thermocouple (PT-1000 with a temperature resolution of 0.01 °C) right under. The maximum power dissipation of the diode is 0.8 Watts, and we did not observe any meaningful temperature variation due to the operation of the LED. Moreover, the temperature in the laboratory was 19.6 ± 0.4 °C, while the corresponding relative humidity level was 38 ± 3% with active temperature and humidity controls to avoid confounding contributions on samples and measured quantities. Finally, as the concentration of PI-SOVs stabilizes within ~90 minutes, we waited for the stabilization of the formation and recovery of PI-SOVs for our measurements.

(31;94)

1.5.4 Time-Resolved Atomic Force Microscopy Measurements

Integrated with new hardware and software, we employed a customized VEECO EnviroScope system for our TR-AFM measurements. Details of microscope customization and principles of TR-AFM measurements can be found elsewhere. Briefly, as summarized in Fig. 1.5, a voltage pulse, V_{bias}, was applied between the sample and the oscillating cantilever probe after the tip was retracted away (e.g., 15 nm) from the surface. The applied V_{bias} results in a time-dependent Coulombic interaction, which causes the migration of charge carriers. The migration of charge carriers leads to a time-dependent tip-sample interaction force, which induces the time-dependent resonance frequency shift of the cantilever probe, Δf. For conventional TR-AFM measurements, the Δf is demodulated with a phase-locked loop and the stretched exponential function is fitted to the time, t, versus Δf data.[25;84;136;137] The time constant associated with the Δf decay, τ^*, corresponds to the charge carrier dynamics of ions, holes, or vacancies depending on the sample system.[25;79;81;82;84;136;137] This measurement principle was formerly employed for Li^+

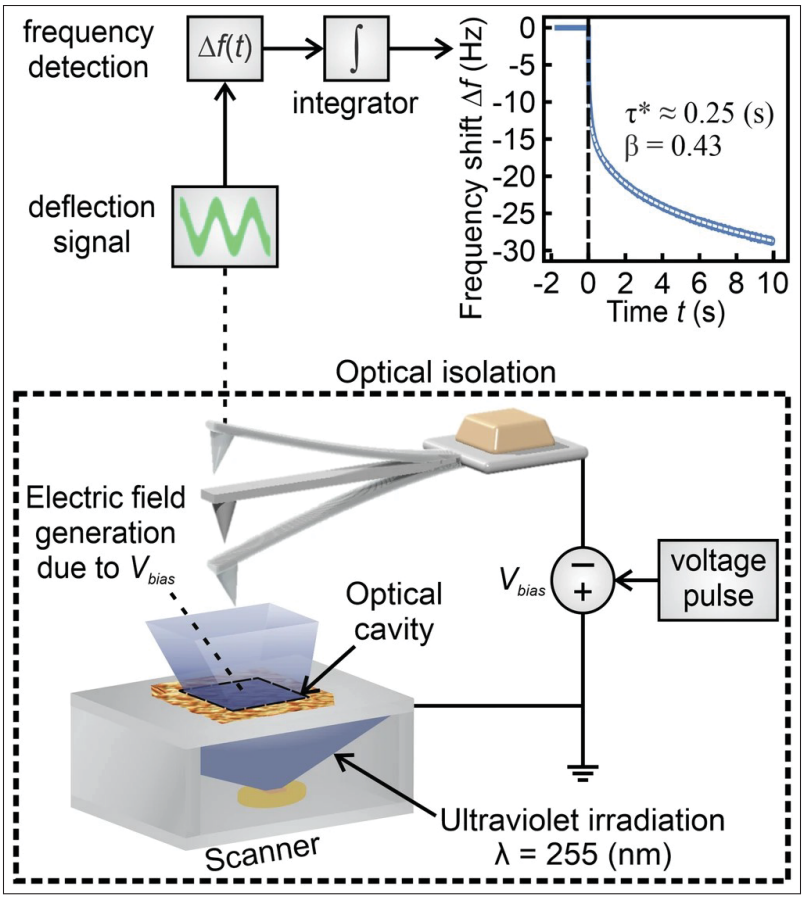

Figure 1.5 Schematic explanation of the time-resolved atomic force microscopy setup and the local measurement of charge carrier dynamics as a function of high-energy ultraviolet (UVC) illumination and metal oxide sample thickness

A voltage pulse, V_{bias} (e.g., a voltage step with an amplitude of 5 V), was applied between the tip and the sample, which resulted in a time-dependent Coulombic interaction. The variation in the induced electric field introduces a time-dependent tip-sample interaction force, which leads to the resonance frequency shift of the oscillating cantilever probe, Δf (demodulated with a phase-locked loop). The experiment was repeated on the same lateral position to enhance the signal-to-noise ratio. A stretched exponential fit was applied to the Δf as a function of time, t, as presented with a dashed line. The decay of the stretched exponential fit, τ^*, is related to the migration dynamics of charge carriers (see main text). The stretching factor, β, is associated with the collective motion of charge carriers (see main text). A UVC source (λ = 255 nm) was employed to back illuminate samples with different illumination densities to explore the effect of back illumination on charge carrier dynamics. The microscope chamber was optically isolated from the outside to eliminate any external UVC contributions. The UVC source was also isolated in a metal box to ensure the back illumination of samples via an optical cavity that was at least 50% smaller than the sample area. The data presented in this figure were recorded at room temperature on a TiO_2 (100) single crystal with a back illumination density of 0.47 mW/cm^2.

transport in $LiAlSiO_4$, K^+ transport in $K_2O{\cdot}2CaO{\cdot}4SiO_2$ glass, and Na^+ transport in $Na_2O{\cdot}GeO_2$ glass, hole migration in TiO_2, and oxygen vacancy migration in $SrTiO_3$.[25;79;81;82;84;136;137] The stretched exponential term, β, can have a value between zero and one while representing the collective motion of charge carriers.[79;81;82] Specifically, decreasing β values imply enhanced collective motion, i.e., stronger particle-to-particle interaction.

We repeated measurements at least 25 different sample locations and at each position 40 times to ensure that the back illumination of the surface covers the entire sample and to enhance the signal-to-noise ratio.[19;138] For all of our measurements, we implemented a gold-coated, conductive microcantilever (OPUSTIPS, 4XC-GG, tip radius < 30 nm, stiffness ~9.0 N/m, and resonance frequency ~150 kHz). To secure the back illumination, the sample was attached to a shielding box with an opening underneath and positioned directly on the UVC source (vide supra). The microscope chamber was also isolated optically. Finally, it was previously shown that the UVC illumination does not change the sensitivity or the temperature of the oscillating cantilever.[26]

CHAPTER 2

TIME-RESOLVED MAPPING OF CHARGE CARRIER DYNAMICS AND DEFECT-MEDIATED MIGRATION BARRIERS IN TIO_2

Bugrahan Guner[1] , Mohammad Safikhani-Mahmoudi[1] , Omur E. Dagdeviren[1]

[1]Department of Mechanical Engineering, École de technologie supérieure,
1100 Notre-Dame Ouest, Montréal, Québec, Canada H3C 1K3

Article published in *Journal of Physical Chemistry C*, 129, 16879–16886 (2025).

2.1 Abstract

The spatiotemporal behavior of charge carriers in metal oxides (MOs) governs their performance in photocatalytic and electronic applications, yet remains poorly understood at the nanoscale. Here, we use time-resolved atomic force microscopy (TR-AFM) to map charge transport in TiO_2 under controlled surface irradiation and thermal conditions. Our measurements reveal pronounced spatial variability in carrier migration times and activation energies, driven by local defect landscapes. Irradiation-induced surface defects are found to lower migration barriers, enhancing carrier relaxation. Notably, we observe electrostatic memory effects, with residual electric fields modulating migration dynamics across hundreds of nanometers. Temperature-dependent studies further reveal a tunable interaction between defect-mediated migration and thermal activation. These findings provide direct insight into nanoscale charge transport in TiO_2 and highlight the role of defect engineering and thermal management in optimizing oxide-based devices for energy conversion and sensing.

2.2 Introduction

Controlled tunability of material properties is a key factor in defining their functionality, and is central to advancing sustainable energy conversion, next-generation electronics, and catalysis. The ability to manipulate matter at the atomic and nanoscale has opened new routes for tailoring materials to meet the demands of increasingly complex.[35;139;140] Metal oxides (MOs), composed of metal cations and oxide anions (e.g., TiO_2), exemplify tunable systems

whose electronic and chemical properties can be engineered, often via defect manipulation, without significantly affecting biocompatibility or toxicity.[17;141] Owing to this versatility, MOs are widely used in batteries,[142] solar cells,[34;143] sensors,[34;143] and biomedical devices.[144] Among the various types of defects, oxygen vacancies (V_O) are particularly influential, as even minor variations in surface stoichiometry can substantially affect the functional properties of MOs.[38;39] V_O not only modify electronic band structures but also influence adsorption energies, catalytic pathways, and long-range carrier recombination processes. In photoelectrochemical systems, they can act as both beneficial charge trapping sites that alter carrier lifetimes and detrimental recombination centers that reduce efficiency. This dual character underscores the need for experimental approaches capable of disentangling their spatially heterogeneous effects. However, probing the spatial and temporal influence of V_O on charge carrier dynamics and migration barriers remains a significant challenge due to their low concentrations under ambient conditions.[145]

Although V_O are known to play a critical role in (photo)catalytic and electronic behavior, understanding its impact on both fast (e.g., electrons) and slow (e.g., holes, polarons, vacancies) charge carriers is essential. Raman spectroscopy under photocatalytic conditions has revealed insights into photoinduced surface oxygen vacancy (PI-SOV) formation and recovery, particularly under high-energy ultraviolet (UVC) irradiation.[52;94] Nevertheless, most conventional techniques yield either volume- or time-averaged data, limiting their ability to resolve the local and time-resolved charge carrier behavior.[37;146] Time-resolved atomic force microscopy (TR-AFM), by contrast, offers direct access to charge carrier dynamics and migration barriers at relevant spatial (tens of nanometers) and temporal (microseconds to hundreds of milliseconds) scales.[19;25;31;138] More specifically, TR-AFM bridges this experimental gap by combining nanoscale imaging with time-resolved probing of transient electrostatic responses. This technique enables simultaneous access to fast electronic relaxation and slower ionic or defect-mediated processes, thereby offering a complete picture of charge transport inaccessible to conventional methods.

In this study, we employ TR-AFM to experimentally investigate the slow and fast charge carrier dynamics in TiO_2 as a function of spatial location, surface irradiation, temperature, and sample

excitation history. Our key findings are as follows: (I) Charge migration dynamics in single crystal TiO_2 are highly localized, contradicting the expectation of uniformity; (II) Surface irradiation alters carrier dynamics, with increased defect density lowering hole migration barriers; (III) Charge migration exhibits history dependence, with effects extending across hundreds of nanometers; and (IV) Fast charge carrier responses are more strongly influenced by temperature than by irradiation. These results provide new insights into the spatial and temporal behavior of charge carriers in MOs and highlight the importance of local measurements for both fundamental science and applied technologies.

2.3 Methods

We employed both conventional[19;25;31;138] and submicrosecond[21;22;26] time-resolved atomic force microscopy (TR-AFM) techniques to measure the dynamics of slow and fast charge carriers in a single crystal TiO_2 (100) sample (see Supporting Information Sections 1–3 for details on sample preparation and experimental methods). As shown in Figure 2.1, a bias voltage (V_{bias} = 7 V) was applied to the tip after positioning it ~15 nm above the sample surface. This bias induces a time-dependent Coulombic interaction within the probing volume, driving charge carrier migration. The resulting change in the electrostatic tip–sample interaction force modulates the deflection signal. By demodulating this signal to recover the frequency shift,[68] Δf, as a function of time, t, we measure charge carrier dynamics: slow dynamics (e.g., electron–hole pair-related.)[19;31;138] and fast dynamics (electron-associated). Activation energies corresponding to electron–hole pair migration, E_a^*, and the effective migration barrier for a single electron–hole pair, E_a, are extracted from temperature-dependent measurements of the time constant (τ^*) and the stretching factor (β) of the $\Delta f(t)$ decay. Note that E_a^* and E_a refer to the effective barriers faced by charge carriers as they migrate within the material,[79;81;138] not specific chemical reaction processes.

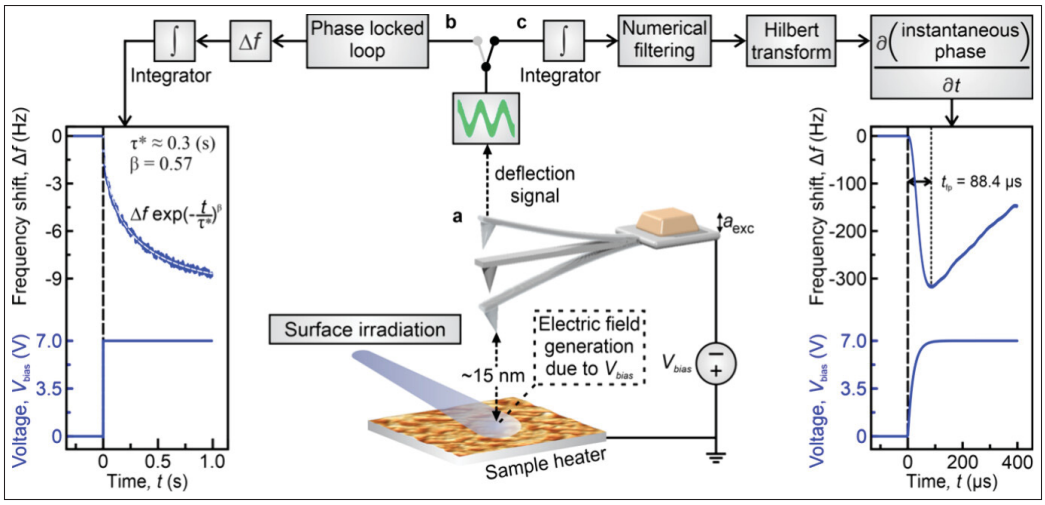

Figure 2.1 Schematic representation of conventional and submicrosecond time-resolved atomic force microscopy (TR-AFM) measurements

(a) TR-AFM was performed on a TiO_2 (100) single crystal under varying sample irradiation and temperature. The cantilever, oscillated with an excitation signal (a_{exc}), was positioned ~15 nm above the sample surface. A tip–sample bias voltage (V_{bias}) was applied, inducing a time-dependent Coulombic interaction that perturbs the deflection signal. Depending on the demodulation method, charge carrier dynamics can be assessed at (b) hundreds of milliseconds and (c) submicroseconds. (b) For conventional TR-AFM, the deflection signal was demodulated as a function of time (t) using a phase-locked loop (a.k.a., PLL) to measure the resonance frequency shift, $\Delta f(t)$. A stretched exponential function was fitted to $\Delta f(t)$, extracting the time constant (τ^*) and stretching factor (β) to assess slow charge carrier (e.g., holes, vacancies, polarons) dynamics. (c) Submicrosecond TR-AFM involves postdemodulation of instantaneous $\Delta f(t)$. The real-time deflection signal was recorded, processed through Hilbert transformation after numerical band-pass filtering (Butterworth, fourth order), and the derivative of the instantaneous phase was used to determine $\Delta f(t)$. The time of the first peak (t_{fp}) provides the relative variation of fast charge carriers (e.g., electrons). The data presented were recorded at 65 °C on a TiO_2 (100) sample.

2.3.1 Preparation of the TiO_2 Single Crystal

We used a single crystal, undoped TiO_2 (100) sample (MSE Supplies LLC). Although the TiO_2 (110) surface is more stable,[40;134] we chose TiO_2 (100) to avoid potential variations in coordination number that could arise from differences in titanium atom coordination. In TiO_2 (110), Ti atoms can be five- or six-coordinated, while in TiO_2 (100), they are exclusively five-coordinated, eliminating ambiguity associated with coordination number variation.[135]

The sample preparation followed an established procedure:[26;28;31] the single crystal was annealed for 10 h at 1000 °C, with ~ 3-h heat-up and cool-down periods. This process resulted in a rutile-terminated surface[31] As Figure II-1 shows, the sample surface is atomically flat and free from carbon clusters. Finally, a rutile termination was preferred over anatase, as the latter is more susceptible to adsorbates at ambient conditions, particularly under surface irradiation.[45;130]

2.3.2 Experimental Setup

Time-resolved scanning probe microscopy measurements were performed using a customized VEECO EnviroScope system. (34) The microscope was modified by integrating additional hardware, including a high-voltage amplifier, a lock-in amplifier with phase-locked loop (PLL) capability (MFLI, Zurich Instruments), and a new control unit, while retaining the environmental control features of the original system. The instrument was operated using the Gnome X Scanning Microscopy (GXSM) software package, (35) equipped with active drift control. For all experiments, we employed gold-coated microcantilever tips (OPUSTIPS 4XC-GG) with a nominal stiffness of ~ 9.0 N/m, a resonance frequency of ~ 150 kHz, and a tip radius of < 30 nm. The cantilever oscillation amplitude was maintained at ~ 10 nm (peak-to-peak).

2.3.3 Conventional Time-Resolved Atomic Force Microscopy Measurements

Conventional TR-AFM measurements[25;136] were carried out by demodulating the cantilever deflection signal to obtain the resonance frequency shift, Δf, as a function of time, t, using standard frequency modulation (FM) mode[68] with a phase-locked loop (PLL), as illustrated in

Figure 2.1. This established TR-AFM methodology has been successfully employed to study charge carrier migration dynamics in various material systems, including glasses,[25;136] ionic materials,[138] perovskites,[19] and, most recently, metal oxides.[28;31]

For data analysis, the $\Delta f(t)$ response was fitted using a stretched exponential function. The decay constant of this fit, denoted as τ^*, provides a quantitative measure of charge migration dynamics, while the stretching factor, β, reflects the degree of collective motion among charge carriers. By performing TR-AFM measurements at different sample temperatures, as Figure 2.3, Arrhenius plots[83] of natural logarithms of τ^* in ms versus $1/(k_B T)$, where k_B is the Boltzmann constant, and T is sample temperature in Kelvin, were constructed to extract the effective activation barrier for electron–hole pair migration, E_a^*. Multiplying E_a^* by the stretching factor β yields the effective migration barrier for a single, uncorrelated electron–hole pair, E_a, which can be directly compared with theoretical predictions.[79;81]

It is important to note that β in this context does not arise from a distribution of energy barriers typically observed in disordered media but rather originates from the collective and correlated motion of charge carriers, particularly electron–hole pairs. All measurements were performed locally at nanometer spatial resolution. On this length scale, the TiO_2 (100) surface remained structurally ordered, with no detectable variation in surface reconstruction across the scanned areas.

2.3.4 Submicrosecond Time-Resolved Atomic Force Microscopy Measurements

To capture the dynamics of fast charge carriers (i.e., electrons), submicrosecond TR-AFM measurements[79;81] were performed, as outlined in Figure 2.1. Submicrosecond TR-AFM relies on applying a bias voltage (V_{bias}) with a well-defined rise time (e.g., τ = 20 μs) at a specific oscillation phase of the cantilever, typically at the zero-crossing point with a positive slope. To acquire the real-time cantilever deflection signal, a high-speed digitizer (i.e., PicoScope 4824A) and an arbitrary function generator (i.e., Tektronix AFG31051) were utilized, as detailed elsewhere.[79;81]

In summary, the oscillation signal was integrated over several cantilever cycles and subsequently processed using a band-pass numerical filter (Butterworth, fourth order). A Hilbert transform was then applied to extract the instantaneous oscillation phase. The time derivative of this phase yielded the instantaneous frequency shift, $\Delta f(t)$. The time for the first peak in $\Delta f(t)$, t_{fp}, was linked to the migration dynamics of the charge carriers. Importantly, in submicrosecond TR-AFM, the relative variation of t_{fp} under external stimuli (e.g., variation in V_{bias} rise time or temperature) is more informative than its absolute value, as the t_{fp} can be influenced by cantilever properties, the specifics of the numerical filtering process, and the τ of V_{bias}.[79;81]

2.3.5 Surface Irradiation

As a wide bandgap semiconductor (bandgap $\sim$ 3.0 eV),[41] the surface stoichiometry and defect density of TiO_2 are highly sensitive to surface irradiation.[31;52;94;97] For this reason, to minimize unintended photochemical effects, all experiments were conducted in an optically isolated microscope chamber. The microscope was equipped with a built-in halogen lamp that could provide broadband illumination to mimic daylight exposure, while a high-energy ultraviolet (UVC) light source (λ = 255 nm, OP255–10P-SM by Crystal IS) was integrated for targeted, well-defined irradiation. The maximum UVC irradiation density was 1.3 mW/cm^2. Although TiO_2 exhibits absorption of wavelengths $\lambda < 400$ nm, only shorter wavelengths ($\lambda < 280$ nm) are known to induce surface oxygen vacancies for crystallized TiO_2.[31;52;94;97] However, for amorphous TiO_2, surface oxygen vacancies can be introduced even with 365 nm UV irradiation.[147] To this end, previous studies have demonstrated that UVC irradiation at λ = 254–255 nm is particularly effective in this regard.[31;52;94]

Using a photodiode power sensor (Slim Photodiode Power Sensor, S130VC by Thorlabs), we measured the ultraviolet component ($\lambda < 400$ nm) of the halogen lamp at maximum illumination, yielding a total intensity of 2.6 $\pm$ 0.1 mW/cm^2. Unless otherwise stated, all reported surface irradiation densities correspond to the UVC source employed for our measurements.

To further distinguish the electronic effects of high-energy UVC exposure, comparative studies were performed using both UVC and ultraviolet (UV) illumination (λ = 375 nm, LED375L by Thorlabs). Figure II-2 shows Kelvin probe force microscopy measurements,[14] which revealed that the work function of the TiO_2 was strongly modulated under UVC irradiation; however, it remained nearly unaffected under UV exposure. This pronounced difference confirms that the changes in surface electronic properties, i.e., charge carrier dynamics variations, are specific to UVC irradiation, consistent with the generation of photoinduced surface oxygen vacancies and previous experimental work.

2.4 Results and Discussion

We first examined the influence of surface irradiation on the time constant, τ^*, as a function of irradiation density across the sample surface. As shown in Figure 2.2, τ^* decreases with increasing surface irradiation density. Following an initial abrupt drop, more pronounced at higher irradiation levels, τ^* decreases asymptotically over time with further irradiation. Specifically, under dark conditions (no irradiation), τ^* was measured to be 1333 ± 137 ms. At a modest illumination density of 0.33 mW/cm^2, τ^* shows a statistically significant decrease to 1041 ± 75 ms. This trend becomes more pronounced at higher irradiation densities: τ^* decreases further to 769 ± 145 ms at 0.65 mW/cm^2 and 677 ± 188 ms at 1.30 mW/cm^2. Although a qualitative decrease in τ^* under UVC irradiation has been reported previously,[31] our results quantitatively correlate τ^* with irradiation density, revealing a continuous and reversible trend. Notably, these changes in τ^* were fully reversible under ambient conditions, even after exposure to the highest irradiation level, strongly suggesting that the observed variation arises from the formation and subsequent recovery of surface defects, particularly PI-SOVs, generated by UVC exposure[97] (see Methods and Supporting Information Section 2 for details). The data support a model in which increased irradiation density leads to enhanced defect formation, thereby accelerating charge carrier relaxation dynamics and reducing τ^*.

The decrease in τ^* indicates reduced carrier mobility (μ), as a higher defect density facilitates faster recombination or trapping of charge carriers.[97] In parallel, we observed a modest increase

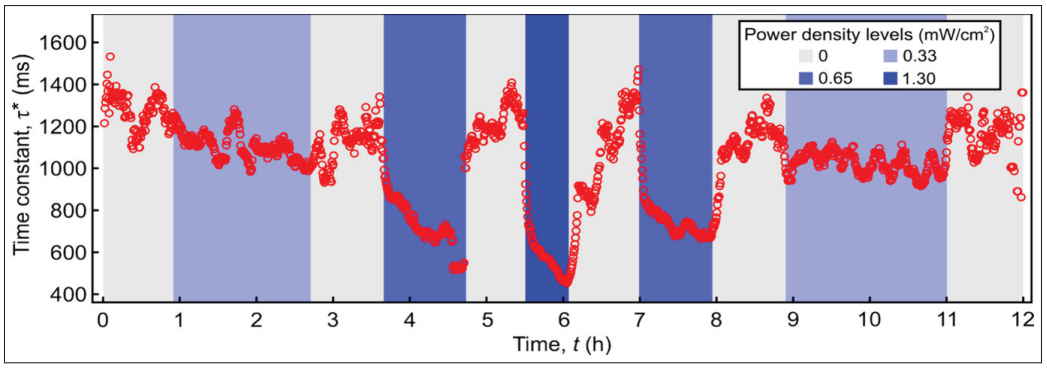

Figure 2.2 Time-resolved atomic force microscopy (TR-AFM) measurements of the characteristic time constant τ^* for slow charge carriers on a TiO_2 (100) surface under varying irradiation conditions

τ^* decreases systematically with increasing surface irradiation density, indicating enhanced carrier relaxation dynamics. At dark conditions, i.e., 0 mW/cm^2 (gray regions), τ^* remains 1333 ± 137 ms. Upon exposure to 0.33 mW/cm^2 (light blue), τ^* drops to 1041 ± 75 ms, and further decreases to 769 ± 145 ms under 0.65 mW/cm^2 (medium blue). At the highest power density, 1.30 mW/cm^2 (blue), τ^* reaches a minimum of 677 ± 188 ms. Particularly, this modulation is reversible: once irradiation is ceased, τ^* gradually returns toward its initial value. This reversible behavior emphasizes the dynamic coupling between surface irradiation and charge carrier dynamics. All measurements were performed at room temperature and analyzed with a rolling average of two successive measurements.

in the stretching factor β, ~ 10%, even at an illumination density of 0.33 mW/cm^2 compared to dark conditions. Since β reflects the degree of collective motion among charge carriers (with $0 \leq \beta \leq 1$, and smaller values corresponding to more collective behavior),[79;81] this increase suggests a slight attenuation in collective transport. This observation hints at two competing effects between enhanced charge carrier generation and defect-mediated trapping: (1) higher surface defect density promotes faster recombination, reducing both τ^* and the opportunity for collective motion; (2) increased carrier density due to photoexcitation could enhance interactions between charge carriers, thereby promoting collective dynamics. However, the faster trapping and recombination at defect sites appear to dominate, resulting in only a slight increase in β. While these observations are consistent with charge carrier dynamics

governed by defect-mediated processes, further studies, such as atomic-scale imaging during carrier migration, are needed to confirm this mechanism. Nevertheless, such characterization lies beyond the scope of the present work.

We performed conventional TR-AFM measurements to investigate the variation in charge carrier dynamics across the sample landscape as a function of temperature and surface irradiation density. For each condition, measurements were taken at 64+ different spatial positions, spaced 40 nm apart. Each data point in Figure 2.3 represents the distribution of time-resolved measurements at a given temperature and irradiation level across the sample landscape. Figure 2.3 shows that τ^* exhibits a strong spatial variation, indicating that it is a local property of the sample. Specifically, τ^* varies by 18% across the sample surface, significantly greater than the systematic error (3%) obtained from repeat measurements at the same location (averaged over 40 repetitions).[19]

This confirms that the observed variation arises from genuine local differences in defect density and charge carrier behavior rather than measurement uncertainty. While TiO_2 (100) single crystals are expected to exhibit uniform defect distribution,[36;48] our results suggest that even small fluctuations in V_O concentration can lead to measurable local changes in τ^*. Moreover, τ^* decreases monotonically with increasing temperature, from 1168 ± 98 ms at 25 °C to 299 ± 63 ms at 65 °C under dark conditions, consistent with thermally attenuated μ in TiO_2. Notably, the spatial variation in τ^* persists at elevated temperatures, although it becomes less pronounced with increasing surface irradiation. For example, at room temperature, the variation of τ^* decreases from 18% in the dark to 7% under 1.3 mW/cm^2 irradiation, suggesting that PI-SOVs become more uniformly distributed under higher UVC exposure.

Temperature-dependent measurements at different spatial locations also enabled the extraction of the effective activation energy barrier, E_a, via Arrhenius plots. Our results show that E_a decreases with increasing irradiation density, from 198 ± 27 meV at dark conditions to 111 ± 11 meV at 1.3 mW/cm^2. While a lower E_a may motivate increased μ, it is important to recognize that μ also depends on other factors, such as the dimensionality of the transport (e.g., 2D migration in thin films vs 3D in bulk crystals) and the average hopping distance between

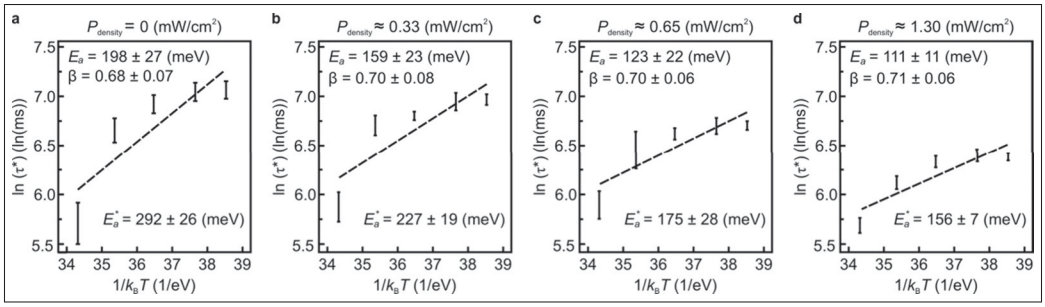

Figure 2.3 Effective activation barrier for electron–hole pair migration in TiO_2 (100) under varying surface irradiation conditions

The characteristic time constant, τ^*, was measured using conventional time-resolved atomic force microscopy. The activation energy corresponding to electron–hole pair migration, E_a^*, was extracted from the slope of the Arrhenius plots of the natural logarithm of τ^* (in ms) versus $1/(k_B T)$, where k_B is the Boltzmann constant and T is the sample temperature in Kelvin. The effective migration barrier for a single electron–hole pair, E_a, can be calculated by multiplying E_a^* with the stretching factor of the exponential fit, β. (a–d) demonstrate that τ^* decreases with increasing temperature across all power densities, consistent with thermally activated migration. Moreover, both E_a^* and E_a systematically decrease as the surface irradiation density increases from dark conditions (no irradiation) to 1.30 mW/cm^2. This reduction in activation barrier suggests that photoexcitation facilitates charge migration by altering the population and/or energy landscape of surface or near-surface defect states, which act as mediators for charge carrier hopping. The vertical error bars show the variation of τ^* across 64+ spatially distributed measurement points (40 nm spacing), each averaged over 40 repetitions to enhance signal-to-noise ratio.

vacancies and charge carriers.[19] For this reason, we believe that these other factors lead to a decrease in μ, as dictated by the decrease in τ^* (see above).

The observed modulation of charge carrier dynamics with surface irradiation has notable implications for solar energy applications, including photocatalysis and photoelectrochemical energy conversion. The reduction in τ^* and E_a with increasing irradiation density indicates faster relaxation dynamics, which are favorable for improving charge separation efficiency.[148;149] Moreover, the reversible nature of PI-SOV formation suggests that light-induced defect

engineering can serve as a tunable and nondestructive strategy to optimize surface properties in real-time, which is beneficial for long-term device stability. The decrease in spatial variation of τ^* under higher irradiation levels further implies that photogenerated defects can homogenize surface transport properties, potentially enhancing large-area device uniformity. Collectively, these findings underline the potential of leveraging controlled light exposure to dynamically tailor the electronic landscape of TiO_2 surfaces for improved solar-driven energy conversion performance.

We performed measurements to investigate the temporal effects on charge carrier migration by applying successive electrical pulses between the probe and the sample with varying time delays, Δt, ranging from 10 to 1000 ms. As shown in Figure 2.4, despite identical initial conditions for each Δt, the residual electric field significantly influences the time-dependent response at shorter delays.

The pronounced dependence of τ^* on Δt suggests that charge carriers do not have sufficient time to migrate to unexcited positions when Δt is small. To further explore this behavior, we carried out temperature-dependent measurements to determine the E_a, as a function of Δt. Notably, for Δt = 100 ms, E_a increases by ~400% between the first and third pulses, whereas for Δt = 1000 ms, the increase is only ~ 15%. This trend indicates that charge carriers face higher energy barriers for migration when they remain in previously excited regions. The relatively small variation in E_a at Δt = 1000 ms suggests that the relaxation time required to fully reset the sample is longer than 1000 ms. However, longer Δt values could not be tested reliably due to thermal drift, particularly at elevated temperatures.

The observed dependence of charge carrier migration on the time delay between successive electrical pulses has important implications for the performance and stability of TiO_2-based electronic and optoelectronic devices. The persistence of residual electric fields and the increase in E_a with shorter delays suggest that charge carriers do not fully relax between excitations, leading to transient memory effects in charge transport. In practical terms, this behavior could result in hysteresis, reduced efficiency, or increased noise in devices operating under

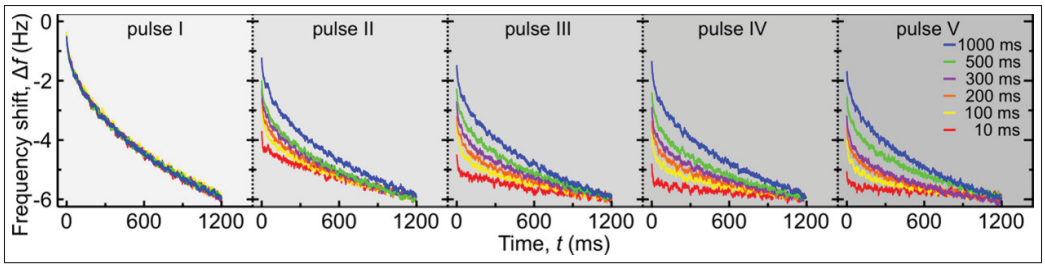

Figure 2.4 Time-resolved atomic force microscopy measurements showing the evolution of charge migration dynamics under repeated electrical pulses

Each panel (pulse I–V) corresponds to successive pulses applied at the same spatial location, with a pulse delay time, Δt, color-coded from 10 ms (red) to 1000 ms (blue). For the initial pulse (pulse I), all delay conditions exhibit an identical response (plotted on top of each other), confirming that measurements were performed at the same spatial position across the sample. As the number of pulses increases (pulse II to V), the decay curves progressively diverge, especially at short pulse delays. This tendency reveals a history-dependent response likely caused by incomplete dissipation of the local electric field between pulses. The persistence of trapped or slowly migrating charges effectively screens the external field, thereby modifying the subsequent charge migration. The observed memory effect, i.e., history dependence, emphasizes the role of electric field screening and defect-mediated trapping in governing charge carrier dynamics.

high-frequency or pulsed conditions, such as memristors, photoelectrochemical sensors, or perovskite solar cells incorporating TiO_2 as a transport layer.[47;150;151] Additionally, the long τ^* implies that charge transport dynamics are sensitive to the device's operational history, potentially influencing long-term stability and limiting performance under rapid cycling. These insights emphasize the need for pulse timing control or defect management strategies in applications where TiO_2 is subjected to repetitive excitation.

To determine the spatial extent of history-dependent effects, we applied a V_{bias} with a constant Δt of 100 ms while incrementally increasing the lateral distance between successive pulses. Since Δt is insufficient for full field recovery, residual electric fields influence the time-resolved response.

As shown in Figure 2.5, this history dependence attenuates with distance and extends ~ 500 nm laterally across the sample. Surface irradiation does not significantly alter this trend, though slight variations arise due to increased defect and carrier concentrations (see Supporting Information Section 4 for details). These findings have important implications for nanoelectronic and optoelectronic devices, where components are often spaced within submicron distances.[152] The persistence of residual electric fields over several hundred nanometers suggests that charge transport and local field distributions can be significantly influenced by prior excitation history. This may impact device behavior such as signal fidelity, noise characteristics, and spatial crosstalk in densely integrated architectures, particularly under high-frequency or pulsed operating conditions. Understanding and controlling this spatial memory effect could be essential for optimizing device performance and long-term operational stability of metal oxide architectures.

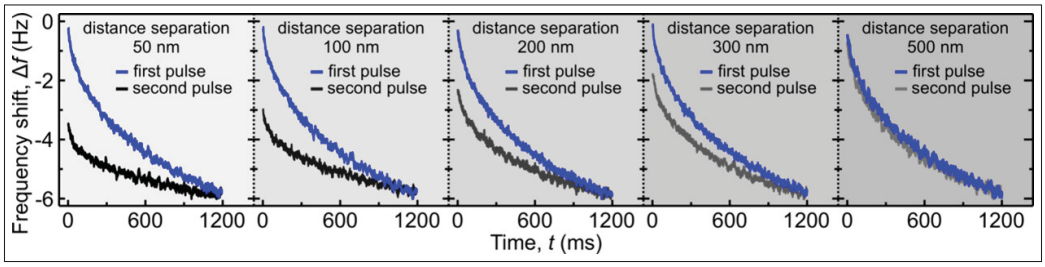

Figure 2.5 Time-resolved atomic force microscopy measurements illustrating the spatial extent of history-dependent charge carrier migration on a TiO_2 (100) surface under dark conditions, i.e., no surface irradiation

Successive pulses were applied with increasing lateral distances, while the pulse delay time was kept constant at 100 ms. The observed variation shows that temporal correlations in the migration dynamics persist over several hundred nanometers, gradually decreasing with distance. This spatial memory effect shows that local electric fields and defect-mediated trapping influence charge migration beyond the immediate vicinity of the applied bias voltage.

Finally, we employed submicrosecond TR-AFM measurements[21;22] on single-crystal TiO_2 (100) to investigate the influence of temperature and surface irradiation on the dynamics of fast charge carriers (i.e., electrons). For benchmarking, similar measurements were performed on a

template-stripped gold sample, where electron transport dominates.[26] Across more than 500 data points, we observed that the characteristic time constant for fast charge carrier migration, t_{fp}, decreased from 90.4 ± 0.6 μs to 88.4 ± 0.6 μs as the sample temperature increased from 25 to 65 °C. In contrast, illumination with a tungsten lamp had a negligible effect on t_{fp} (90.3 ± 0.6 μs, the variation is within the error margin), while prior results show that UVC exposure reduces t_{fp} (~1.0 μs) through PI-SOV formation,[26] which acts as charge-trapping centers. It is important to note that the extracted t_{fp} values reflect a convolution of both intrinsic carrier dynamics and the response of the measurement system; thus, observed trends are more meaningful than absolute values.[26]

2.5 Conclusions

We provided new insights into the time-resolved and spatially localized charge carrier dynamics in single crystal TiO_2, uncovering how surface irradiation, temperature, and excitation history influence migration barriers and carrier relaxation behavior. Through time-resolved atomic force microscopy (TR-AFM), we demonstrate that photoinduced surface oxygen vacancies (PI-SOVs) significantly lower migration barriers and modulate carrier dynamics. Moreover, the persistence of residual electric fields and history-dependent effects over hundreds of nanometers reveals a form of spatial and temporal memory in charge transport. These findings have direct implications for the design of TiO_2-based devices, including memristors, sensors, and photoelectrochemical systems, where precise control over local charge dynamics is essential.

We also revealed that by leveraging defect engineering through light exposure and temperature control, it is possible to tune charge transport properties in real time, potentially empowering more efficient, uniform, and stable device performance. Our approach offers a novel platform for guiding the development of next-generation oxide electronics and energy conversion technologies.

CHAPTER 3

DEFECT- AND GEOMETRY-CONTROLLED FERMI-LEVEL DYNAMICS IN TIO_2

Mohammad Safikhani-Mahmoudi[1] , Nuray Basaran[1] , Bugrahan Guner[1,2] , Tugce Hacaloglu[1] , Omur E. Dagdeviren[1]

[1]Department of Mechanical Engineering, École de technologie supérieure,
1100 Notre-Dame Ouest, Montréal, Québec, Canada H3C 1K3
[2]Department of Mechanical Engineering, Yale University,
New Haven, Connecticut 06520, USA

Article under review in *Advanced Materials*.

3.1 Abstract

The Fermi level dictates charge distribution and redox activity, yet its dynamic evolution under illumination remains poorly resolved. Using Kelvin probe force microscopy, we map time-dependent Fermi-level shifts in a model sample system, a single-crystal TiO_2, under front- and back-side ultraviolet irradiation at two photon energies. High-energy ultraviolet irradiation lowers the surface Fermi level through the formation of persistent photoinduced surface oxygen vacancies, while low-energy ultraviolet irradiation induces only short-lived electron–hole generation with rapid surface recovery. Moreover, front-side irradiation yields a transient response, followed by a uniform surface modification, whereas back-side excitation produces slower, bulk-mediated shifts. In addition, gold nanoparticle decoration of the surface further modifies the Fermi-level kinetics through the Schottky barrier at the interface. By decoupling photon energy from illumination geometry, this work reveals the paired dynamics of carrier transport and defect-mediated formation that shape oxide energetics. These findings establish a foundation for Fermi-level engineering in photocatalysis, sensing, and optoelectronic applications.

3.2 Introduction

The Fermi level sits at the heart of condensed-matter chemistry:[55;59;77;153] it defines the dissemination of electrons across energy levels and, in doing so, dictates charge distribution, redox activity and energy transduction in solids. From quantum-mechanical principles to the operation of modern semiconductors, precise control of this thermodynamic quantity highlights advances in catalysis,[56] optoelectronics[57;58] and energy conversion.[139;143] Within inorganic semiconductors, most prominently the technologically indispensable metal oxides, the Fermi level responds exquisitely to both intrinsic factors (e.g., dopants, stoichiometry) and external stimuli (e.g., temperature, photon flux).[53;60;95] Even mV-scale shifts can reorder band alignments at heterointerfaces, redefining reaction kinetics, device efficiencies, and lifetimes.[54;154;155] Yet the chemist's toolbox for mapping such shifts with relevant spatial and temporal resolution remains limited, particularly under ambient, operando conditions.

Point defects offer a gateway to Fermi-level engineering.[54;154;155] Photo-induced surface oxygen vacancies (PI-SOVs) in TiO_2, for example, donate shallow electrons or create trap states that remodel surface energetics and catalytic pathways.[29;52;92;95] Detecting and quantifying their influence is challenging because their steady-state population is dilute and their lifetime dictates non-equilibrium behaviour.[39] Moreover, conventional spectroscopies average over microns and (milli)seconds, obscuring local, defect-specific dynamics.[156–159] Former scanning probe microscopy-based work concentrated on low-energy irradiation at a single wavelength, exploring the electrochemical nature of the variation upon surface irradiation.[156–159] Furthermore, illumination geometry is rarely considered, leaving the distinct roles of front-side versus back-side excitation and the separate contributions of high-energy vacancy formation versus low-energy electron–hole generation unresolved.

Here, we employ Kelvin-probe force microscopy to track Fermi level evolution in a single-crystal TiO_2 (100), exposed to ultraviolet light from opposing surfaces and at two photon energies. High-energy irradiation (i.e., UVC) lowers the surface Fermi level irrespective of direction, yet the subsequent relaxation diverges. More specifically, front-side excitation produces a

transient variation before further decay, whereas back-side excitation yields a monotonic decline, implying direction-dependent carrier migration through the bulk. Moreover, drop casting gold nanoparticles (Au-NPs) on the surface yields trapping centers, leading to a Schottky barrier between the Au-NPs, which modifies the dynamics of the Fermi level variation upon high-energy irradiation. In contrast, low-energy illumination (i.e., UVA) has a negligible effect, confirming that persistent PI-SOVs, and not short-lived photocarriers, dominate the energetic landscape. By decoupling irradiation geometry from photon energy, our study exposes the spatiotemporal manipulation of defect-mediated Fermi level shifts. These insights link surface photochemistry with solid-state defect physics and can, in principle, guide the design of oxide-based photocatalysts, sensors, and electronic devices whose performance is governed by both electrons and vacancies.

3.3 Summary of Methods

Off-resonance, amplitude-modulated KPFM[15;74;76] was employed to investigate a single-crystal, 500 μm-thick, rutile-terminated TiO_2 (100) sample under front- and back-illumination conditions using a custom-built microscope system (see Supporting Information for details of sample preparation, surface irradiation, and the experimental setup). As illustrated in Figure 3.1, surface topography was acquired by exciting the cantilever near its resonance frequency, while an alternating, i.e., oscillating, bias voltage was superimposed on a constant bias to extract the contact potential difference (CPD), i.e., work function difference between the sample and the probe tip, corresponding to the Volta potential.[160] Ultraviolet surface irradiation was performed with UVC and UVA light sources (λ = 255 nm and λ = 375 nm, respectively) within an optically isolated microscope chamber.[31;61] A standard configuration was used for front-side illumination, while back-side illumination was achieved by mounting the sample over an optical cavity, ensuring ultraviolet isolation via a dedicated source enclosure. Au-NPs were drop-casted with a micropipette on a heated substrate (see Supporting Information for details of the preparation of Au-NPs.)[52]

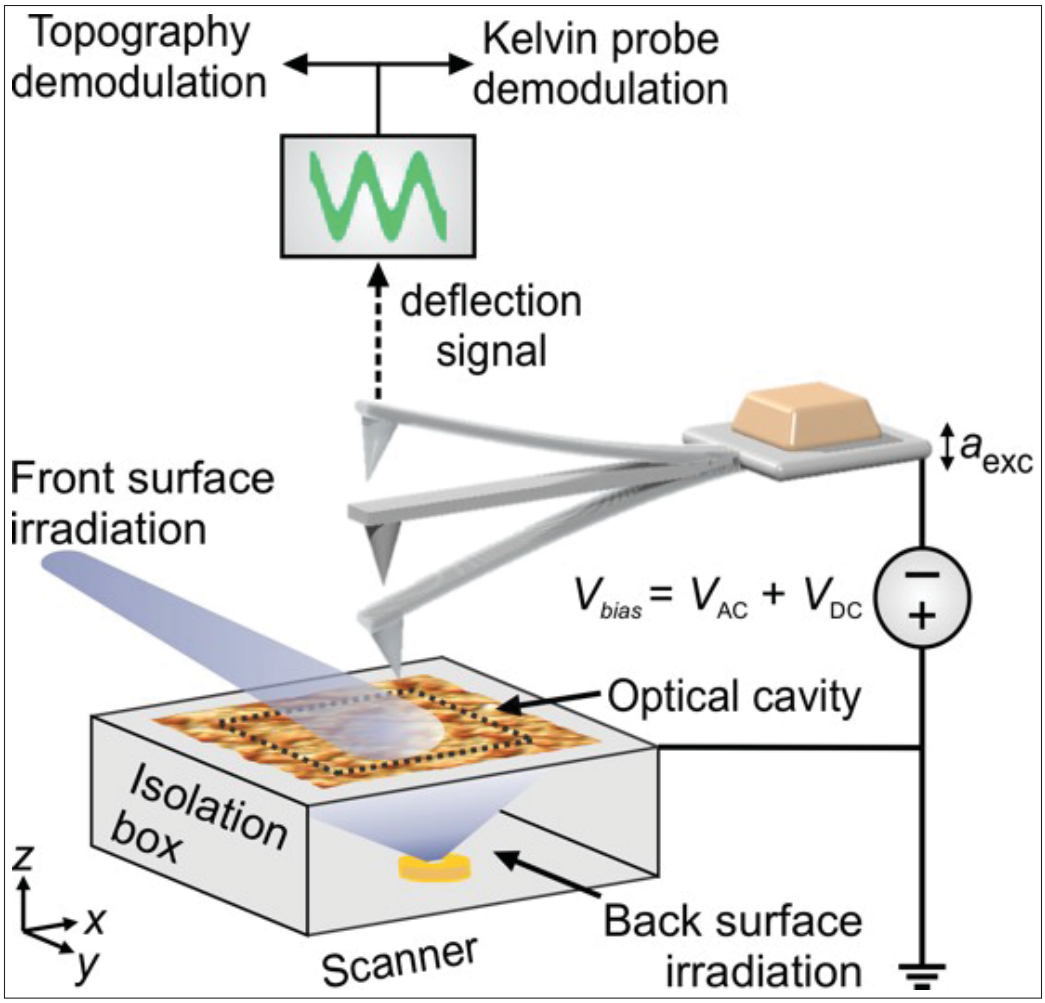

Figure 3.1 Schematic of simultaneous topography and Kelvin probe force microscopy measurements under front- and back-surface ultraviolet irradiation

The atomic force microscopy cantilever was driven off-resonance using an excitation signal (a_{exc}), while a tip–sample bias voltage (V_{bias}) consisted of both alternating (AC) and constant (DC) components. The deflection signal was demodulated using a phase-locked loop integrated with a lock-in amplifier to control the tip–sample distance, yielding topographical data, and to extract the Kelvin probe signal, providing the contact potential difference. High- and/or low-energy ultraviolet sources were used to irradiate either the front or back surface of the sample to modulate electronic states during measurement.

3.4 Results and Discussion

TiO_2 is a wide-bandgap semiconductor that absorbs photons primarily in the ultraviolet region.[41;61] UVC irradiation can alter both charge carrier density and defect concentration, affecting the surface and subsurface regions of the material.[31;95;97] While the penetration depth of UVC was traditionally considered to be only a few tens of nanometers,[30;98;100;101;103] recent studies indicate that photons can penetrate hundreds of micrometres into the bulk.[27] Although the most pronounced variations in carrier concentration and lifetime occur near the surface, a fraction of incident UVC photons reaches the interior and contributes to bulk carrier generation or defect modification.[27]

We first compared the evolution of the CPD under front- and back-side UVC illumination, referencing each trend to its respective dark-state average, as shown in Figure 3.2. Distinct temporal features emerge for the two configurations. Under front-side irradiation, as shown by the inset, the CPD exhibits an initial sub-second drop, characteristic of a surface photovoltage (SPV) generated by electron–hole pairs within the depletion region.[30;64;65] This rapid response is followed by oscillations within the first ~300 s before settling into a monotonic decay. Two competing processes are expected to govern this transient behavior: (i) PI-SOVs, which inject electrons into the conduction band and drive the CPD negative, and (ii) slow re-adsorption or chemisorption of oxygen and/or water molecules, which results in electron-hole recombination and partially restores band bending.[161] In contrast, back-side illumination produces a nearly monotonic CPD decrease with no discernible sub-second feature, and the minor oscillations observed originate from imaging, i.e., trace and retrace of scan range (2 mm). Even though the same surface region was scanned both for forward and backward illumination, under steady state conditions, i.e., after 45 minutes of surface irradiation, the variation across the surface for backward irradiation exceeds that of the front irradiation, with -0.374 ± 0.018 V, while -0.392 ± 0.012 V for the forward irradiation. This implies that the front irradiation leads to a more uniform surface modification compared to the backward irradiation.

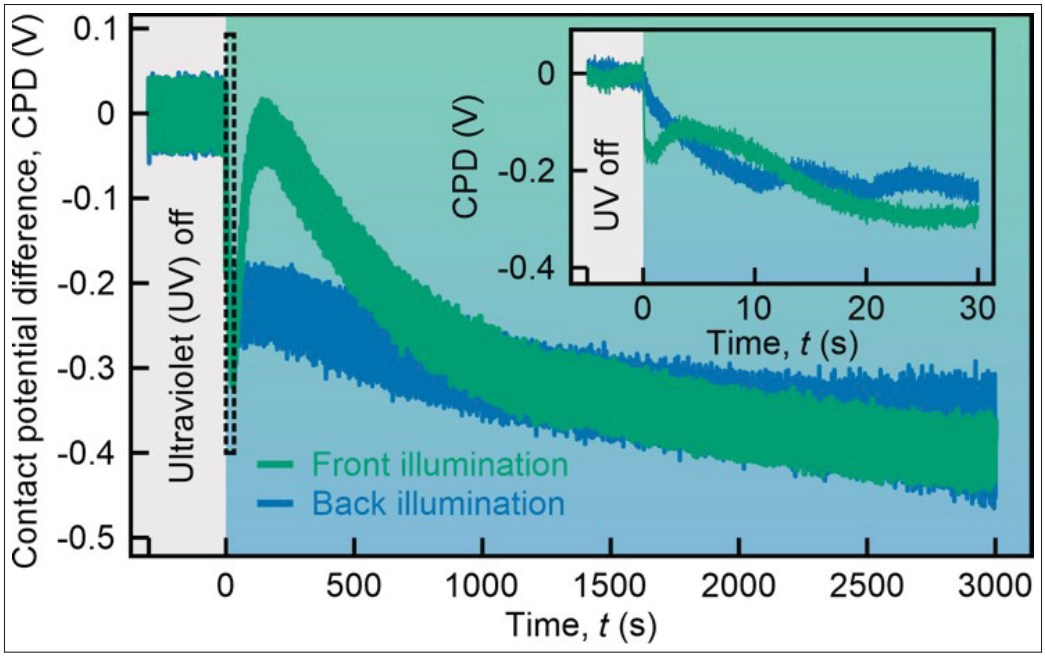

Figure 3.2 Time-dependent contact potential difference (CPD) response of TiO_2 (100) under high-energy UVC irradiation for front-side (green curve) and back-side (blue curve) illumination

Front-side excitation produces an abrupt initial CPD drop, highlighted in the magnified inset, followed by a transient recovery and subsequent decay. In contrast, back-side illumination yields a smooth, monotonic CPD decay, with minor oscillations originating from trace–retrace scan cycling. Front-side irradiation also leads to a more spatially uniform CPD distribution across the surface compared to back-side excitation: -0.392 ± 0.012 V and -0.374 ± 0.018 V, respectively. All measurements were acquired on the same surface region using the same cantilever to ensure direct comparability.

The divergent responses to front- and back-side irradiation can be rationalized by differences in carrier generation, recombination, and diffusion dynamics. Carrier recombination rates depend sensitively on both the location of generation and the local defect concentration, with surface-generated carriers exhibiting slower recombination.[43;62;162] Furthermore, photoinduced defect formation primarily involves adsorbed species and radicals rather than direct Ti-O bond photolysis.[162;163] Because adsorbates exist only on the surface, such reactions cannot occur within the bulk. Carriers generated in the bulk thus migrate toward the surface, where hole traps

can quickly saturate under high photon flux, allowing photogenerated holes to reach surface sites.[44;162;164] Finally, surface bridging oxygen atoms, coordinated to fewer Ti atoms than bulk oxygen, require less energy to form vacancies.[31] The accumulation of photoinduced holes further weakens Ti-O bonds, rendering surface bridging oxygens more labile and increasing the probability of oxygen vacancy formation,[31] as implied by a slightly lower contact potential difference for the same irradiation density.

The observed direction-dependent CPD dynamics have important implications for applications in photocatalysis, sensors, and oxide-based electronic devices. Front-side illumination produces rapid, oscillatory surface responses and more uniform steady-state modifications, suggesting controlled generation of PI-SOVs and stable band bending, features that can enhance catalytic activity and charge separation at the surface. In contrast, back-side illumination drives a slower, monotonic bulk-mediated electron flux with greater spatial heterogeneity, which may be advantageous for devices requiring directional carrier transport or bulk defect engineering. The sensitivity of carrier recombination and defect formation to generation location, local adsorbates, and surface atomic coordination highlights the possibility of tailoring Fermi-level landscapes via illumination geometry. By selectively controlling surface versus bulk excitation, it becomes feasible to engineer both local electronic structure and vacancy distributions, offering design rules for optimizing oxide-based photocatalysts, sensors, and optoelectronic devices with improved efficiency and spatial precision.

We repeated front- and back-illumination experiments across nine surface regions (Figure 3.3), consistently reproducing the direction-dependent CPD dynamics. To directly compare both geometries under identical tip conditions, sequential on/off cycles of front, back, and dual UV illumination were applied while scanning the same surface region. All cycles exhibited two distinct kinetic regimes: front illumination produced a rapid drop of CPD followed by a damped overshoot (vide supra), whereas back illumination induced a slower, monotonic decrease. Moreover, the CPD evolution is better described by a stretched-exponential function rather than a simple exponential, indicating that collective carrier interactions, rather than isolated events, dominate the dynamics.[79;82] The decay constant of the stretched exponential fit, denoted as τ,

provides a quantitative measure of time-dependent CPD variation, while the stretching factor, β, reflects the degree of collective motion among charge carriers.[79;82] Upon light removal, recovery occurred with $\tau \sim 25$–76 s. Notably, the overshoot and oscillatory relaxation appeared exclusively during front illumination, even when both LEDs were active, demonstrating that vacancy generation and adsorbate re-equilibration are confined to the illuminated surface, while back illumination drives a steady, unidirectional electron flux through the bulk. Together, these insights enable rational design of oxide-based devices in which surface and bulk properties can be selectively engineered, opening pathways for enhanced photocatalysis, sensing, and optoelectronic performance.

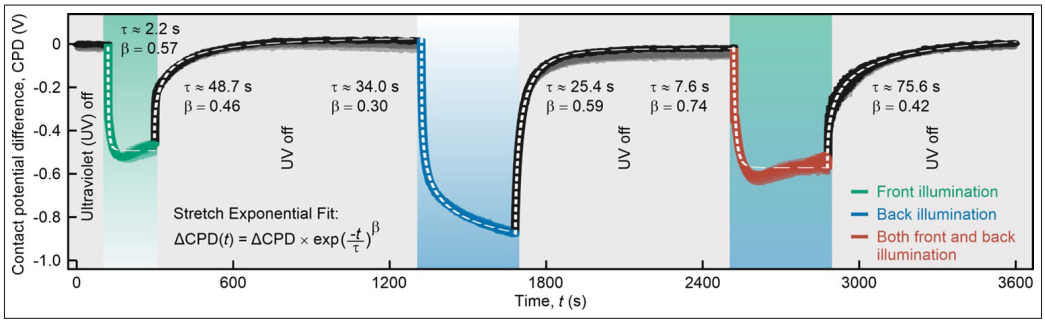

Figure 3.3 Time-dependent contact potential difference (CPD) response of TiO_2 (100) under successive front-side (green curve), back-side (blue curve), and simultaneous front–back (orange curve) UVC illumination

Front illumination produces an instantaneous CPD drop followed by a damped overshoot, whereas back illumination yields a monotonic, stretched-exponential decay. Simultaneous irradiation results in a cumulative response combining features of both illumination geometries. In all cases, the CPD recovery in the dark follows similar stretched-exponential kinetics. Data from nine independent measurements are presented in this figure, with solid lines representing the averaged response.

To probe the influence of ultraviolet irradiation flux, back-illumination measurements were performed at varying UVC intensities, as shown in Figure 3.4. The CPD variation scales directly with flux, indicating that higher photon densities generate larger carrier populations. Across all fluxes, the CPD evolution follows a stretched-exponential behavior, reflecting collective

carrier interactions and cooperative migration through the bulk. As shown in Figure 3.4, the characteristic time constant τ decreases with increasing flux, while β remains nearly constant, demonstrating that higher flux produces steeper driving gradients for carrier transport. In contrast, the recovery kinetics after turning off the illumination exhibit a weaker dependence on prior flux, consistent with slower vacancy re-oxidation by ambient oxygen and/or water molecules. These results highlight the ability to tune bulk carrier dynamics and defect-mediated transport in TiO_2 by controlling UVC flux, providing a route for designing devices with optimized directional charge flow, controlled defect distributions, and enhanced performance.

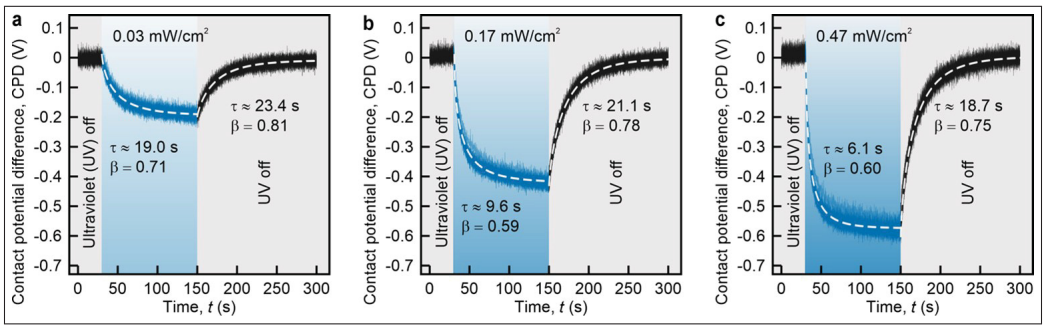

Figure 3.4 Effect of back-side UVC irradiation density on the time-dependent contact potential difference (CPD) of TiO_2 (100)

(a–c) Increasing irradiation density leads to larger CPD shifts and systematically shorter characteristic time constants, reflecting accelerated carrier-driven dynamics. In contrast, the dark recovery remains largely insensitive to the prior irradiation density. In all cases, the CPD change under illumination and conditions follow stretched-exponential kinetics. Data from nine independent measurements are plotted in this figure, with solid lines denoting the averaged response.

We conducted measurements under front-side UVA irradiation. To ensure robust evaluation of the irradiation effect, we subsequently irradiated the back side with UVC light, thereby eliminating any region- or probe-dependent inconsistencies. Figure III-1 shows that the successive measurements reveal that the effect of UVA irradiation on the CPD differs markedly from that of UVC irradiation. While UVA primarily generates electron–hole pairs, UVC produces both PI-SOVs and electron–hole pairs.[31;61] Under UVA irradiation, an abrupt initial

CPD decrease is followed by gradual recovery even during continued exposure. This distinct behavior indicates that PI-SOV formation is the primary driver of the observed time-dependent CPD variations. Finally, no effect was detected under backside UVA irradiation, confirming that the surface remains inert under such conditions. The distinct effects of UVA and UVC irradiation on the surface potential of TiO_2 provide a pathway for rational defect and charge-state engineering. Controlled generation or suppression of PI-SOVs enables precise tuning of surface reactivity, charge separation, and adsorption dynamics. These insights can be directly applied to optimize TiO_2-based photocatalysts, enhance photoelectrochemical water-splitting efficiency, improve UV-assisted pollutant degradation, and develop stable, responsive optoelectronic or sensing interfaces.

In the final stage of the measurements, Au-NPs were drop-cast onto the TiO_2 surface, followed by back-side UVC irradiation to probe the time-dependent evolution of the CPD. Au-NPs, widely used to tailor photochemical activity, serve as an efficient electron trap, while the Au-NP / TiO_2 interface forms a Schottky barrier that acts as a hole trap and slows carrier diffusion.[26;52;94]

Although both Au NP–covered and bare TiO_2 regions exhibit qualitatively similar CPD dynamics under back-side UVC illumination, quantitative analysis reveals distinct kinetics. As shown in Figure 3.5, the stretched-exponential fitting of the CPD transients indicates slower and more strongly interacting processes in the Au NP–covered regions compared to bare TiO_2 regions being exposed to deionized water during decoration. Upon termination of illumination, both regions display comparable recovery behavior, suggesting that vacancy re-oxidation dominates the relaxation pathway in the dark.

The altered CPD dynamics in Au-NP–decorated TiO_2 reveal how interfacial charge transfer can be harnessed to optimize functional oxide performance. The Schottky barrier at the Au-NP / TiO_2 junction suppresses hole diffusion and prolongs charge separation, effectively stabilizing photoinduced oxygen vacancies and reshaping local band alignment. This interfacial control provides a powerful design strategy for improving photocatalytic and photoelectrochemical systems, where extended carrier lifetimes directly translate to enhanced reaction efficiencies.

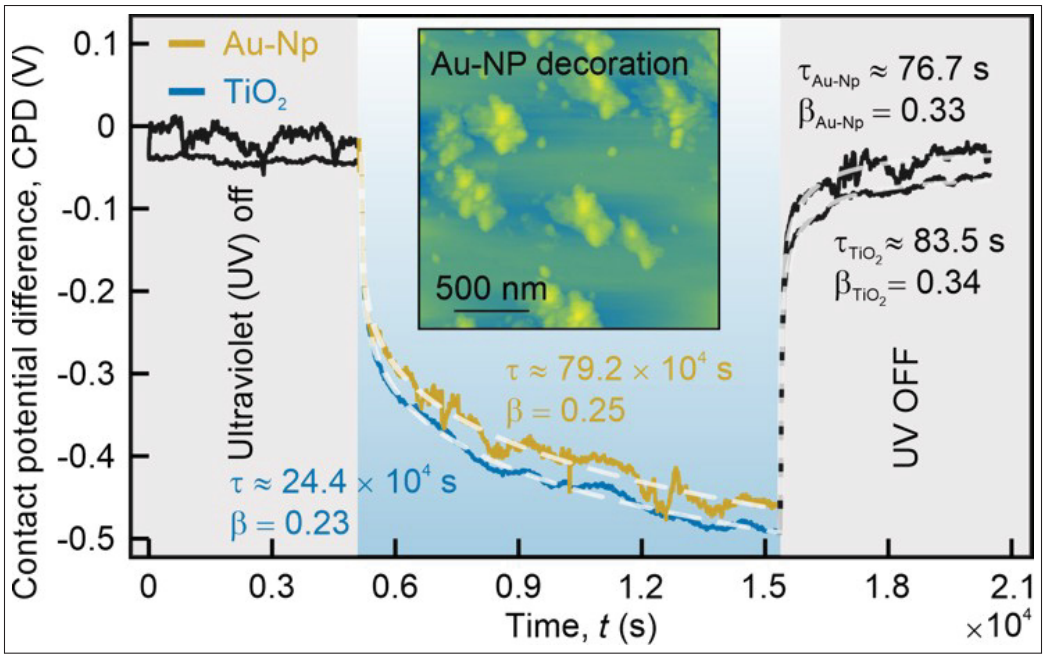

Figure 3.5 Effect of gold nanoparticle (Au-NP) decoration on the contact potential difference (CPD) dynamics of TiO_2 (100) under back-side high-energy ultraviolet irradiation

Both pristine and Au-NP-decorated TiO_2 exhibit qualitatively similar time-dependent CPD responses; however, the formation of a Schottky barrier at the Au-NP / TiO_2 interface induces interfacial band bending that suppresses hole diffusion into the bulk and promotes spatial charge separation and electron trapping at the metal–semiconductor junction. Following termination of irradiation, both regions exhibit comparable recovery dynamics, consistent with bulk recombination and surface charge relaxation processes. The inset shows the surface topography of the Au-NP-decorated TiO_2.

Moreover, the tunable charge-trapping behavior at metal–oxide interfaces offers new opportunities for engineering UV-responsive sensors, plasmonic catalysts, and hybrid optoelectronic devices with programmable surface energetics and defect dynamics.

3.5 Conclusions

By directly monitoring contact potential variations under controlled front- and back-side ultraviolet excitation, we reveal how illumination geometry and photon energy govern Fermi-

level dynamics in TiO_2. High-energy ultraviolet irradiation drives persistent photoinduced surface oxygen vacancies, whereas low-energy ultraviolet excitation induces only transient electron–hole generation with rapid recovery. The contrasting temporal and spatial behaviors expose the coupled kinetics of defect formation, carrier migration, and re-oxidation at the oxide surface.

Beyond clarifying the microscopic origin of Fermi-level shifts, these findings establish illumination geometry as a powerful handle for engineering charge states, carrier transport, and surface energetics in metal oxides. This framework enables rational defect and band-edge control for next-generation photocatalysts, sensors, and optoelectronic devices operating under ambient or operando conditions.

CONCLUSION AND RECOMMENDATIONS

Re-Statement of the Core Scientific Problem

The performance, stability, and functionality of modern metal oxide–based materials and devices are governed by processes that occur at the nanoscale and evolve over time. In systems such as titanium dioxide (TiO_2), electronic behavior is strongly influenced by the interplay between charge carrier transport, oxygen vacancy defects, surface energetics, and external stimuli including illumination, temperature, and electrical excitation. These processes are inherently spatially heterogeneous and temporally dynamic, often spanning length scales from nanometers to hundreds of micrometers and timescales from microseconds to seconds. Despite their central importance, direct experimental access to such coupled spatiotemporal phenomena remains limited.

Conventional characterization techniques typically provide either high temporal resolution with limited spatial specificity, or high spatial resolution under quasi-equilibrium conditions. Macroscopic electrical and optical measurements average over large areas and obscure local defect-driven behavior. Conversely, scanning probe techniques offer nanoscale spatial resolution but have historically emphasized static or steady-state properties. As a result, a fundamental gap persists in the ability to directly correlate local energetics with time-dependent charge carrier dynamics under nonequilibrium conditions.

This limitation is particularly critical in photoactive metal oxides, where ultraviolet irradiation can induce photoinduced surface oxygen vacancies (PI-SOVs), modify band alignment, alter migration barriers, and introduce history-dependent electrostatic behavior. The extent to which such defect-mediated processes penetrate into the bulk, interact collectively, and reshape local Fermi-level dynamics has remained incompletely understood. Furthermore, distinguishing slow

defect-mediated migration from fast electronic redistribution requires measurement approaches capable of resolving multiple timescales within the same nanoscale probing volume.

The core scientific problem addressed in this thesis is therefore the lack of a unified experimental framework capable of probing spatially resolved, time-dependent charge carrier dynamics and defect-mediated electronic processes in metal oxides across multiple timescales. Addressing this challenge requires integrating electrostatic sensitivity with time-resolved nanoscale measurements in order to bridge the gap between local energetics and dynamic transport behavior.

By developing and applying advanced electrostatic and time-resolved atomic force microscopy (TR-AFM) methodologies, this work aims to directly interrogate how oxygen vacancies, illumination geometry, excitation history, and thermal activation govern charge migration and Fermi-level evolution in TiO_2. Through this approach, the thesis seeks to establish a coherent framework for understanding and quantifying dynamic nanoscale electronic processes in functional oxide materials.

Integrated Synthesis of the Main Scientific Findings

This thesis systematically investigated nanoscale charge carrier dynamics and defect-mediated electronic processes in TiO_2 by integrating electrostatic and time-resolved atomic force microscopy techniques across multiple timescales. Rather than treating ultraviolet irradiation, defect formation, charge migration, and Fermi-level evolution as isolated phenomena, this work established a coherent experimental framework to correlate local energetics with dynamic transport behavior under nonequilibrium conditions.

Bulk Influence of Ultraviolet Irradiation and Defect Propagation

A central finding of this thesis is that high-energy ultraviolet (UVC) irradiation influences TiO_2 far beyond the conventionally assumed surface-limited region. Although optical transmission

measurements confirm that approximately 99% of incident UVC radiation is absorbed within the first tens of nanometers, time-resolved AFM measurements reveal that the electronic consequences of irradiation extend across hundreds of micrometers into the bulk. The observed monotonic reduction of the characteristic time constant τ^* with increasing back-side UVC illumination density demonstrates that photoinduced surface oxygen vacancies (PI-SOVs) alter charge migration dynamics throughout the crystal.

These results challenge the traditional assumption that UVC-induced modifications are confined to near-surface regions. Instead, the data indicate that defect-mediated processes can propagate or influence electronic behavior across macroscopic thicknesses. This finding has important implications for oxide-based devices in which TiO_2 functions as a charge transfer layer or ultraviolet protection layer, suggesting that irradiation-induced defect landscapes may impact bulk transport properties even when absorption is strongly surface-weighted.

Defect-Mediated Charge Migration and Collective Transport

Time-resolved AFM measurements further revealed that oxygen vacancy density strongly modulates charge carrier migration dynamics. The systematic decrease in τ^* with increasing UVC illumination density indicates attenuation of carrier mobility, consistent with enhanced trapping and modified migration barriers induced by increased vacancy concentration. Concurrently, the reduction of the stretching parameter β under high irradiation conditions signifies increasingly collective or cooperative carrier motion.

These observations establish a direct nanoscale link between defect concentration and transport dynamics. Rather than exhibiting single-exponential relaxation behavior, charge migration in TiO_2 follows stretched exponential kinetics, reflecting heterogeneous energy landscapes and correlated motion among carriers. Temperature-dependent measurements enabling extraction

of effective migration barriers further demonstrate that defect landscapes actively reshape the energetic pathways governing charge transport.

Together, these findings provide quantitative evidence that oxygen vacancies do not merely alter static electronic structure but fundamentally govern the time-dependent migration behavior of charge carriers at the nanoscale.

Multi-Timescale Carrier Dynamics: Separation of Slow and Fast Processes

A key methodological and scientific contribution of this thesis is the separation of slow defect-mediated migration processes from fast electronic redistribution dynamics. Conventional time-resolved AFM accessed carrier relaxation over millisecond-to-second timescales, primarily capturing polaron-mediated hole migration. In contrast, sub-microsecond time-resolved measurements enabled interrogation of rapid electronic responses following electrical excitation.

The ability to resolve both regimes within the same experimental framework demonstrates that charge dynamics in TiO_2 are intrinsically multi-timescale. Slow relaxation reflects thermally activated, defect-mediated transport, while fast responses correspond to immediate electronic redistribution and polarization effects. Distinguishing these processes is essential for constructing a physically meaningful model of charge transport in oxide semiconductors.

By bridging these temporal regimes, this thesis advances beyond steady-state characterization and provides a more complete representation of how electronic systems respond dynamically to external perturbations.

Fermi-Level Dynamics and Illumination Geometry Effects

Electrostatic AFM and Kelvin probe force microscopy measurements further revealed that local Fermi-level evolution is highly sensitive to illumination geometry, excitation history, and

interfacial conditions. Front-side, back-side, and simultaneous illumination configurations produce distinct contact potential difference (CPD) dynamics, indicating that defect generation and carrier redistribution are not solely functions of photon energy but also of spatial excitation pathways.

Moreover, the presence of metal–oxide interfaces modifies CPD evolution under irradiation, demonstrating that interfacial energetics strongly influence nonequilibrium charge redistribution. These findings highlight that Fermi-level dynamics in TiO_2 are governed by a complex interplay between defect formation, charge trapping, and geometric boundary conditions.

Collectively, the electrostatic and time-resolved measurements establish that nanoscale energetic landscapes and dynamic transport behavior are inseparable. Fermi-level shifts, defect concentration, and migration kinetics evolve together under external stimulation, reinforcing the need for integrated measurement strategies.

Unified Perspective

Taken together, the results of this thesis demonstrate that nanoscale charge carrier dynamics in TiO_2 are governed by three interconnected factors: defect distribution, excitation history, and measurement timescale. Ultraviolet irradiation reshapes defect landscapes; defect landscapes redefine migration barriers; and migration dynamics manifest across distinct temporal regimes. By experimentally correlating these elements, this work establishes a unified nanoscale framework linking defect physics, electrostatic energetics, and time-dependent charge transport in metal oxides.

Methodological Contributions and Scientific Impact

Beyond the specific findings related to TiO_2, this thesis makes methodological contributions that extend the capabilities of atomic force microscopy for studying functional materials under

nonequilibrium conditions. A central advancement of this work lies in the deliberate integration of electrostatic sensitivity with time-resolved measurement strategies to construct a unified nanoscale probing framework.

Establishing Time-Resolved AFM as a Quantitative Tool

While time-resolved atomic force microscopy has previously been employed to probe dynamic processes, it has often been used qualitatively to observe relaxation behavior. In this thesis, time-resolved AFM is implemented in a systematic and quantitative manner. By extracting characteristic time constants, stretching parameters, and effective migration barriers, the technique is elevated from a phenomenological imaging modality to a quantitative probe of carrier transport physics.

The use of stretched exponential analysis enables interpretation of heterogeneous relaxation dynamics and cooperative transport phenomena. Furthermore, temperature-dependent measurements allow extraction of effective activation energies, directly linking experimental observables to thermally activated migration processes. These methodological refinements demonstrate that time-resolved AFM can provide transport-relevant parameters at the nanoscale, bridging the gap between local measurements and macroscopic transport models.

Bridging Slow and Fast Temporal Regimes

A significant methodological contribution of this thesis is the implementation of sub-microsecond time-resolved AFM through real-time cantilever signal analysis. By processing the instantaneous phase of the cantilever oscillation, rapid electronic redistribution processes are resolved without reliance on conventional phase-locked loop demodulation. This approach enables access to dynamic behavior that is typically obscured in standard AFM measurements.

The ability to probe both slow defect-mediated migration (milliseconds to seconds) and fast electronic redistribution (microseconds) within a single experimental framework represents a substantial expansion of AFM temporal capability. This multi-timescale strategy provides a more comprehensive view of charge carrier dynamics and establishes a blueprint for future nanoscale dynamic investigations in semiconductors and oxides.

Correlating Energetics with Transport at the Nanoscale

By combining Kelvin probe force microscopy with time-resolved electrostatic measurements, this thesis establishes a direct experimental correlation between local Fermi-level evolution and charge carrier migration dynamics. Rather than treating energetic mapping and dynamic transport measurements independently, this work demonstrates that they must be interpreted collectively.

This integrated approach provides a pathway toward operando-like nanoscale characterization of functional materials. It enables direct observation of how illumination geometry, defect generation, and excitation history reshape both energetic landscapes and transport kinetics. Such correlation is critical for advancing defect engineering strategies in oxide electronics, photocatalysis, and energy conversion devices.

Advancing Nanoscale Characterization of Functional Oxides

The methodological framework developed in this thesis extends beyond TiO_2 and is broadly applicable to a wide class of metal oxides and semiconductor materials. Systems such as $SrTiO_3$, $KTaO_3$, and other defect-sensitive oxides exhibit similar coupling between vacancy formation, charge transport, and electrostatic behavior. The experimental strategies demonstrated here provide a transferable toolkit for investigating such materials under controlled external stimuli.

Importantly, this work shifts the role of atomic force microscopy from static surface imaging toward dynamic nanoscale transport characterization. By integrating electrostatic detection, controlled excitation, and multi-timescale resolution, the thesis contributes to redefining AFM as a powerful platform for studying coupled spatiotemporal electronic phenomena.

Potential Applications and Broader Impact

The potential applications of this thesis can be broadly categorized into three main directions. First, although TiO_2 was specifically considered as the model sample system, the methodologies used in this thesis can be extended to many other material systems, particularly those in which high-resolution mapping of charge carrier dynamics and light–matter interactions is important. The combination of time-resolved AFM, electrostatic force detection, and KPFM-based surface-potential mapping provides a powerful framework for studying local charge redistribution, defect-mediated transport, and photoinduced electronic processes. Therefore, beyond TiO_2, similar approaches could be applied to emerging photovoltaic materials, solar-cell interfaces, ion-battery materials, oxide semiconductors, and other functional materials where the interaction between charge carriers, defects, and optical or ultraviolet excitation strongly affects device performance.

Second, for TiO_2 itself, the results of this thesis provide deeper insight into the role of photoinduced oxygen vacancies in controlling charge carrier dynamics, surface energetics, and light-induced material response. Since many applications of TiO_2 are based on its interaction with light, including photocatalysis, photoelectrochemical energy conversion, UV photodetection, and oxide-based optoelectronic devices, the knowledge gained from this work can support better engineering of TiO_2-based materials and devices. In particular, this thesis shows that photoinduced oxygen vacancies, which may contribute to degradation pathways in light-absorbing materials, can influence charge carrier dynamics at depths greater than previously expected. This understanding can help guide the redesign of TiO_2-based solar cells, photocatalytic coatings, and

UV-sensitive devices with the goal of improving stability, reducing degradation, and extending operational lifetime.

Third, the unexpectedly large effective penetration depth of UV-induced effects in TiO_2 may also be viewed as a potential advantage when considered from a sensing perspective. Although only a limited fraction of ultraviolet light penetrates through TiO_2, this thesis shows that such penetration can still significantly modify charge carrier dynamics at the opposite surface. This finding suggests a possible concept for indirect or remote UV sensing in enclosed environments. For example, UV-generating chambers are used in applications such as UV/ozone cleaning, photochemical processing, germicidal irradiation, and water-treatment reactors, where direct access to the internal environment may be limited or undesirable. In a possible sensing configuration, a TiO_2 layer could be placed as part of the chamber boundary, with one side exposed to the internal UV environment and the opposite side accessible from outside the chamber. By continuously monitoring the charge carrier dynamics or surface-potential response from the external side, it may be possible to infer the presence or intensity of UV radiation inside the chamber without direct optical access. While this concept would require further calibration, device-level design, and validation, the results of this thesis provide a physical basis for considering TiO_2 as an active platform for indirect UV detection and environmentally isolated sensing applications.

Scientific Impact

Collectively, the methodological advances presented in this thesis contribute to closing the long-standing gap between high spatial resolution and high temporal sensitivity in nanoscale characterization. The framework developed herein enables systematic interrogation of defect-mediated electronic processes under nonequilibrium conditions and provides quantitative insight into migration barriers, cooperative transport, and Fermi-level dynamics.

By establishing this integrated experimental strategy, the thesis not only advances understanding of TiO_2 but also contributes to the broader field of nanoscale materials characterization. It lays the groundwork for future investigations aimed at coupling local electrostatic energetics with dynamic charge transport in functional materials and device architectures.

Future Research Directions

The methodological developments presented in this thesis open several important research directions aimed at advancing time-resolved atomic force microscopy (TR-AFM) beyond its current operational limits. While the present work established a framework for correlating electrostatic energetics with dynamic charge transport phenomena across multiple timescales, a natural next step involves refining and optimizing the measurement platform itself in order to approach fundamental sensitivity and temporal limits.

A primary direction of ongoing research concerns the systematic optimization of Fast Free Time-Resolved Atomic Force Microscopy (FF-TR-AFM) for enhanced signal-to-noise performance. In contrast to conventional frequency-modulated TR-AFM approaches, the effectiveness of FF-TR-AFM is not fundamentally constrained by hardware electronics but is instead governed by the mechanical properties of the cantilever and the selection of experimental parameters. This characteristic provides an opportunity: rather than accepting instrument limitations, the method can be deliberately engineered and tuned to maximize performance.

Previous optimization efforts have largely focused on improving temporal resolution. However, for emerging nanoscale applications, sensitivity to extremely small electrostatic forces is equally critical. When probing migration processes involving only a few charge carriers, the forces acting on the cantilever become minute and can easily be obscured by thermal noise, damping, or signal processing artifacts. Enhancing detectability under such conditions requires systematic investigation of how cantilever stiffness, resonance frequency, oscillation amplitude,

tip–sample separation, excitation magnitude, and post-processing strategies collectively influence measurement fidelity. Optimization must therefore be treated as a constrained multiparameter engineering problem rather than a single-variable adjustment.

A more ambitious trajectory aims to push TR-AFM toward the detection of migration events involving only a few, or potentially individual, charge carriers. In conventional bias-driven measurements, the number of participating carriers scales with the excitation amplitude and the effective nano-capacitive coupling beneath the tip. Reducing excitation to involve fewer carriers necessarily reduces the magnitude of the Coulomb force acting on the cantilever, thereby challenging detectability. Achieving reliable detection at this limit requires simultaneous optimization of mechanical design, excitation protocols, and signal analysis. If successful, such capability would represent a conceptual shift for scanning probe microscopy, enabling interrogation of discrete electronic events rather than ensemble-averaged transport behavior.

Beyond parameter optimization, an additional and potentially transformative research direction involves the integration of machine learning methodologies into dynamic AFM signal analysis. The governing equation of motion of the AFM cantilever under transient electrostatic forcing is inherently nonlinear and, in many experimentally relevant regimes, does not admit closed-form analytical solutions. When forces are both rapidly time-varying and extremely small in magnitude, extracting the underlying force profile from the measured cantilever response becomes an inverse problem of considerable complexity.

Theoretically, the mechanical bandwidth and sensitivity of AFM are sufficient to respond to such fast and weak forces. However, experimental methodologies capable of reliably decoding these signals have not yet been fully realized. Machine learning techniques offer a promising pathway to bridge this gap. Rather than attempting to derive analytical inversion formulas, a data-driven approach may be employed in which known transient forces with varying amplitudes and time constants are systematically applied in controlled experiments or high-fidelity simulations. The

resulting cantilever responses can then be used to train models that learn the mapping between dynamic force characteristics and measurable tip motion.

Such models would effectively serve as physics-informed inversion engines, capable of estimating force amplitude, temporal profile, or decay constant directly from complex cantilever dynamics. Importantly, this approach does not replace physical modeling but augments it: the governing mechanical equations provide the structure of the problem, while machine learning addresses regimes where analytical inversion becomes intractable. By combining mechanistic simulation with data-driven inference, it may become possible to recover information about ultrafast and weak transient forces that are currently obscured within noisy experimental signals.

In the longer term, the convergence of mechanical optimization and intelligent signal reconstruction could significantly enhance both temporal and effective spatial resolution in TR-AFM. Improved decoding of transient force signatures would allow finer discrimination of localized charge redistribution events, potentially enabling experimental exploration of defect-level transport phenomena at unprecedented scales.

More broadly, continued development along these directions may redefine the role of atomic force microscopy in functional materials research. Rather than serving primarily as a static surface characterization tool, AFM can evolve into a dynamically optimized and computationally enhanced platform for resolving transient nanoscale electronic events. By systematically improving mechanical design, excitation strategies, signal processing, and data-driven inversion techniques, future work aims to approach the fundamental measurement limits of nanoscale electrostatic force detection.

Achieving these objectives would not only advance TR-AFM methodology but also enable new classes of experiments targeting discrete carrier migration, localized defect interactions, and ultrafast electrostatic phenomena. Such progress would contribute to bridging the gap between

nanoscale experimental probing and microscopic transport theory, opening pathways toward fundamentally new insight into dynamic processes in complex material systems.

APPENDIX I

SUPPLEMENTAL INFORMATION OF THE ARTICLE "ULTRAVIOLET IRRADIATION PENETRATION DEPTH ON TIO_2"

Bugrahan Guner[1,4] , Mohammad Safikhani-Mahmoudi[1,4] , Fengmiao Li[2,3] , Ke Zou[2,3] , Omur E. Dagdeviren[1]

[1]Department of Mechanical Engineering, École de technologie supérieure, 1100 Notre-Dame Ouest, Montréal, Québec, Canada H3C 1K3
[2]Department of Physics and Astronomy, University of British Columbia, 6224 Agricultural Road, Vancouver, BC, Canada V6T 1Z1
[3]Quantum Matter Institute, University of British Columbia, 6224 Agricultural Road, Vancouver, BC, Canada V6T 1Z1
[4]These authors contributed equally.

Article published in *Communications Chemistry*, 8, 83 (2025).
DOI: https://doi.org/10.1038/s42004-025-01487-1

1. X-ray Diffraction Measurements

X-ray diffraction (XRD) measurements were performed by employing a PANalytical X'Pert PRO, which was operated with a Co X-ray source with Co Kα_1 (λ = 1.78901 Å) and Co Kα_2 (λ = 1.7929 Å) emitted with an intensity ratio (Kα_2 / Kα_1) of 0.5 at a resolution of 0.0167° by employing a generator voltage of 45 kV and tube current of 40 mA at 200 seconds per step sampling rate. Figure I-1 shows the XRD measurements of the single-crystal TiO_2 sample. The supplier, MSE Supplies LLC, reported that the TiO_2 crystal has (100) orientation, confirmed by our XRD measurements, revealing a sharp, intense peak at $2\theta \approx 46°$ [165;166] Due to destructive interference (a.k.a., systematic absence), the (100) peak of TiO_2 is suppressed.[166] A second peak is visible at $2\theta \approx 42°$, corresponding to the (101) plane; however, it has two orders of magnitude less intensity than the (200) peak.[165;167–169] The powder form of rutile would ordinarily give (110) and (101) the most intense peaks.[165;167–169] However, these peaks are absent relative to the (200) peak These observations support the supplier report of the (100) surface. The lattice constant corresponding to the most dominant peak, i.e., (200), is calculated

as 4.5786 Å, while the tetragonal lattice constant ($a = b \neq c$) of rutile TiO_2 is $a = 4.5937$ Å.[170]

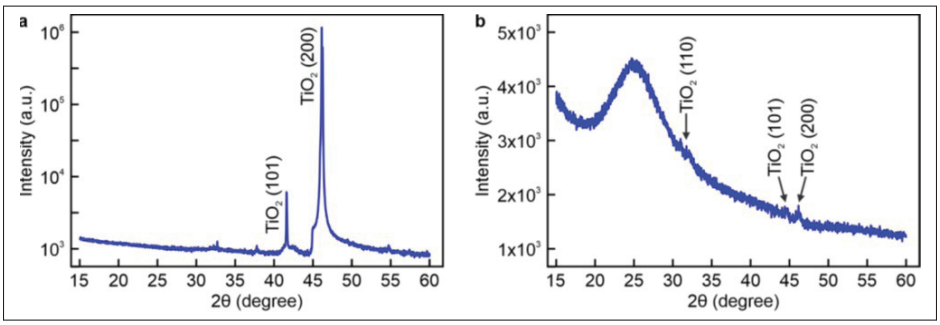

Figure-A I-1 X-ray diffraction (XRD) measurements of single crystal TiO_2 and 46-nm thick TiO_2 film grown on quartz

(a, b) TiO_2 single crystal has a dominant peak while thin film has a background due to the quartz substrate and demonstrates multiple crystallographic directions. We did not observe any trace of anatase in either sample.

Figure I-1b shows the XRD measurement of 46-nm thick, polycrystalline TiO_2 film on the quartz substrate. The XRD data has a background due to the quartz substrate, e.g., ~25° peak, which is consistent with the literature.[31] Distinct reflections appear around 31°, 44°, and 46°, which are relevant with polycrystalline rutile TiO_2, specifically the (110), (101), and (200) planes.[165;167–169] The thin-film nature (~46 nm) and polycrystalline microstructure cause these peaks to be broad and low-intensity, in contrast to the stronger reflections typically observed in bulk.[171] We did not observe characteristics of anatase, indicating that the film is predominantly rutile.

APPENDIX II

SUPPLEMENTAL INFORMATION OF THE ARTICLE "TIME-RESOLVED MAPPING OF CHARGE CARRIER DYNAMICS AND DEFECT-MEDIATED MIGRATION BARRIERS IN TIO_2"

Bugrahan Guner[1] , Mohammad Safikhani-Mahmoudi[1] , Omur E. Dagdeviren[1]

[1]Department of Mechanical Engineering, École de technologie supérieure, 1100 Notre-Dame Ouest, Montréal, Québec, Canada H3C 1K3

Article published in *Journal of Physical Chemistry C*, 129, 16879–16886 (2025).

1. Surface topography of the TiO_2 (100) single crystal

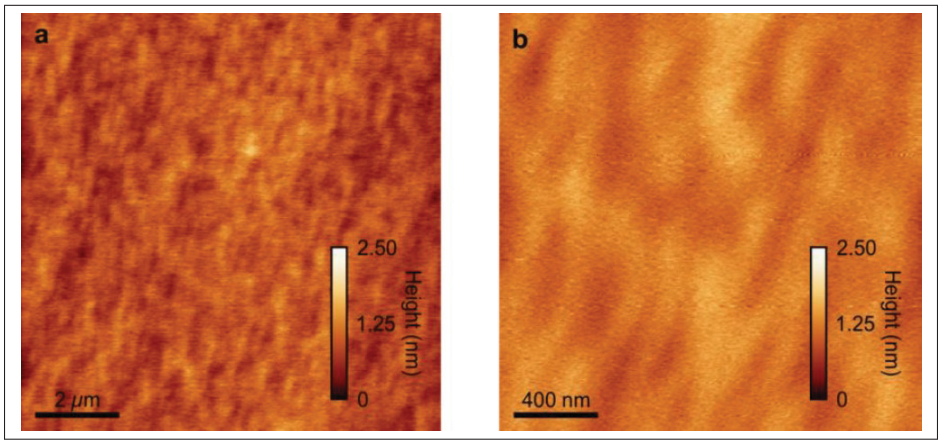

Figure-A II-1 High-resolution characterization of the TiO_2 (100) sample via atomic force microscopy (AFM) imaging. (a, b) AFM-based topography images (raw, flattened data) show that the TiO_2 surface is free of carbon clusters and atomically flat. The surface roughness was measured as ~0.20 nm and ~0.17 nm in (a) and (b), respectively..

2. Effect of surface irradiation on contact potential difference measurements

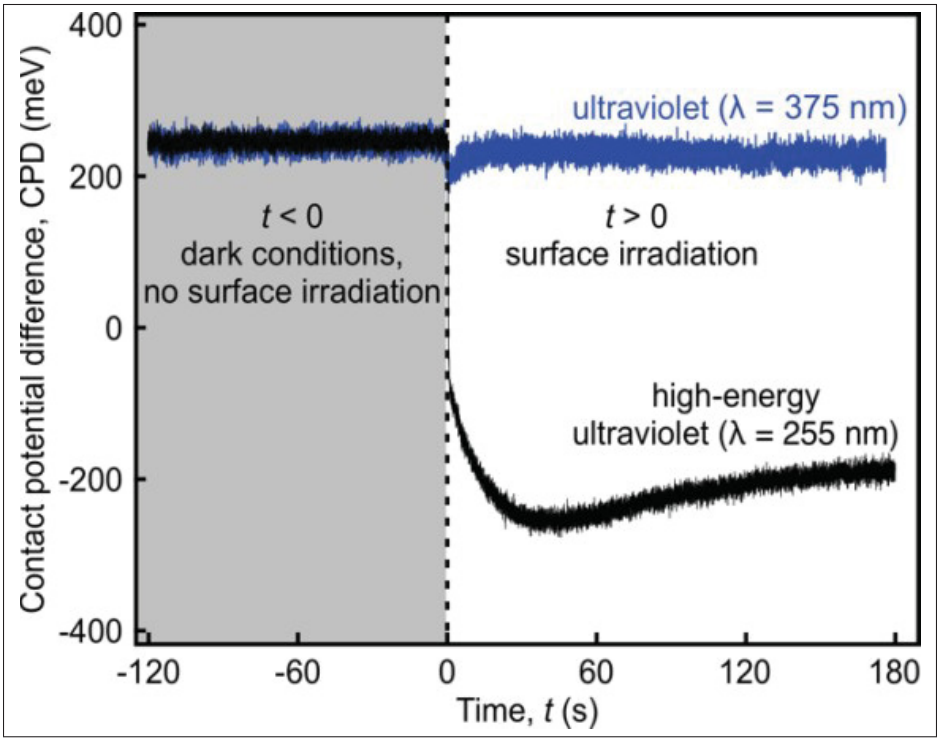

Figure-A II-2 Effect of ultraviolet (UV, λ = 375 nm) and high-energy ultraviolet (UVC, λ = 255 nm) surface irradiation on the contact potential difference (CPD) as a function of time, t, for the TiO_2 (100) surface

Under dark conditions ($t < 0$), the surface exhibits a CPD value of 244 ± 10 meV. Upon UV irradiation, the CPD changes marginally by ~16 meV under steady-state conditions. In contrast, UVC irradiation modifies CPD almost instantaneously with a shift of ~ −450 meV, indicating a substantial modification of the surface electronic structure. These results confirm that the observed variations in charge carrier dynamics are specific to UVC irradiation and are consistent with the formation of photo-induced surface oxygen vacancies, in agreement with previous reports.

3. Combinations of experimental parameters

We investigated the effects of spatial and temporal variations in charge carrier migration as a function of surface irradiation and sample temperature using both conventional and sub-microsecond time-resolved atomic force microscopy (TR-AFM) techniques. As illustrated in Figure 1.3, we systematically explored different combinations of external stimuli. For instance, to assess the local heterogeneity of charge carrier dynamics, we performed measurements at 64+ distinct locations across the TiO_2 (100) sample. To probe the influence of residual electric fields on migration behavior, we applied sequences of electric pulses with varying pulse delay times (Δt). Additionally, the spatial extent of history-dependent migration was characterized by increasing the distance between successive pulses (Δd) while maintaining a constant delay. Finally, we investigated the response of charge carrier migration under varying surface irradiation densities and temperatures to elucidate the coupling between photo-induced defect formation and thermally activated migration dynamics.

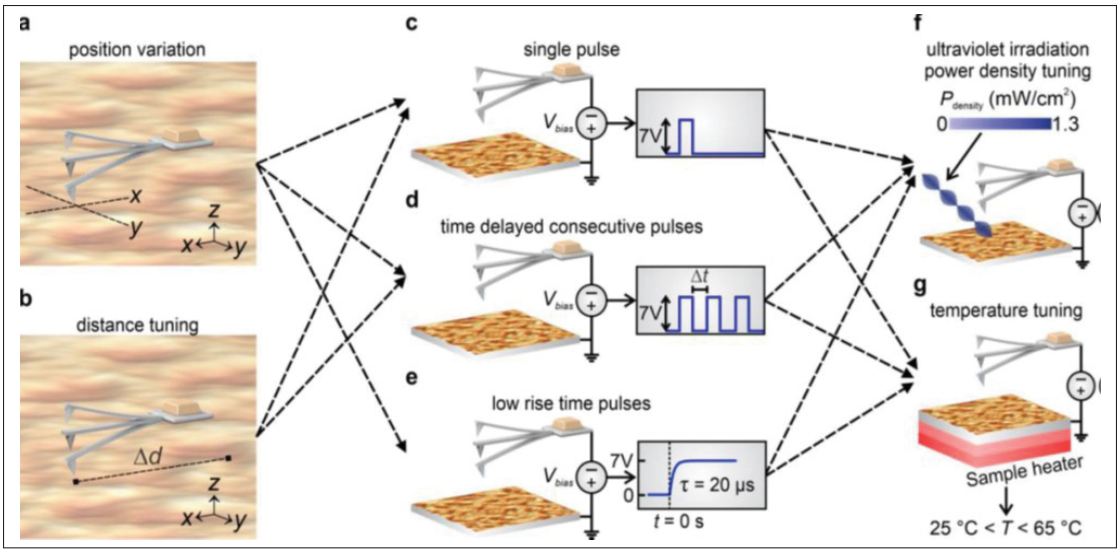

Figure-A II-3 Schematic representation of the experimental conditions explored in this work

We performed measurements at different sample locations (a) and varied the spatial separation of excitations to probe distance-dependent residual effects, i.e., history dependence (Δd) (b). Different bias waveforms were applied to excite charge carriers (c), induce history dependence (Δt) (d), and enable sub-microsecond time-resolved atomic force microscopy measurements (e). Surface irradiation (f) and temperature (g) were systematically altered to study photo-induced and thermally activated processes.

4. The spatial extent of history-dependent migration under high-energy surface irradiation

We performed conventional time-resolved atomic force microscopy (TR-AFM) measurements to investigate the spatial extent of history-dependent charge carrier migration under high-energy ultraviolet (UVC) surface irradiation for a time delay of 100 ms. A comparison between Figure II-4 and Figure 2.5 in the main text reveals no systematic change in the spatial extent of history-dependent migration under UVC exposure. This observation indicates that residual electric fields persist over several hundred nanometers even with surface irradiation, suggesting that UVC irradiation does not significantly suppress the long-range memory effects in charge migration.

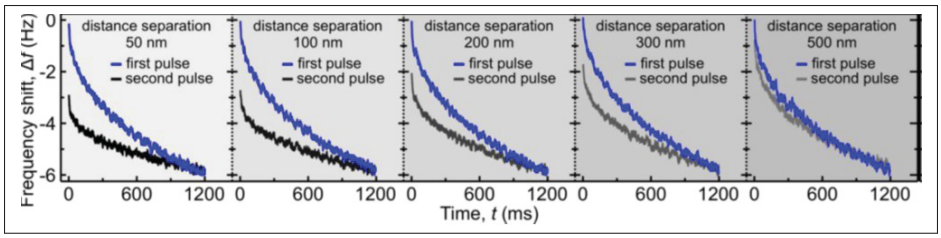

Figure-A II-4 Time-resolved atomic force microscopy measurements illustrating the spatial extent of history-dependent charge carrier migration on a TiO_2 (100) surface under high-energy ultraviolet (UVC) irradiation

Successive pulses were applied with increasing lateral distances, while the pulse delay time was kept constant at 100 ms. The observed variation shows that temporal correlations in the migration dynamics persist over several hundred nanometers, gradually attenuating with distance. This spatial memory effect suggests that local electric fields and defect-mediated trapping persist/influence charge migration beyond the immediate vicinity of the applied bias voltage under UVC irradiation.

APPENDIX III

SUPPLEMENTAL INFORMATION OF THE ARTICLE "DEFECT- AND GEOMETRY-CONTROLLED FERMI-LEVEL DYNAMICS IN TIO_2"

Mohammad Safikhani-Mahmoudi[1] , Nuray Basaran[1] , Bugrahan Guner[1,2] , Tugce Hacaloglu[1] , Omur E. Dagdeviren[1]

[1]Department of Mechanical Engineering, École de technologie supérieure,
1100 Notre-Dame Ouest, Montréal, Québec, Canada H3C 1K3
[2]Department of Mechanical Engineering, Yale University,
New Haven, Connecticut 06520, USA

Article under review in *Advanced Materials*.

1. Preparation of the TiO_2 single crystal

We used an undoped, single crystal TiO2 (100) sample (provided by MSE Supplies LLC). We employed a well-established sample preparation routine:[26;28;31] the single crystal TiO2 (100) was annealed for 10 hours at 1000 °C, with 3-hour heat-up and cool-down periods. This annealing process led to a rutile-terminated surface,[31] with an atomically flat sample surface and free from carbon clusters. Even though the TiO2 (110) surface is more stable[40;134], we employed TiO2 (100) to null potential variations in coordination number, which can be induced by differences in titanium atom coordination. TiO2 (110) has five- or six-coordinated Ti atoms, while in TiO2 (100), Ti atoms are solely five-coordinated, eliminating ambiguity associated with coordination number variation.[135] Finally, a rutile termination was preferred over anatase, as anatase termination is more susceptible to adsorbates at ambient conditions, particularly under surface irradiation.[45;130]

2. Surface irradiation

High-energy ultraviolet (UVC) irradiation was provided by a fixed-wavelength light-emitting diode (LED) source (λ = 255 nm; OP255-10P-SM, Crystal IS), while low-energy ultraviolet (UVA) irradiation employed a 375 nm LED (LED375L, Thorlabs). Identical UVC and UVA

diodes were used for both front- and back-irradiation measurements. For back-illumination experiments, the ultraviolet sources were optically shielded such that the sample surface was irradiated exclusively through the cavity beneath the substrate. The transmitted power density was monitored using a photodiode power sensor (Slim Photodiode Power Sensor, S130VC, Thorlabs), maintaining a constant sensor-to-sample distance across all measurements. The optical setup was fully enclosed to eliminate stray light, ensuring uniform illumination over the entire backside of the sample.

The ultraviolet diodes were mounted on a stainless-steel heat sink equipped with an embedded thermocouple (PT-1000, temperature resolution 0.01 °C) positioned directly beneath the LEDs. The maximum power dissipation of the diodes was 0.8 W, and no measurable temperature variation was observed during operation. Laboratory environmental conditions were maintained at 19.6 ± 0.4 °C and 38 ± 3 % relative humidity with active temperature and humidity control. No ultraviolet-dependent variation in cantilever sensitivity or calibration was detected, as verified independently and described elsewhere.

3. Experimental setup

Kelvin probe force microscopy (KPFM) measurements were performed using a customized VEECO EnviroScope system.[9] The microscope was customized with additional hardware, including a high-voltage amplifier, a lock-in amplifier with phase-locked loop (PLL) capability (MFLI, Zurich Instruments), and a new control unit, while retaining the environmental control features of the original system. Moreover, the microscope was operated using the Gnome X Scanning Microscopy (GXSM) software package,[172] equipped with active drift control. For all measurements, we employed gold-coated microcantilever tips (OPUSTIPS 4XC-GG) with a nominal stiffness of ~9.0 N/m, a resonance frequency of ~150 kHz, and a tip radius of < 30 nm. The cantilever oscillation amplitude was adjusted for ~10 nm (peak-to-peak).

We conducted off-resonance amplitude-modulated KPFM measurements.[15;74;76] In this method, the cantilever is driven near its primary mechanical resonance frequency (~150 kHz for our

case) to acquire topographical data, while a combined alternating and constant bias is applied between the tip and the sample to probe electrostatic interactions. This bias induces a modulated electrostatic force at a secondary frequency (e.g., 3 kHz), which is well-separated from the cantilever's resonance to minimize crosstalk between topographic and electrostatic channels. The low-frequency response, demodulated via lock-in detection, is used to extract the contact potential difference (CPD). The frequency separation between these signals enables simultaneous acquisition of topography and CPD in a single-pass scan, eliminating the need for a secondary lift pass.

4. Preparation and the deposition of gold nanoparticles

Gold nanoparticles (Au-NPs) were deposited on TiO_2 (100) using a previously reported method,[26] summarized here for completeness. Citrate-stabilized Au-NPs (nominal diameter $\approx$ 40 nm; Sigma-Aldrich, PubChem SID 329765547) were first functionalized with 4-mercaptobenzoic acid (4-MBA; Tokyo Chemical Industry, CAS 1074-36-8). The functionalization was carried out by mixing the Au-NP dispersion with 4-MBA under gentle stirring, followed by centrifugation at 5000 rpm for 10 min to remove excess ligands. The precipitate was washed with deionized water and redispersed to obtain the purified Au-NP suspension. ~3 μL of the suspension was drop-cast onto the TiO_2 (100) substrate using a micropipette. The sample was then placed on a preheated hot plate at 100 °C for ~30 s to evaporate the solvent and ensure uniform nanoparticle adhesion. As presented in Figure 3.5 of the main text, the deposition was visible and justified by topography measurements.

5. Successive front-side low-energy ultraviolet (UVA) and back-side high-energy ultraviolet (UVC) irradiations

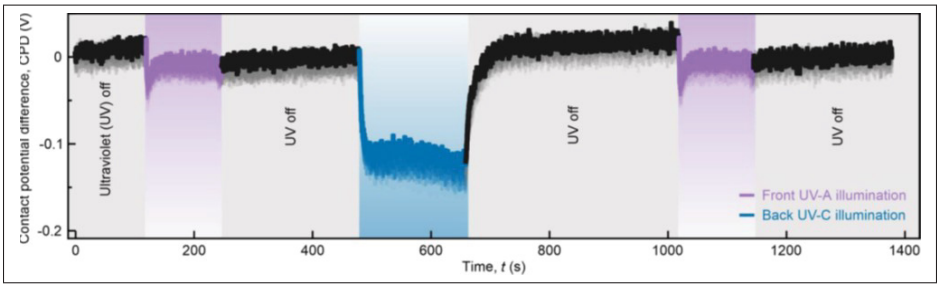

Figure-A III-1 Time-dependent contact potential difference (CPD) response of TiO_2 (100) under successive front-side UVA (purple curve), back-side (blue curve) UVC, and successive front-side UVA illumination

Front UVA illumination produces an instantaneous CPD drop followed by a recovery, whereas back UVC illumination yields a monotonic, stretched-exponential decay, as explained in detail in the main text. Successive front UVA illumination followed by back-UVC ensures the repeatability of the effect of the front-side UVA illumination. Data from nine independent measurements are presented in this figure, with solid lines representing the averaged response.

APPENDIX IV

SUPPLEMENTAL INFORMATION: DETAILED MEASUREMENT PARAMETERS FOR KPFM METHOD

Several established KPFM implementations were considered before selecting the CPD measurement method used in this thesis, including AM lift-mode KPFM, AM second-eigenmode KPFM, off-resonance AM-KPFM, FM sideband KPFM, and FM heterodyne KPFM. The main goal of the KPFM measurements was to continuously monitor changes in the contact potential difference (CPD) during UV illumination. Therefore, the selected method had to provide stable CPD tracking over time, minimize measurement noise, and remain compatible with the available instrumental configuration.

Methods requiring high-frequency excitation or detection were less suitable under the present setup because they produced noisier responses and lower reproducibility for long-duration CPD monitoring. Although FM sideband KPFM is attractive because of its high signal-to-noise capability, it requires dual-frequency excitation/detection and additional lock-in amplifier functionality, which was not available in the current experimental configuration. Lift-mode KPFM was also not ideal because the increased tip–sample distance during the second pass can weaken the electrostatic signal, reduce spatial sensitivity, and limit continuous monitoring of CPD variations during illumination. Based on these considerations, off-resonance AM-KPFM was selected as the most practical and reliable method for the UV-dependent CPD measurements performed in this thesis. The rationale for this selection is summarized in Table IV-1.

The CPD values obtained using off-resonance AM-KPFM were further cross-checked through an independent DC-bias sweep measurement. In this verification test, the tip–sample configuration was kept fixed while the applied DC bias was varied incrementally, and the corresponding Z-piezo response was monitored. Under the present feedback configuration, the lowest Z-piezo response was observed near the electrostatic compensation condition. The corresponding bias value was compared with the CPD measured by off-resonance AM-KPFM, and the values

Table-A IV-1 Excitation and detection requirements of the KPFM methods considered in this thesis.

Method	Electrical excitation	Electrical detection	Feedback condition	Main limitation for this thesis	Used
AM lift-mode KPFM	$\omega_E = \omega_0$	ω_0	$X(\omega_0) = \min$	Requires a second lifted scan, which increases the tip–sample distance, weakens the electrostatic signal, and is less suitable for continuous monitoring of CPD changes during UV illumination.	×
AM second-eigenmode KPFM	$\omega_E = \omega_1$	ω_1	$X(\omega_1) = \min$	Requires excitation and detection at a higher cantilever eigenmode. Under the available setup, this high-frequency operation produced a noisier response and lower reproducibility.	×
Off-resonance AM-KPFM	$\omega_E \ll \omega_0$	ω_E	$X(\omega_E) = \min$	Selected because it allows CPD detection at a low off-resonance modulation frequency, provides stable contrast, and is suitable for continuous monitoring of UV-dependent CPD changes.	✓
FM sideband KPFM	$\omega_E \ll \omega_0$	$\omega_0 \pm \omega_E$	$X(\omega_0 + \omega_E) - X(\omega_0 - \omega_E)$	Requires sideband detection near the cantilever resonance and, depending on implementation, detection of one or both sidebands. This increases frequency-domain complexity and requires additional lock-in capability.	×
FM heterodyne KPFM	$\omega_E = \omega_1 - \omega_0$	ω_1	$X(\omega_1) = \min$	Requires multi-frequency excitation/detection involving different cantilever modes. The additional instrumental and software complexity was not necessary for the CPD trends investigated here.	×

Here, ω_E is the electrical modulation frequency, ω_0 is the first cantilever resonance frequency, and ω_1 is a higher cantilever eigenmode. The term X represents the in-phase component of the detected oscillation response used for CPD feedback. Off-resonance AM-KPFM was selected because it allowed continuous CPD detection at a low off-resonance modulation frequency, while avoiding lift-mode operation, higher-eigenmode excitation, and multi-frequency sideband or heterodyne detection.

obtained from the two approaches were in acceptable agreement. This agreement supports the reliability of the selected method under the experimental conditions used in this thesis.

In addition, the CPD contrast obtained with off-resonance AM-KPFM was sufficiently clear and reproducible for resolving local surface-potential variations, including those associated with Au nanoparticle-decorated TiO_2 surfaces.

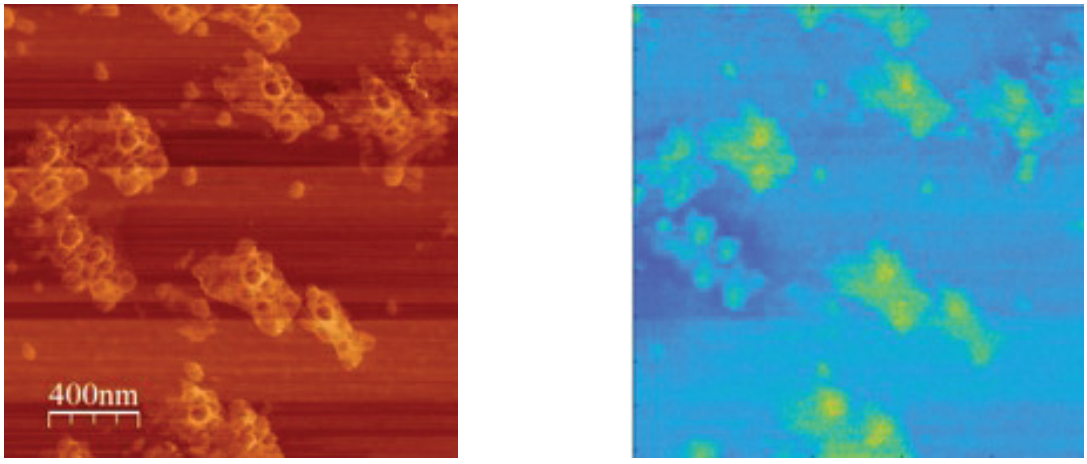

Figure-A IV-1 Representative off-resonance AM-KPFM measurement on Au nanoparticle-decorated TiO_2

(a) AFM topography image showing Au nanoparticles distributed on the TiO_2 surface. (b) Corresponding CPD map acquired from the same region using off-resonance AM-KPFM. The CPD image shows clear spatial contrast.

To explicitly detail the instrumental configuration used to achieve this contrast, the system parameters and probe specifications are documented below.

All measurements were performed using commercially available, overall gold-coated multiprobe cantilevers (Model 4XC-GG, OPUS). The specific cantilever utilized for these experiments had a manufacturer-specified nominal spring constant of 9 N/m and a nominal resonance frequency of 150 kHz. It should be noted that these are nominal values, and the exact operational mechanical properties may vary slightly in practice.

During these ambient measurements, single-pass, off-resonance amplitude modulation KPFM (AM-KPFM) was employed to continuously monitor the contact potential difference (CPD) while simultaneously maintaining active topographic feedback. Unlike standard two-pass lift-mode techniques, the tip remained engaged with the surface throughout the measurement, avoiding spatial resolution degradation.

We observed that actively nulling the CPD during imaging noticeably enhanced the topographic contrast. By monitoring the Z-piezo extension, we found that the tip moved closer to the sample surface upon engaging the KPFM feedback loop. This behavior provides direct evidence for the successful suppression of long-range attractive electrostatic forces between the tip and sample. Consequently, with the electrostatic contribution minimized, the topographic feedback was primarily governed by short-range van der Waals interactions, resulting in higher fidelity surface tracking and improved image resolution. The detailed instrumental parameters for both the physical probe and the software controllers are summarized in Table IV-2.

Table-A IV-2 Detailed probe specifications and instrumental parameters for single-pass off-resonance AM-KPFM.

Subsystem	Parameter	Value
Probe Specifications	Probe Model	OPUS 4XC-GG
	Coating	Overall Gold (Au)
	Nominal Spring Constant (k)	9 N/m
	Nominal Resonance Freq. (f_0)	150 kHz
Topography (AFM)	Microscope Mode	Tapping (AM)
	Scan Rate	0.100 Hz
	Resolution (Pixels)	512×512
	Amplitude Setpoint	0.3118 V
	Proportional Gain (P)	0.5000
	Integral Gain (I)	0.2000
	Drive Amplitude	20.60 mV
KPFM Modulation (LIA)	AC Modulation Voltage (V_{ac})	1.500 V (pk)
	AC Modulation Frequency (f_{mod})	3.000 kHz
	LIA Filter Bandwidth	50.00 Hz
	LIA Filter Order	4
KPFM Feedback (PID)	Control Mode	Amplitude Nulling (Demod X)
	Proportional Gain (P)	+816.3375
	Integral Gain (I)	$+182.086 \times 10^3$ s^{-1}

BIBLIOGRAPHY

[1] William D. Callister Jr and David G. Rethwisch. *Materials science and engineering: an introduction*. John wiley & sons, 2020.

[2] G. B. Olson. Computational Design of Hierarchically Structured Materials. *Science*, 277(5330):1237–1242, August 1997.

[3] Max Born and Emil Wolf. *Principles of optics: electromagnetic theory of propagation, interference and diffraction of light*. Elsevier, 2013.

[4] Gabor A. Somorjai and Yimin Li. *Introduction to surface chemistry and catalysis*, volume 2. Wiley New York, 1994.

[5] Yang Leng. *Materials characterization: introduction to microscopic and spectroscopic methods*. John Wiley & Sons, 2013.

[6] G. Binnig, C. F. Quate, and Ch. Gerber. Atomic Force Microscope. *Physical Review Letters*, 56(9):930–933, March 1986.

[7] Ernst Meyer, Roland Bennewitz, and Hans J. Hug. *Scanning Probe Microscopy: The Lab on a Tip*. Graduate Texts in Physics. Springer International Publishing, Cham, 2021.

[8] Greg Haugstad. *Atomic force microscopy: understanding basic modes and advanced applications*. John Wiley & Sons, 2012.

[9] Bugrahan Guner, Simon Laflamme, and Omur E. Dagdeviren. Customization of an atomic force microscope for multidimensional measurements under environmental conditions. *Review of Scientific Instruments*, 94(6), 2023.

[10] R.F. Egerton. *Physical Principles of Electron Microscopy*. Springer International Publishing, Cham, 2016.

[11] Ricardo Garcıa and Ruben Perez. Dynamic atomic force microscopy methods. *Surface science reports*, 47(6-8):197–301, 2002.

[12] Omur E. Dagdeviren, Chao Zhou, Eric I. Altman, and Udo D. Schwarz. Quantifying Tip-Sample Interactions in Vacuum Using Cantilever-Based Sensors: An Analysis. *Physical Review Applied*, 9(4):044040, April 2018.

[13] Riccardo Borgani and David B. Haviland. Intermodulation spectroscopy as an alternative to pump-probe for the measurement of fast dynamics at the nanometer scale. *Review of Scientific Instruments*, 90(1), 2019.

[14] M. Nonnenmacher, M. P. O'Boyle, and H. K. Wickramasinghe. Kelvin probe force microscopy. *Applied Physics Letters*, 58(25):2921–2923, June 1991.

[15] Ulrich Zerweck, Christian Loppacher, Tobias Otto, Stefan Grafström, and Lukas M. Eng. Accuracy and resolution limits of Kelvin probe force microscopy. *Physical Review B*, 71(12):125424, March 2005.

[16] U. Diebold. The surface science of titanium dioxide. *Surf. Sci. Rep.*, 48, 2003.

[17] Roger Rousseau, Vassiliki-Alexandra Glezakou, and Annabella Selloni. Theoretical insights into the surface physics and chemistry of redox-active oxides. *Nature Reviews Materials*, 5(6):460–475, June 2020.

[18] Zeno Schumacher, Andreas Spielhofer, Yoichi Miyahara, and Peter Grutter. The lower limit for time resolution in frequency modulation atomic force microscopy. *Applied Physics Letters*, 110(5):053111, January 2017. arXiv:1609.02362 [cond-mat].

[19] Omur E. Dagdeviren, Aaron Mascaro, Shuaishuai Yuan, Javad Shirani, Kirk H. Bevan, and Peter Grütter. Ergodic and Nonergodic Dynamics of Oxygen Vacancy Migration at the Nanoscale in Inorganic Perovskites. *Nano Letters*, 20(10):7530–7535, October 2020.

[20] Bugrahan Guner, Mohammad Safikhani-Mahmoudi, and Omur E. Dagdeviren. Time-Resolved Mapping of Charge Carrier Dynamics and Defect-Mediated Migration Barriers in TiO2. *The Journal of Physical Chemistry C*, 129(37):16879–16886, September 2025.

[21] Durmus U. Karatay, Jeffrey S. Harrison, Micah S. Glaz, Rajiv Giridharagopal, and David S. Ginger. Fast time-resolved electrostatic force microscopy: Achieving sub-cycle time resolution. *Review of Scientific Instruments*, 87(5), 2016.

[22] Rajiv Giridharagopal, Glennis E. Rayermann, Guozheng Shao, David T. Moore, Obadiah G. Reid, Andreas F. Tillack, David. J. Masiello, and David S. Ginger. Submicrosecond Time Resolution Atomic Force Microscopy for Probing Nanoscale Dynamics. *Nano Letters*, 12(2):893–898, February 2012.

[23] Aaron Mascaro, Yoichi Miyahara, Tyler Enright, Omur E. Dagdeviren, and Peter Grütter. Review of time-resolved non-contact electrostatic force microscopy techniques with applications to ionic transport measurements. *Beilstein Journal of Nanotechnology*, 10(1):617–633, 2019.

[24] Ryan P. Dwyer, Sarah R. Nathan, and John A. Marohn. Microsecond photocapacitance transients observed using a charged microcantilever as a gated mechanical integrator. *Science Advances*, 3(6):e1602951, June 2017.

[25] A. Schirmeisen, A. Taskiran, H. Fuchs, B. Roling, S. Murugavel, H. Bracht, and F. Natrup. Probing ion transport at the nanoscale: Time-domain electrostatic force spectroscopy on glassy electrolytes. *Applied Physics Letters*, 85(11):2053–2055, September 2004.

[26] Bugrahan Guner, Orcun Dincer, and Omur E. Dagdeviren. Fast and Slow Time-Scale Effects of Photoinduced Surface Oxygen Vacancies on the Charge Carrier Dynamics of TiO2. *ACS Applied Energy Materials*, 7(6):2292–2298, March 2024.

[27] Bugrahan Guner, Mohammad Safikhani-Mahmoudi, Fengmiao Li, Ke Zou, and Omur E. Dagdeviren. Ultraviolet irradiation penetration depth on TiO2. *Communications Chemistry*, 8(1):83, March 2025.

[28] Orcun Dincer, Bugrahan Guner, and Omur E. Dagdeviren. Effect of methanol and photoinduced surface oxygen vacancies on the charge carrier dynamics in TiO2. *APL Materials*, 12(2), 2024.

[29] Akira Fujishima, Xintong Zhang, and Donald A. Tryk. TiO2 photocatalysis and related surface phenomena. *Surface Science Reports*, 63(12):515–582, December 2008.

[30] Jenny Schneider, Masaya Matsuoka, Masato Takeuchi, Jinlong Zhang, Yu Horiuchi, Masakazu Anpo, and Detlef W. Bahnemann. Understanding TiO2 Photocatalysis: Mechanisms and Materials. *Chemical Reviews*, 114(19):9919–9986, October 2014.

[31] Omur E. Dagdeviren, Daniel Glass, Riccardo Sapienza, Emiliano Cortés, Stefan A. Maier, Ivan. P. Parkin, Peter Grütter, and Raul Quesada-Cabrera. The Effect of Photoinduced Surface Oxygen Vacancies on the Charge Carrier Dynamics in TiO $_2$ Films. *Nano Letters*, 21(19):8348–8354, October 2021.

[32] Mohammad S. Mahmoudi, Bugrahan Guner, Simon Laflamme, and Omur OE. Dagdevirenmur. An Optimization of Time-Resolved Atomic Force Microscopy, August 2024.

[33] Bugrahan Guner, Mohammad S. Mahmoudi, Simon Laflamme, and Omur E. Dagdeviren. Multidimensional Contact Potential Difference Measurements at the Nanoscale in Inorganic Oxides, August 2024.

[34] Danielle Schweke, Yuval Mordehovitz, Mahdi Halabi, Lee Shelly, and Shmuel Hayun. Defect Chemistry of Oxides for Energy Applications. *Advanced Materials*, 30(41):1706300, 2018. _eprint: https://advanced.onlinelibrary.wiley.com/doi/pdf/10.1002/adma.201706300.

[35] Song Bai, Ning Zhang, Chao Gao, and Yujie Xiong. Defect engineering in photocatalytic materials. *Nano Energy*, 53:296–336, November 2018.

[36] Adawiyah J. Haider, Zainab N. Jameel, and Imad H. M. Al-Hussaini. Review on: Titanium Dioxide Applications. *Energy Procedia*, 157:17–29, January 2019.

[37] Nikolai Tsvetkov, Qiyang Lu, Lixin Sun, Ethan J. Crumlin, and Bilge Yildiz. Improved chemical and electrochemical stability of perovskite oxides with less reducible cations at the surface. *Nature Materials*, 15(9):1010–1016, September 2016.

[38] G. Pacchioni. Oxygen vacancy: the invisible agent on oxide surfaces. *ChemPhysChem*, 4, 2003.

[39] F. Gunkel, D. V. Christensen, Y. Z. Chen, and N. Pryds. Oxygen vacancies: The (in)visible friend of oxide electronics. *Applied Physics Letters*, 116(12), 2020.

[40] Benjamin J. Morgan and Graeme W. Watson. A DFT + *U* description of oxygen vacancies at the TiO2 rutile (1 1 0) surface. *Surface Science*, 601(21):5034–5041, November 2007.

[41] Yoshio Nosaka and Atsuko Y. Nosaka. Reconsideration of Intrinsic Band Alignments within Anatase and Rutile TiO2. *The Journal of Physical Chemistry Letters*, 7(3):431–434, February 2016.

[42] Meredith CK Sellers and Edmund G. Seebauer. Manipulation of polycrystalline TiO2 carrier concentration via electrically active native defects. *Journal of Vacuum Science & Technology A*, 29(6), 2011.

[43] X. Pan, M. . Q. Yang, X. Fu, N. Zhang, and Y. . J. Xu. Defective TiO2 with oxygen vacancies: synthesis, properties and photocatalytic applications. *Nanoscale*, 5, 2013.

[44] Ming Kong, Yuanzhi Li, Xiong Chen, Tingting Tian, Pengfei Fang, Feng Zheng, and Xiujian Zhao. Tuning the Relative Concentration Ratio of Bulk Defects to Surface Defects in TiO2 Nanocrystals Leads to High Photocatalytic Efficiency. *Journal of the American Chemical Society*, 133(41):16414–16417, October 2011.

[45] A. Sclafani and J. M. Herrmann. Comparison of the Photoelectronic and Photocatalytic Activities of Various Anatase and Rutile Forms of Titania in Pure Liquid Organic Phases and in Aqueous Solutions. *The Journal of Physical Chemistry*, 100(32):13655–13661, January 1996.

[46] Joseph Muscat, Varghese Swamy, and Nicholas M. Harrison. First-principles calculations of the phase stability of TiO 2. *Physical Review B*, 65(22):224112, June 2002.

[47] T. Bak, D. Chu, A. R. Francis, W. Li, and J. Nowotny. Concentration of electrons at grain boundaries in TiO2 (rutile): Impact on charge transport and reactivity. *Catal. Today*, 224, 2014.

[48] M. K. Nowotny, T. Bak, and J. Nowotny. Electrical properties and defect chemistry of TiO2 single crystal. I. Electrical conductivity. *J. Phys. Chem. B*, 110, 2006.

[49] B. J. Morgan and G. W. Watson. Polaronic trapping of electrons and holes by native defects in anatase TiO2. *Phys. Rev. B*, 80, 2009.

[50] P. Deák, B. Aradi, and T. Frauenheim. Quantitative theory of the oxygen vacancy and carrier self-trapping in bulk TiO2. *Phys. Rev. B*, 86, 2012.

[51] M. K. Nowotny, L. R. Sheppard, T. Bak, and J. Nowotny. Defect chemistry of titanium dioxide. application of defect engineering in processing of TiO2-based photocatalysts. *J. Phys. Chem. C.*, 112, 2008.

[52] Daniel Glass, Emiliano Cortés, Sultan Ben-Jaber, Thomas Brick, William J. Peveler, Christopher S. Blackman, Christopher R. Howle, Raul Quesada-Cabrera, Ivan P. Parkin, and Stefan A. Maier. Dynamics of Photo-Induced Surface Oxygen Vacancies in Metal-Oxide Semiconductors Studied Under Ambient Conditions. *Advanced Science*, 6(22):1901841, 2019. _eprint: https://advanced.onlinelibrary.wiley.com/doi/pdf/10.1002/advs.201901841.

[53] Andreas Klein, Karsten Albe, Nicole Bein, Oliver Clemens, Kim Alexander Creutz, Paul Erhart, Markus Frericks, Elaheh Ghorbani, Jan Philipp Hofmann, Binxiang Huang, Bernhard Kaiser, Ute Kolb, Jurij Koruza, Christian Kübel, Katharina N. S. Lohaus, Jürgen Rödel, Jochen Rohrer, Wolfgang Rheinheimer, Roger A. De Souza, Verena Streibel, Anke Weidenkaff, Marc Widenmeyer, Bai-Xiang Xu, and Hongbin Zhang. The Fermi energy as common parameter to describe charge compensation mechanisms: A path to Fermi level engineering of oxide electroceramics. *Journal of Electroceramics*, 51(3):147–177, November 2023.

[54] H. Ishii, N. Hayashi, E. Ito, Y. Washizu, K. Sugi, Y. Kimura, M. Niwano, Y. Ouchi, and K. Seki. Kelvin probe study of band bending at organic semiconductor/metal interfaces: examination of Fermi level alignment. *physica status solidi (a)*, 201(6):1075–1094, 2004.

[55] Jun Wang, Ganghai Ni, Wanru Liao, Kang Liu, Jiawei Chen, Fangyang Liu, Zongliang Zhang, Ming Jia, Jie Li, Junwei Fu, Evangelina Pensa, Liangxing Jiang, Zhenfeng Bian, Emiliano Cortés, and Min Liu. Subsurface Engineering Induced Fermi Level De-pinning in Metal Oxide Semiconductors for Photoelectrochemical Water Splitting. *Angewandte Chemie International Edition*, 62(9):e202217026, 2023.

[56] Vaidyanathan Subramanian, Eduardo E. Wolf, and Prashant V. Kamat. Catalysis with TiO2/Gold Nanocomposites. Effect of Metal Particle Size on the Fermi Level Equilibration. *Journal of the American Chemical Society*, 126(15):4943–4950, April 2004.

[57] Seungho Bang, Wooyoung Kang, Dohyeong Kim, Hyeong Chan Suh, Dong Hyeon Kim, Chan Kwon, Jieun Jo, Ji-hong Kim, Hayoung Ko, Ki Kang Kim, Jinho Ahn, and Mun Seok Jeong. Harnessing Persistent Photocurrent in a 2D Semiconductor–Polymer Hybrid Structure: Electron Trapping and Fermi Level Modulation for Optoelectronic Memory. *Nano Letters*, 24(32):9889–9897, August 2024.

[58] Mingrui Shao, Chang Ji, Jibing Tan, Baoqiang Du, Xiaofei Zhao, Jing Yu, Baoyuan Man, Kaichen Xu, Chao Zhang, and Zhen Li. Ferroelectrically modulate the Fermi level of graphene oxide to enhance SERS response. *Opto-Electronic Advances*, 6(11):230094–1–230094–10, November 2023.

[59] Xiaochi Liu, Min Sup Choi, Euyheon Hwang, Won Jong Yoo, and Jian Sun. Fermi Level Pinning Dependent 2D Semiconductor Devices: Challenges and Prospects. *Advanced Materials*, 34(15):2108425, 2022.

[60] Andreas Klein, Christoph Körber, André Wachau, Frank Säuberlich, Yvonne Gassenbauer, Steven P. Harvey, Diana E. Proffit, and Thomas O. Mason. Transparent Conducting Oxides for Photovoltaics: Manipulation of Fermi Level, Work Function and Energy Band Alignment. *Materials*, 3(11):4892–4914, 2010.

[61] Akihiro Furube, Tsuyoshi Asahi, Hiroshi Masuhara, Hiromi Yamashita, and Masakazu Anpo. Charge Carrier Dynamics of Standard TiO2 Catalysts Revealed by Femtosecond Diffuse Reflectance Spectroscopy. *The Journal of Physical Chemistry B*, 103(16):3120–3127, April 1999.

[62] G. Rothenberger, J. Moser, M. Graetzel, N. Serpone, and D. K. Sharma. Charge carrier trapping and recombination dynamics in small semiconductor particles. *J. Am. Chem. Soc.*, 107, 1985.

[63] Liam Collins, Jason I. Kilpatrick, Sergei V. Kalinin, and Brian J. Rodriguez. Towards nanoscale electrical measurements in liquid by advanced KPFM techniques: a review. *Reports on Progress in Physics*, 81(8):086101, July 2018.

[64] Monica Luna, Mariam Barawi, Sacha Gómez-Moñivas, Jaime Colchero, Micaela Rodríguez-Peña, Shanshan Yang, Xiao Zhao, Yi-Hsien Lu, Ravi Chintala, Patricia Reñones, Virginia Altoe, Lidia Martínez, Yves Huttel, Seiji Kawasaki, Alexander Weber-Bargioni, Victor A. de la Peña ÓShea, Peidong Yang, Paul D. Ashby, and Miquel Salmeron. Photoinduced Charge Transfer and Trapping on Single Gold Metal Nanoparticles on TiO2. *ACS Applied Materials & Interfaces*, 13(42):50531–50538, October 2021.

[65] Alex Henning, Gino Günzburger, Res Jöhr, Yossi Rosenwaks, Biljana Bozic-Weber, Catherine E. Housecroft, Edwin C. Constable, Ernst Meyer, and Thilo Glatzel. Kelvin probe force microscopy of nanocrystalline TiO2 photoelectrodes. *Beilstein Journal of Nanotechnology*, 4:418–428, 2013.

[66] Clemens Möller, Mike Allen, Virgil Elings, Andreas Engel, and Daniel J. Müller. Tapping-mode atomic force microscopy produces faithful high-resolution images of protein surfaces. *Biophysical journal*, 77(2):1150–1158, 1999.

[67] M. Bammerlin. True atomic resolution on the surface of an insulator via ultrahigh vacuum dynamic force microscopy. *Probe Micros.*, 1:3–9, 1997.

[68] T. R. Albrecht, P. Grütter, D. Horne, and D. Rugar. Frequency modulation detection using high-Q cantilevers for enhanced force microscope sensitivity. *Journal of Applied Physics*, 69(2):668–673, January 1991.

[69] John E. Sader and Suzanne P. Jarvis. Accurate formulas for interaction force and energy in frequency modulation force spectroscopy. *Applied physics letters*, 84(10):1801–1803, 2004.

[70] Ricardo Garcia and Elena T. Herruzo. The emergence of multifrequency force microscopy. *Nature nanotechnology*, 7(4):217–226, 2012.

[71] Jose R. Lozano and Ricardo Garcia. Theory of Multifrequency Atomic Force Microscopy. *Physical Review Letters*, 100(7):076102, February 2008.

[72] Sergei V. Kalinin and Alexei Gruverman. *Scanning probe microscopy: electrical and electromechanical phenomena at the nanoscale*, volume 1. Springer Science & Business Media, 2007.

[73] S. Hudlet, M. Saint Jean, C. Guthmann, and J. Berger. Evaluation of the capacitive force between an atomic force microscopy tip and a metallic surface. *The European Physical Journal B*, 2(1):5–10, April 1998.

[74] J. Colchero, A. Gil, and A. M. Baró. Resolution enhancement and improved data interpretation in electrostatic force microscopy. *Physical Review B*, 64(24):245403, November 2001.

[75] William R. Silveira, Erik M. Muller, Tse Nga Ng, David Dunlap, and John A. Marohn. High-Sensitivity Electric Force Microscopy of Organic Electronic Materials and Devices. In Sergei Kalinin and Alexei Gruverman, editors, *Scanning Probe Microscopy*, pages 788–830. Springer New York, New York, NY, 2007.

[76] Amelie Axt, Ilka M. Hermes, Victor W. Bergmann, Niklas Tausendpfund, and Stefan AL Weber. Know your full potential: Quantitative Kelvin probe force microscopy on nanoscale electrical devices. *Beilstein journal of nanotechnology*, 9(1):1809–1819, 2018.

[77] Antoine Kahn. Fermi level, work function and vacuum level. *Materials Horizons*, 3(1):7–10, 2016.

[78] Aaron Mascaro. *Time resolved electrostatic force microscopy measurements of ionic transport*. McGill University (Canada), 2019.

[79] K. L. Ngai, Y. N. Wang, and L. B. Magalas. Theoretical basis and general applicability of the coupling model to relaxations in coupled systems. *Journal of Alloys and Compounds*, 211-212:327–332, September 1994.

[80] S. Havriliak and S. Negami. A complex plane representation of dielectric and mechanical relaxation processes in some polymers. *Polymer*, 8:161–210, 1967.

[81] K. L. Ngai and O. Kanert. Comparisons between the coupling model predictions, Monte Carlo simulations and some recent experimental data of conductivity relaxations in glassy ionics. *Solid State Ion.*, 53-56, 1992.

[82] K. Funke. Jump relaxation in solid electrolytes. *Progress in Solid State Chemistry*, 22(2):111–195, January 1993.

[83] Svante Arrhenius. Über die Dissociationswärme und den Einfluss der Temperatur auf den Dissociationsgrad der Elektrolyte. *Zeitschrift für physikalische Chemie*, 4(1):96–116, 1889.

[84] A. Schirmeisen, A. Taskiran, H. Bracht, and B. Roling. Ion jump dynamics in nanoscopic subvolumes analyzed by electrostatic force spectroscopy. *Z. für. Phys. Chem.*, 224, 2010.

[85] G. T. S. How, A. Pandikumar, H. N. Ming, and L. H. Ngee. Highly exposed {001} facets of titanium dioxide modified with reduced graphene oxide for dopamine sensing. *Sci. Rep.*, 4, 2014.

[86] R. Ghamarpoor, A. Fallah, and M. Jamshidi. Investigating the use of titanium dioxide (TiO2) nanoparticles on the amount of protection against UV irradiation. *Sci. Rep.*, 13, 2023.

[87] W. Souza. The two faces of titanium dioxide nanoparticles bio-camouflage in 3D bone spheroids. *Sci. Rep.*, 9, 2019.

[88] J. Bai and B. Zhou. Titanium dioxide nanomaterials for sensor applications. *Chem. Rev.*, 114, 2014.

[89] M. Vasilopoulou. Hydrogen and nitrogen codoping of anatase TiO2 for efficiency enhancement in organic solar cells. *Sci. Rep.*, 7, 2017.

[90] X. Du. One-step preparation of nanoarchitectured TiO2 on porous Al as integrated anode for high-performance lithium-ion batteries. *Sci. Rep.*, 6, 2016.

[91] Y. Zeng. Oxygen-vacancy and surface modulation of ultrathin nickel cobaltite nanosheets as a high-energy cathode for advanced Zn-ion batteries. *Adv. Mater.*, 30, 2018.

[92] Hao Wu, Hua Wang, and Guanghai Li. Metal oxide semiconductor SERS-active substrates by defect engineering. *Analyst*, 142(2):326–335, 2017.

[93] Gunkel, F., Christensen, D. V., Chen, Y. Z. & Pryds, N. Oxygen vacancies: The (in)visible friend of oxide electronics. Appl. Phys. Lett.116, 120505 (2020).

[94] Daniel Glass, Raul Quesada-Cabrera, Steven Bardey, Premrudee Promdet, Riccardo Sapienza, Valérie Keller, Stefan A. Maier, Valérie Caps, Ivan P. Parkin, and Emiliano Cortés. Probing the Role of Atomic Defects in Photocatalytic Systems through Photoinduced Enhanced Raman Scattering. *ACS Energy Letters*, 6(12):4273–4281, December 2021.

[95] Cesare Franchini, Michele Reticcioli, Martin Setvin, and Ulrike Diebold. Polarons in materials. *Nature Reviews Materials*, 6(7):560–586, July 2021.

[96] N. Rahimi, R. A. Pax, and E. M. Gray. Review of functional titanium oxides. I: TiO2 and its modifications. *Prog. Solid State Chem.*, 44, 2016.

[97] Tykhon Zubkov, Dirk Stahl, Tracy L. Thompson, Dimitar Panayotov, Oliver Diwald, and John T. Yates. Ultraviolet Light-Induced Hydrophilicity Effect on TiO2(110)(1×1). Dominant Role of the Photooxidation of Adsorbed Hydrocarbons Causing Wetting by Water Droplets. *The Journal of Physical Chemistry B*, 109(32):15454–15462, August 2005.

[98] Manuel Cardona and Gunther Harbeke. Optical Properties and Band Structure of Wurtzite-Type Crystals and Rutile. *Physical Review*, 137(5A):A1467–A1476, 1965.

[99] T. Siefke. Materials pushing the application limits of wire grid polarizers further into the deep ultraviolet spectral range. *Adv. Opt. Mater.*, 4, 2016.

[100] Ana Stevanovic, Michael Büttner, Zhen Zhang, and John T. Yates. Photoluminescence of TiO2: Effect of UV Light and Adsorbed Molecules on Surface Band Structure. *Journal of the American Chemical Society*, 134(1):324–332, January 2012.

[101] Jiyuan Zhang, Jiajia Wang, Zongyan Zhao, Tao Yu, Jianyong Feng, Yongjun Yuan, Zekun Tang, Yunhong Liu, Zhaosheng Li, and Zhigang Zou. Reconstruction of the (001) surface of TiO2 nanosheets induced by the fluorine-surfactant removal process under UV-irradiation for dye-sensitized solar cells. *Physical Chemistry Chemical Physics*, 14(14):4763–4769, 2012.

[102] Edward D. Palik. *Handbook of optical constants of solids*, volume 3. Academic press, 1998.

[103] Axel Wahl and Jan Augustynski. Charge Carrier Transport in Nanostructured Anatase TiO2 Films Assisted by the Self-Doping of Nanoparticles. *The Journal of Physical Chemistry B*, 102(40):7820–7828, October 1998.

[104] I. Tanabe and Y. Ozaki. Far- and deep-ultraviolet spectroscopic investigations for titanium dioxide: electronic absorption, Rayleigh scattering, and Raman spectroscopy. *J. Mater. Chem. C.*, 4, 2016.

[105] B. Liu. Intrinsic intermediate gap states of TiO2 materials and their roles in charge carrier kinetics. *J. Photochem. Photobiol. C: Photochem. Rev.*, 39, 2019.

[106] D. Meroni. Oxygen vacancies in the Spotlight: On the engineering of intrinsic defects in highly defective TiO2 photocatalysts. *J. Photochem. Photobiol. A: Chem.*, 444, 2023.

[107] H. Yaghoubi. Toward a visible light-driven photocatalyst: the effect of midgap-states-induced energy gap of undoped TiO2 nanoparticles. *ACS Catal.*, 5, 2015.

[108] V. Etacheri, C. Valentin, J. Schneider, D. Bahnemann, and S. C. Pillai. Visible-light activation of TiO2 photocatalysts: Advances in theory and experiments. *J. Photochem. Photobiol. C: Photochem. Rev.*, 25, 2015.

[109] X. Kang, X. . Z. Song, Y. Han, J. Cao, and Z. Tan. Defect-engineered TiO2 hollow spiny nanocubes for phenol degradation under visible light irradiation. *Sci. Rep.*, 8, 2018.

[110] Z. Pei. Facile synthesis of defect-mediated TiO2x with enhanced visible light photocatalytic activity. *J. Mater. Chem. A*, 1, 2013.

[111] J. Zhang, C. Y. Toe, P. Kumar, J. Scott, and R. Amal. Engineering defects in TiO2 for the simultaneous production of hydrogen and organic products. *Appl. Catal. B: Environ. Energy*, 333, 2023.

[112] S. . G. Wang. Formation of oxygen vacancies on the TiO2(110) surfaces. *Surf. Sci.*, 577, 2005.

[113] Charles Kittel and Paul McEuen. *Introduction to solid state physics*. John Wiley & Sons, 2018.

[114] Z. Zhang. Manipulating the carrier concentration and phase transition via Nb content in SrTiO3. *Sci. Rep.*, 12, 2022.

[115] H. Huang. TiO2 surface oxygen vacancy passivation towards mitigated interfacial lattice distortion and efficient perovskite solar cell. *Appl. Surf. Sci.*, 544, 2021.

[116] Y. Nam, L. Li, J. Y. Lee, and O. V. Prezhdo. Strong influence of oxygen vacancy location on charge carrier losses in reduced TiO2 nanoparticles. *J. Phys. Chem. Lett.*, 10, 2019.

[117] A. Klasen. Removal of surface oxygen vacancies increases conductance through TiO2 thin films for perovskite solar cells. *J. Phys. Chem. C. Nanomater Interfaces*, 123, 2019.

[118] A. C. Papageorgiou. Electron traps and their effect on the surface chemistry of TiO2 (110). *Proc. Natl Acad. Sci.*, 107, 2010.

[119] G. Horowitz and M. E. Hajlaoui. Grain size dependent mobility in polycrystalline organic field-effect transistors. *Synth. Met.*, 122, 2001.

[120] S. Emin, E. Pavlica, H. Okuyucu, M. Valant, and G. Bratina. Charge carrier transport in polycrystalline CH3NH3PbI3 perovskite thin films in a lateral direction characterized by time-of-flight photoconductivity. *Mater. Chem. Phys.*, 220, 2018.

[121] R. T. Weitz. The importance of grain boundaries for the time-dependent mobility degradation in organic thin-film transistors. *Chem. Mater.*, 21, 2009.

[122] I. Jelovica Badovinac. Grain size effect on photocatalytic activity of TiO2 thin films grown by atomic layer deposition. *Thin Solid Films*, 709, 2020.

[123] James Quirk, Mathias Rothmann, Wei Li, Daniel Abou-Ras, and Keith Patrick McKenna. Grain boundaries in polycrystalline materials for energy applications: First principles modeling and electron microscopy. *Applied Physics Reviews*, 11(1), 2024.

[124] F. Y. Bruno. Band structure and spin–orbital texture of the (111)-KTaO3 2D electron gas. *Adv. Electron. Mater.*, 5, 2019.

[125] W. Meevasana. Creation and control of a two-dimensional electron liquid at the bare SrTiO3 surface. *Nat. Mater.*, 10, 2011.

[126] S. M. Walker. Carrier-density control of the SrTiO3 (001) Surface 2D Electron gas studied by ARPES. *Adv. Mater.*, 27, 2015.

[127] R. Engel-Herbert, B. Jalan, J. Cagnon, and S. Stemmer. Microstructure of epitaxial rutile TiO2 films grown by molecular beam epitaxy on r-plane Al2O3. *J. Cryst. Growth*, 312, 2009.

[128] X. Weng, P. Fisher, M. Skowronski, P. A. Salvador, and O. Maksimov. Structural characterization of TiO2 films grown on LaAlO3 and SrTiO3 substrates using reactive molecular beam epitaxy. *J. Cryst. Growth*, 310, 2008.

[129] O. E. Dagdeviren. Surface phase, morphology, and charge distribution transitions on vacuum and ambient annealed SrTiO3 (100). *Phys. Rev. B*, 93, 2016.

[130] J. Augustynski. The role of the surface intermediates in the photoelectrochemical behaviour of anatase and rutile TiO2. *Electrochim. Acta*, 38, 1993.

[131] H. Z. Banfield and F. Jillian. Thermodynamic analysis of phase stability of nanocrystalline titania. *J. Mater. Chem.*, 8, 1998.

[132] S. J. S. Woodfield. Heat capacities and thermodynamic functions of TiO2 anatase and rutile: Analysis of phase stability. *Am. Mineral.*, 94, 2022.

[133] D. A. H. Hanaor and C. C. Sorrell. Review of the anatase to rutile phase transformation. *J. Mater. Sci.*, 46, 2010.

[134] F. Maleki, G. Liberto, and G. Pacchioni. pH- and facet-dependent surface chemistry of TiO2 in aqueous environment from first principles. *ACS Appl. Mater. Interfaces*, 15, 2023.

[135] Baohuan Wei, Frederik Tielens, and Monica Calatayud. Understanding the Role of Rutile TiO2 Surface Orientation on Molecular Hydrogen Activation. *Nanomaterials*, 9(9):1199, September 2019.

[136] André Schirmeisen, Ahmet Taskiran, Harald Fuchs, Hartmut Bracht, Sevi Murugavel, and Bernhard Roling. Fast Interfacial Ionic Conduction in Nanostructured Glass Ceramics. *Physical Review Letters*, 98(22):225901, May 2007.

[137] A. Taskiran, A. Schirmeisen, H. Fuchs, H. Bracht, and B. Roling. Time-domain electrostatic force spectroscopy on nanostructured lithium-ion conducting glass ceramics: analysis and interpretation of relaxation times. *Phys. Chem. Chem. Phys.*, 11, 2009.

[138] Aaron Mascaro, Zi Wang, Pierre Hovington, Yoichi Miyahara, Andrea Paolella, Vincent Gariepy, Zimin Feng, Tyler Enright, Connor Aiken, and Karim Zaghib. Measuring spatially resolved collective ionic transport on lithium battery cathodes using atomic force microscopy. *Nano letters*, 17(7):4489–4496, 2017. ISBN: 1530-6984.

[139] James Utama Surjadi and Carlos M. Portela. Enabling three-dimensional architected materials across length scales and timescales. *Nature Materials*, 24(4):493–505, April 2025.

[140] Dongtao Liu, Deying Luo, Affan N. Iqbal, Kieran W. P. Orr, Tiarnan A. S. Doherty, Zheng-Hong Lu, Samuel D. Stranks, and Wei Zhang. Strain analysis and engineering in halide perovskite photovoltaics. *Nature Materials*, 20(10):1337–1346, October 2021.

[141] Zhuyan Gao, Puning Ren, Lulu Sun, Nengchao Luo, and Feng Wang. Photocatalysts for steering charge transfer and radical reactions in biorefineries. *Nature Synthesis*, 3(4):438–451, April 2024.

[142] Meinan He, Louis G. Hector, Fang Dai, Fan Xu, Suryanarayana Kolluri, Nathaniel Hardin, and Mei Cai. Industry needs for practical lithium-metal battery designs in electric vehicles. *Nature Energy*, 9(10):1199–1205, October 2024.

[143] George Kiriakidis and Vassilios Binas. Metal oxide semiconductors as visible light photocatalysts. *Journal of the Korean Physical Society*, 65(3):297–302, August 2014.

[144] Jimin Kim, Jia-An Lin, Jinhyun Kim, Inwhan Roh, Soohyung Lee, and Peidong Yang. A red-light-powered silicon nanowire biophotochemical diode for simultaneous CO2 reduction and glycerol valorization. *Nature Catalysis*, 7(9):977–986, September 2024.

[145] Ludwig Hüttenhofer, Felix Eckmann, Alberto Lauri, Javier Cambiasso, Evangelina Pensa, Yi Li, Emiliano Cortés, Ian D. Sharp, and Stefan A. Maier. Anapole Excitations in Oxygen-Vacancy-Rich TiO2–x Nanoresonators: Tuning the Absorption for Photocatalysis in the Visible Spectrum. *ACS Nano*, 14(2):2456–2464, February 2020.

[146] Krzysztof Szot, Wolfgang Speier, Gustav Bihlmayer, and Rainer Waser. Switching the electrical resistance of individual dislocations in single-crystalline SrTiO3. *Nature Materials*, 5(4):312–320, April 2006.

[147] Dongwei Ma, Kaiming Li, and Jia Hong Pan. Ultraviolet-Induced Interfacial Crystallization of Uniform Nanoporous Biphasic TiO2 Spheres for Durable Lithium-Ion Battery. *ACS Applied Energy Materials*, 3(5):4186–4192, May 2020.

[148] Shuo Wang, Chenyang Li, Yu Qi, Jiaming Zhang, Ningning Wang, Meng Liu, Boyang Zhang, Xuefen Cai, Hongbo Zhang, Su-huai Wei, Guijun Ma, Jingxiu Yang, Shanshan Chen, and Fuxiang Zhang. Etched BiVO4 photocatalyst with charge separation efficiency exceeding 90%. *Nature Communications*, 16(1):3776, April 2025.

[149] Shanshan Dong, Jinyuan Hu, Shucai Xia, Binli Wang, Zhiqiang Wang, Tianjun Wang, Wei Chen, Zefeng Ren, Hongjun Fan, Dongxu Dai, Jun Cheng, Xueming Yang, and Chuanyao Zhou. Origin of the Adsorption-State-Dependent Photoactivity of Methanol on TiO2(110). *ACS Catalysis*, 11(5):2620–2630, March 2021.

[150] David Kitto, Carolina Espinoza, José C. Díaz, Jacquelyn Zamora, and Jovan Kamcev. Fast and selective ion transport in ultrahigh-charge-density membranes. *Nature Chemical Engineering*, 2(4):252–260, April 2025.

[151] Theo Emmerich, Yunfei Teng, Nathan Ronceray, Edoardo Lopriore, Riccardo Chiesa, Andrey Chernev, Vasily Artemov, Massimiliano Di Ventra, Andras Kis, and Aleksandra Radenovic. Nanofluidic logic with mechano–ionic memristive switches. *Nature Electronics*, 7(4):271–278, April 2024.

[152] Xiaoli Zheng, Qin Kuang, Keyou Yan, Yongcai Qiu, Jianhang Qiu, and Shihe Yang. Mesoporous TiO2 Single Crystals: Facile Shape-, Size-, and Phase-Controlled Growth and Efficient Photocatalytic Performance. *ACS Applied Materials & Interfaces*, 5(21):11249–11257, November 2013.

[153] N. W. and Mermin Ashcroft. *Solid State Physics*. Sounders College, Philadelphia, 1981.

[154] R. Stadler and K. W. Jacobsen. Fermi level alignment in molecular nanojunctions and its relation to charge transfer. *Physical Review B*, 74(16):161405, 2006.

[155] John K. Tomfohr and Otto F. Sankey. Complex band structure, decay lengths, and Fermi level alignment in simple molecular electronic systems. *Physical Review B*, 65(24):245105, 2002.

[156] R. A. De Souza. Oxygen Diffusion in SrTiO3 and Related Perovskite Oxides. *Advanced Functional Materials*, 25(40):6326–6342, 2015.

[157] Amit Kumar, Francesco Ciucci, Anna N. Morozovska, Sergei V. Kalinin, and Stephen Jesse. Measuring oxygen reduction/evolution reactions on the nanoscale. *Nature Chemistry*, 3(9):707–713, September 2011.

[158] Yuchao Yang and Ru Huang. Probing memristive switching in nanoionic devices. *Nature Electronics*, 1(5):274–287, May 2018.

[159] Yuchao Yang, Xiaoxian Zhang, Liang Qin, Qibin Zeng, Xiaohui Qiu, and Ru Huang. Probing nanoscale oxygen ion motion in memristive systems. *Nature Communications*, 8(1):15173, May 2017.

[160] Sascha Sadewasser and Thilo Glatzel, editors. *Kelvin Probe Force Microscopy, Measuring and Compensating Electrostatic Forces*. Springer, Berlin, 2012.

[161] Michael A. Henderson, William S. Epling, Charles H. F. Peden, and Craig L. Perkins. Insights into Photoexcited Electron Scavenging Processes on TiO2 Obtained from Studies of the Reaction of O2 with OH Groups Adsorbed at Electronic Defects on TiO2(110). *The Journal of Physical Chemistry B*, 107(2):534–545, January 2003.

[162] Tracy L. Thompson and John T. Yates. Surface Science Studies of the Photoactivation of TiO2New Photochemical Processes. *Chemical Reviews*, 106(10):4428–4453, October 2006.

[163] Chi Lun Pang, Robert Lindsay, and Geoff Thornton. Chemical reactions on rutile TiO2(110). *Chemical Society Reviews*, 37(10):2328–2353, 2008.

[164] Tracy L. Thompson and John T. Yates. Monitoring Hole Trapping in Photoexcited TiO2(110) Using a Surface Photoreaction. *The Journal of Physical Chemistry B*, 109(39):18230–18236, October 2005.

[165] Thomas Degen, Mustapha Sadki, Egbert Bron, Uwe König, and Gwilherm Nénert. The HighScore suite. *Powder Diffraction*, 29(S2):S13–S18, December 2014.

[166] Theo Hahn, Uri Shmueli, and JC Wilson Arthur. *International tables for crystallography*, volume 1. Reidel Dordrecht, 1983.

[167] T. A. Al-Dhahir. Quantitative phase analysis for titanium dioxide from X-ray powder diffraction data using the Rietveld method. *Diyala journal for pure sciences*, 2(9):108–119, 2013.

[168] M. Nasir Khan, K. Shahzad, and J. Bashir. Thermal atomic displacements in nanocrystalline titanium dioxide studied by synchrotron x-ray diffraction. *Journal of Physics D: Applied Physics*, 41(8):085409, 2008.

[169] O. Le Bacq, E. Salinas, A. Pisch, C. Bernard, and A. Pasturel. First-principles structural stability in the strontium–titanium–oxygen system. *Philosophical Magazine*, 86(15):2283–2292, May 2006.

[170] Robert B. Cook. Handbook of mineralogy. *Rocks and Minerals*, 76(4):278, 2001.

[171] Bernard Dennis Cullity and RJPT Smoluchowski. Elements of X-ray Diffraction. *Physics Today*, 10(3):50–50, 1957.

[172] Percy Zahl, Markus Bierkandt, Stefan Schröder, and Andreas Klust. The flexible and modern open source scanning probe microscopy software package GXSM. *Review of Scientific Instruments*, 74(3):1222–1227, March 2003.